PhD-FSTC-2018-46

The Faculty of Sciences, Technology and Communication

DISSERTATION

Defense held on 29/06/2018 in Luxembourg

to obtain the degree of

DOCTEUR DE L'UNIVERSITÉ DU LUXEMBOURG
EN INFORMATIQUE

by

Danilo SPANO

Born on 11 November 1989 in Lecce, Italy

ADVANCED SYMBOL-LEVEL PRECODING SCHEMES FOR INTERFERENCE EXPLOITATION IN MULTI-ANTENNA MULTI-USER WIRELESS COMMUNICATIONS

Dissertation defense committee

Dr. Symeon Chatzinotas, Dissertation Supervisor,

Senior Research Scientist, SnT, University of Luxembourg

Dr. Björn Ottersten, Vice-chairman,

Professor and Director of SnT, University of Luxembourg

Dr. Gabriele Lenzini, Chairman,

Senior Research Scientist, SnT, University of Luxembourg

Dr. Kai-Kit Wong,

Professor at University College London, United Kingdom

Dr. Jens Krause,

Senior Manager, Satellite Telecommunications Systems, SES, Luxembourg

ADVANCED SYMBOL-LEVEL PRECODING SCHEMES FOR INTERFERENCE EXPLOITATION IN MULTI-ANTENNA MULTI-USER WIRELESS COMMUNICATIONS

Danilo Spano

Abstract

The utilization of multi-antenna transmitters relying on full frequency reuse has proven to be an effective strategy towards fulfilling the constantly increasing throughput requirements of wireless communication systems. As a consequence, in the last two decades precoding has been a prolific research area, due to its ability to handle the interference arising among simultaneous transmissions addressed to different co-channel users. The conventional precoding strategies aim at mitigating the multi-user interference (MUI) by exploiting the knowledge of the channel state information (CSI). More recently, novel approaches have been proposed where the aim is not to eliminate the interference, but rather to control it so as to achieve a constructive interference effect at each receiver. In these schemes, referred to as symbol-level precoding (SLP), the data information (data symbols) is used together with the CSI in the precoding design, which can be addressed following several optimization strategies.

In the context of SLP, the work carried out in this thesis is mainly focused on developing more advanced optimization strategies suitable to non-linear systems, where the per-antenna high-power amplifiers introduce an amplitude and phase distortion on the transmitted signals. More specifically, the main objective is to exploit the potential of SLP not only to achieve the constructive interference at the receivers, but also to control the per-antenna instantaneous transmit power, improving the power dynamics of the transmitted waveforms. In fact, a reduction of the power variation of the signals, both in the spatial dimension (across the different antennas) and in the temporal dimension, is particularly important for mitigating the non-linear effects.

After a detailed review of the state of the art of SLP, the first part of the thesis is focused on improving the power dynamics of the transmitted signals in the spatial dimension, by reducing the instantaneous power imbalances across the different antennas. First, a SLP per-antenna power minimization scheme is presented, followed by a related max-min fair formulation with per-antenna power constraints. These approaches allow to reduce the power peaks of the signals across the antennas. Next, more advanced SLP schemes are formulated and solved, with the objective of further improving the spatial dynamics of the signals. Specifically, a first approach performs a peak power minimization under a lower bound constraint on the per-antenna transmit power, while a second strategy minimizes the spatial peak-to-average power ratio.

The second part of this thesis is devoted to developing a novel SLP method, referred to as spatio-temporal SLP, where the temporal variation of the transmit power is also considered in the SLP optimization. This new model allows to minimize the peak-to-average power ratio of the transmitted waveforms both in the spatial and in the temporal

dimensions, thus further improving the robustness of the signals to non-linear effects. Then, this thesis takes one step further, by exploiting the developed spatio-temporal SLP model in a different context. In particular, a spatio-temporal SLP scheme is proposed which enables faster-than-Nyquist (FTN) signaling over multi-user systems, by constructively handling at the transmitter side not only the MUI but also the inter-symbol interference (ISI). This strategy allows to benefit from the increased throughput provided by FTN signaling without imposing additional complexity at the user terminals. Extensive numerical results are presented throughout the thesis, in order to assess the performance of the proposed schemes with respect to the state of the art in SLP. The thesis concludes summarizing the main research findings and identifying the open problems, which will constitute the basis for the future work.

To my father Ottavio, a great dad and a strong man,
for he taught me that Life is the most valuable thing.
You always were, and always will be, the most beautiful part of me.
In Loving Memory.

Acknowledgements

First of all, I would like to thank my supervisor, Dr. Symeon Chatzinotas, for his continuous support and technical guidance throughout my doctoral studies. His daily supervision and his positive attitude had a pivotal role in the accomplishment of this thesis. I would also like to thank Prof. Björn Ottersten, for giving me the chance to pursue my PhD studies in an excellent research group, and for his valuable advices and constructive comments. Further, I would like to thank Dr. Jens Krause from SES, for helping me to understand several concepts in the context of satellite communications. I also thank Prof. Kai-Kit Wong and Dr. Gabriele Lenzini for accepting to be in my defense committee.

I would like to thank all my (current and past) colleagues of the SIGCOM group of SnT, for many fruitful research collaborations, and for creating an enjoyable working environment. A big gratitude is owed to all the new friends that came into my life in these years while living in Luxembourg, who made me feel at home away from home.

I am grateful to my friends from Italy, who stayed close to me even from far away. Among all, I owe a special thanks to my friends William De Carlo and Giuseppe Candido, who have always been next to me, in good and bad times. Their support in the most difficult moments has been invaluable. The biggest thanks goes to my family, for giving me the possibility to pursue my studies and for the unquestionable support throughout all the path. A special mention goes to my father, Ottavio, my model of strength. With his being a purely good man, he taught me that honesty and simplicity are more important than anything else. With his ceaseless struggle, he taught me that Life is the most valuable thing, in spite of everything. My biggest accomplishment has been making him proud of me, and my mission in life is to carry his name higher and higher. This thesis is dedicated to him.

Danilo Spano
Vernole, 27 May 2018

Contents

List of Figures

List of Tables

Acronyms

ACM	adaptive coding and modulation
AM-PM	amplitude-to-phase
AM-AM	amplitude-to-amplitude
APSK	amplitude phase shift keying
AWGN	additive white Gaussian noise
BER	bit error rate
BPSK	binary phase shift keying
CCDF	complementary cumulative distribution function
CSI	channel state information
DPC	dirty paper coding
FEC	forward error correction
FPP	feasible point pursuit
FTN	faster-than-Nyquist
HPA	high-power amplifier
IAPR	instantaneous-to-average power ratio
IBO	input back-off
ISI	inter-symbol interference
KKT	Karush-Kuhn-Tucker
LDPC	low-density parity check
MIMO	multiple-input multiple-output
MISO	multiple-input single-output
MMSE	minimum mean square error
MRT	maximum ratio transmission
MUI	multi-user interference
NSD	negative semi-definite
OFDM	orthogonal frequency-division multiplexing
PAC	per-antenna power constraint
PAPR	peak-to-average power ratio
PPM	peak power minimization

PSK	phase shift keying
QAM	quadrature amplitude modulation
QoS	Quality-of-Service
QPSK	quadrature phase shift keying
RF	radio frequency
SCA	successive convex approximation
SDR	semi-definite relaxation
SER	symbol error rate
SINR	signal-to-interference-plus-noise ratio
SLP	symbol-level precoding
SNR	signal-to-noise ratio
SOCP	second-order cone program
SPAPR	spatial peak-to-average power ratio
SPC	sum power constraint
SPM	sum power minimization
SRRC	squared root raised cosine
SSPA	solid state power amplifier
ST-PAPR	spatio-temporal peak-to-average power ratio
TDD	time-division duplexing
THP	Tomlinson-Harashima precoding
TWTA	traveling-wave tube amplifier
WPPMLB	weighted peak power minimization with lower bound
ZF	zero forcing

Notations

x	Scalar variable
$\boldsymbol{x}$	Vector variable
$\boldsymbol{X}$	Matrix variable
$(\cdot)^T$	Transpose
$(\cdot)^*$	Conjugate
$(\cdot)^\dagger$	Conjugate transpose
$\lvert\cdot\rvert$	Magnitude (amplitude)
$\angle(\cdot)$	Argument (phase)
$\mathrm{Re}(\cdot)$	Real part
$\mathrm{Im}(\cdot)$	Imaginary part
ι	Imaginary unit
$\lVert\cdot\rVert$	Euclidean norm of a vector
$\lVert\cdot\rVert_\infty$	l_∞ norm of a vector
$\lVert\cdot\rVert_F$	Frobenius norm of a matrix
$\mathrm{diag}(\cdot)$	Diagonal
$\mathrm{vec}(\cdot)$	Vectorization
$\otimes$	Kronecker product
$\circ$	Element-wise Hadamard operations
$\mathbb{E}[\cdot]$	Statistical expectation
$\Pr(\cdot)$	Probability
$\mathbf{1}_{a\times b}$	$a \times b$ matrix of all ones
$\mathbf{0}_{a\times b}$	$a \times b$ matrix of all zeros
$\boldsymbol{I}_a$	$a \times a$ identity matrix
max	Maximization
min	Minimization

$\frac{\partial}{\partial \boldsymbol{x}}$	Gradient operator with respect to $\boldsymbol{x}$
$\frac{\partial}{\partial \boldsymbol{x}^*}$	Gradient operator with respect to $\boldsymbol{x}^*$
$\triangleright$	Operator denoting the correct detection region
$\trianglerighteq$	Generalized inequality ($\geq$ or $=$, depending on the data)
$\gtrless$	Generalized inequality ($>$,$<$ or $=$, depending on the data)

By striving to do the impossible, man has always achieved what is possible. Those who have cautiously done no more than they believed possible have never taken a single step forward.

M. A. Bakunin

Chapter 1

Introduction

Current research in the context of wireless communications is facing the need to break the existent throughput gridlock, in order to fulfill the ever-increasing demand for interactive services and multimedia content delivery. Since the wireless spectrum is a scarce resource, which is becoming more and more congested, a main challenge is to find novel system architectures and advanced signal processing techniques able to stretch the data rate achievable utilizing the available bandwidth. In this direction, one solution relies on the use of multi-antenna transceivers, which allow aggressive reuse of the frequency spectrum by exploiting the additional degrees of freedom given by the spatial dimension. This strategy allows to deliver information to different co-channel users sharing the same time and frequency resources, through a space division multiple access scheme [1], thus it can significantly boost the throughput performance. The related architectures are known as multi-user multiple-input multiple-output (MIMO), when multiple antennas are utilized both at the transmitter and at the receivers, or multi-user multiple-input single-output (MISO), when a multi-antenna transmitter serves single-antenna users. However, one crucial limitation of full frequency reuse schemes is the interference arising among the simultaneous transmissions towards the different co-channel users, referred to as multi-user interference (MUI). As a consequence, it is pivotal to employ appropriate signal processing techniques in order to handle the MUI. In this framework, precoding schemes have been shown to be effective in tackling the interference, while guaranteeing specific system performance requirements. In a broad sense, precoding can be defined as the design of the transmitted signals of a multi-antenna system aimed to efficiently deliver the intended data stream to each user, tackling the MUI by exploiting the data and channel state information. Precoding has found applications in many practical communication systems, such as terrestrial cellular networks [2–6], satellite communications (SatComs) [7–9], and visible light communications [10–12].

Conventional precoding techniques use knowledge of the channel state information (CSI) to mitigate the MUI, therefore they can be referred to as channel-level precoding. In this class of techniques, the generic scheme relies on the design of a precoding weight matrix (or precoder), which depends only on the CSI. As a consequence, the precoder remains constant for a whole block of symbols whose length is related to the coherence time of the channel. In this framework, different strategies have been considered for the precoder design. The optimal precoding strategy for the minimization of the total transmit power, whilst guaranteeing some Quality-of-Service (QoS) targets at each user was given in [13, 14], while the problem of precoding for maximizing the minimum signal-to-interference-plus-noise ratio (SINR) across the users, under sum power constraints, was optimally solved in [15]. The goal of the latter formulation is to increase the fairness of the system, hence the approach is also referred to as *max-min fair*. This work on channel-level precoding was extended in [16] accounting for per-antenna power constraints, and in [17] considering generalized power constraints. Furthermore, the problem of channel-level precoding in a multigroup multicast framework has been tackled in [18, 19].

In the recent years, a new paradigm has been developed in the context of precoding, known as symbol-level precoding (SLP), which is the main focus of this thesis work. The term SLP refers to a class of precoding schemes where the transmitted signals are designed exploiting the knowledge of both the CSI and the data information, constituted by the symbols to be delivered to the users [20–25]. Differently from the conventional channel-level schemes, the aim of SLP is not to cancel the interference, but rather to control it so to have a constructive interference effect at each user. The classification of the interference as constructive or destructive was given in [20], where a selective channel inversion scheme was proposed in order to eliminate the destructive interference. A more advanced SLP scheme was proposed in [21], based on the rotation of the destructive interference so as to transform it into useful power. Several optimization strategies have been considered in the literature for SLP, including the sum power minimization and the max-min fair problem for phase shift keying (PSK) modulations [22], as well as extensions to the case of multi-level modulations [23]. A detailed overview of the state of the art in channel-level and symbol-level precoding is provided in chapter 2.

This thesis work goes beyond the state of the art in SLP, which is mainly focused on a constructive exploitation of the MUI. On one hand, novel SLP strategies are proposed which, besides leveraging the constructive interference effect at the receivers, account for per-antenna power limitations and improve the robustness of the transmitted waveforms to non-linear channels. On the other hand, SLP is also used to enable faster-than-Nyquist (FTN) signaling over multi-user systems, by constructively handling at the transmitter side not only the MUI but also the inter-symbol interference (ISI). Motivation and scope of this thesis are specifically discussed in the following section.

1.1 Motivation and Scope

The main motivation of this thesis is given by the considerations below:

- In practical systems it is common that each individual antenna has a dedicated amplifier, resulting in a reduced flexibility in the power allocation amongst the different radio frequency (RF) chains of the transmitter. This dictates the need to consider the power limitations independently for each antenna, while performing the precoding operation.
- While per-antenna power constraints have been considered in several works in the context of channel-level precoding (see for instance [16]), the SLP schemes available in the literature consider solely sum power constraints at the transmitter. Therefore, they are not suitable to per-antenna power limited systems.
- The power amplifiers usually introduce non-linear effects which can degrade the transmitted waveform [26, 27]. Therefore, good dynamic properties of the per-antenna transmit power are required to limit the distortion effects. For single-user links, predistortion techniques are used to deal with this problem [28]. However, their extension to multi-user systems relying on precoding is not straightforward, due to the complex nature of the constellations produced by the precoding operation. The non-linear effects are even more detrimental when multiple transmitting antennas, each one having a dedicated amplifier, are considered. In fact, in this case a phase distortion, dependent on the instantaneous transmitted power, applies independently to each transmitted stream. As a consequence, a high variation across the instantaneous power transmitted by different antennas determines different phase shifts in the amplification stages, and this differential effect is a further source of performance degradation.
- Based on the above point, in order to counteract the non-linear effects in the context of SLP, it is important to control the per-antenna instantaneous transmit power and, in particular, to reduce its variation both in the temporal dimension and in the spatial one (i.e. among the different antennas). Although this issue has already been addressed in the precoding literature resorting to peak-to-average power ratio (PAPR) reduction or constant envelope precoding schemes [29–32], this has not been done in the context of SLP based on constructive interference and accounting for QoS constraints.

Based on these considerations, a first aim of this thesis is to develop novel optimization strategies for SLP allowing to exploit the constructive interference effect and, at the same

time, to control the instantaneous per-antenna power levels. Firstly, this is done solely in the spatial dimension, by minimizing the per-antenna power amongst the antennas under QoS constraints, as well as by improving the spatial power dynamics. The reason of this space-only optimization is related to the inherent symbol-by-symbol processing of SLP schemes, which prevents from controlling the power variations in the temporal dimension. To fill this gap, in the second part of the thesis a novel SLP method is proposed, referred to as spatio-temporal SLP, which models the transmitted waveforms both in the spatial and in the temporal domain in the optimization procedure. This method allows to optimize the power dynamics also in the temporal dimension, thus further improving the robustness of the signals to non-linearities. A second aim of this thesis is to use the introduced spatio-temporal SLP method to enable FTN signaling over multi-user systems. In this regard, moving away from the traditional discrete memoryless channel, SLP can jointly exploit the interference in the spatial dimension (the MUI) and the interference in the temporal dimension (the ISI), using the pulse shaping filters as additional side information for the precoding design. This strategy allows to benefit from the increased throughput provided by FTN signaling without imposing additional complexity at the user terminals. The novelty of this approach lies in its ability to merge together the aggressive frequency reuse relying on precoding, the FTN signaling, and the constructive interference effect, which involves both the MUI and the ISI. An overview on the state of the art on FTN signaling is provided in chapter 2.

1.2 Thesis Outline

The main thread of the thesis is the development of novel SLP schemes which account for per-antenna power limitations and improve the robustness of the signals to the non-linear effects of practical systems. Nevertheless, in its second part the thesis goes beyond this main thread, by introducing a multi-user FTN framework based on spatio-temporal SLP. The outline of the thesis is as follows.

- Chapter 2 gives an overview on the state of the art in precoding, in particular SLP, and in FTN signaling. Further, it presents the main working assumptions and highlights with more detail the contributions of this thesis, related to the existent literature.
- In chapter 3 a SLP per-antenna power minimization scheme under QoS constraints is proposed, which allows to reduce the spatial power peaks of the transmitted signals. Further, a related max-min fair approach under per-antenna power constraints is formulated and solved.

- In chapter 4 two different more advanced symbol-level precoding strategies are proposed, with the objective of reducing the power imbalances between the multiple transmit antennas, and therefore to have improved performance over non-linear channels. In both the proposed approaches QoS constraints are considered to guarantee a per-user required SINR. The first presented algorithm minimizes the per-antenna transmit power, and imposes a lower bound to the power carried by each transmitted signal. In this approach, the imbalances between the different RF chains are reduced by constraining the per-antenna transmit power within a specific range. The second proposed scheme directly tackles a minimization of the spatial peak-to-average power ratio (SPAPR) amongst the multiple transmit antennas.

- In chapter 5 the spatio-temporal SLP method is presented, which is able to optimize the power dynamics of the waveforms both in the spatial and in the temporal dimensions, thus further enhancing the robustness of the signals to non-linear effects. Specifically, the proposed scheme performs a minimization of the spatio-temporal PAPR of the transmitted waveforms, under QoS constraints.

- Chapter 6 presents a spatio-temporal SLP scheme which enables FTN signaling over multi-user MISO systems, managing at the transmitter side not only the interference in the spatial dimension (the MUI), but also the interference in the temporal dimension (the ISI). More specifically, two optimization schemes are presented, one splitting the data streams in symbol blocks and tackling only the ISI within each block, and another sequentially handling also the inter-block ISI.

- Finally, in chapter 7 conclusions are drawn and the open research challenges are discussed.

1.3 Publications

The work presented in this thesis has resulted in a number of peer-reviewed conference and journal papers, currently published or under revision, as well as in a patent filing. The publications (fully or partially) included in this thesis are listed here below.

Journals

- J1: D. Spano, M. Alodeh, S. Chatzinotas and B. Ottersten, "Symbol-Level Precoding for the Nonlinear Multiuser MISO Downlink Channel," *IEEE Transactions on Signal Processing*, vol. 66, no. 5, pp. 1331-1345, March 2018.

- J2: D. Spano, S. Chatzinotas, S. Andrenacci, J. Krause, and B. Ottersten, "Per-antenna Power Minimization in Symbol-level Precoding for the Multi-beam Satellite Downlink", *International Journal of Satellite Communications and Networking*, May 2018.

- J3: D. Spano, M. Alodeh, S. Chatzinotas, and B. Ottersten, "Faster-than-Nyquist signaling through spatio-temporal symbol-level precoding for the multiuser MISO downlink channel," *IEEE Transactions on Wireless Communications*, July 2018.

- J4: M. Alodeh, D. Spano, A. Kalantari, C. Tsinos, D. Christopoulos, S. Chatzinotas, and B. Ottersten, "Symbol-level and multicast precoding for multiuser multi-antenna downlink: A state-of-the-art, classification and challenges," *IEEE Communications Surveys and Tutorials*, May 2018.

Conferences

- C1: D. Spano, M. Alodeh, S. Chatzinotas and B. Ottersten, "Per-Antenna Power Minimization in Symbol-Level Precoding," 2016 *IEEE Global Communications Conference (GLOBECOM)*, Washington, DC, 2016, pp. 1-6.

- C2: D. Spano, S. Chatzinotas, J. Krause and B. Ottersten, "Symbol-level precoding with per-antenna power constraints for the multi-beam satellite downlink," *2016 8th Advanced Satellite Multimedia Systems Conference and the 14th Signal Processing for Space Communications Workshop (ASMS/SPSC)*, Palma de Mallorca, 2016, pp. 1-8.

- C3: D. Spano, M. Alodeh, S. Chatzinotas, J. Krause and B. Ottersten, "Spatial PAPR reduction in symbol-level precoding for the multi-beam satellite downlink," *2017 IEEE 18th International Workshop on Signal Processing Advances in Wireless Communications (SPAWC)*, Sapporo, 2017, pp. 1-5.

- C4: M. Alodeh, D. Spano, S. Chatzinotas and B. Ottersten, "Faster-than-Nyquist spatiotemporal symbol-level precoding in the downlink of multiuser MISO channels," *2017 IEEE International Conference on Acoustics, Speech and Signal Processing (ICASSP)*, New Orleans, LA, 2017, pp. 3779-3783.

- C5: D. Spano, M. Alodeh, S. Chatzinotas, and B. Ottersten, "PAPR minimization through spatio-temporal symbol-level precoding for the non-linear multi-user MISO channel," in *2018 IEEE International Conference on Acoustics, Speech and Signal Processing (ICASSP)*, April 2018, to appear.

Patents

- P1: M. Alodeh, D. Spano, and S. Chatzinotas, "Spatio-temporal precoding for faster-than-Nyquist signal transmissions," March 2017, Patent LU100110.

1.4 Publications not included in this thesis

The following publications, carried out in the context of the PhD work, are not included in this thesis to keep it consistent. Nonetheless, they are still relevant to this thesis, as they include preliminary results or extensions of the described ideas.

- BC1: D. Christopoulos, S. Andrenacci, D. Spano, S. Chatzinotas, J. Krause, and B. Ottersten, "Multibeam joint processing satellites: cooperative relays, high above," Book chapter in *Advanced Relay Technologies in Next Generation Wireless Communication*, IET 2016.

- C6: D. Spano, D. Christopoulos, S. Andrenacci, S. Chatzinotas, J. Krause, and B. Ottersten, "Total degradation analysis of precoded signals onto non-linear satellite channels," in *21st Ka and Broadband Communications Conference*, October 2015.

- C7: M. Alodeh, D. Spano, S. Chatzinotas and B. Ottersten, "Peak power minimization in symbol-level precoding for cognitive MISO downlink channels," *2016 IEEE International Conference on Digital Signal Processing (DSP)*, Beijing, October 2016, pp. 240-244.

- C8: S. Andrenacci, D. Spano, D. Christopoulos, S. Chatzinotas, J. Krause and B. Ottersten, "Optimized link adaptation for DVB-S2X precoded waveforms based on SNIR estimation," 2016 *50th Asilomar Conference on Signals, Systems and Computers*, Pacific Grove, CA, November 2016, pp. 502-506.

- C9: D. Spano, S. Chatzinotas, and B. Ottersten, "Sequential spatio-temporal symbol-level precoding enabling faster-than-Nyquist signaling for multi-user MISO systems," *2018 26th European Signal Processing Conference (EUSIPCO)*, 2018, to appear.

Chapter 2

Background and Contributions

In this chapter, an overview of the state of the art in precoding and in faster-than-Nyquist (FTN) signaling is given, and the contributions of this thesis are highlighted. First, the conventional channel-level precoding schemes are reviewed, describing their common model and different optimization strategies. Then, the symbol-level precoding (SLP) paradigm is described, by highlighting its peculiarities and discussing various techniques proposed in the literature. Further, the chapter discusses the problem of channel non-linearities and the concept of FTN signaling. Finally, an overview of the contributions of this thesis is given.

2.1 Channel-level Precoding

Conventionally, precoding schemes treat the interference as a harmful factor to be mitigated, and they exploit the knowledge of the channel state information (CSI) to tackle it. One of the earliest schemes concerning interference cancellation is dirty paper coding (DPC) [33, 34], a non-linear technique which pre-subtracts the interference and has been shown to achieve the multiple-input multiple-output (MIMO) downlink capacity. Albeit optimal, DPC methods are in general very complex [35] and assume codewords with infinite length for the encoding of the data. A suboptimal counterpart of DPC is Tomlinson-Harashima precoding (THP) [36, 37], which offers a complexity reduction at a comparable performance. Nonetheless, the associated complexity is still prohibitive and makes it impractical for current communication systems. On the other hand, several linear precoding schemes have been proposed in the literature, having a much lower complexity and therefore resulting more suitable for practical applications. Although linear precoding does not achieve the optimum capacity bound of DPC, it has been shown effective for several applications for handling the multi-user interference (MUI)

while guaranteeing, at the same time, specific service requirements [13–15, 38–40]. Hereinafter, the focus will be on linear precoding schemes.

The generic scheme for linear precoding relies on the design of a precoding weight matrix (or precoder), which is used to pre-filter the data streams prior to transmission. The precoder depends solely on the channel and remains constant for a whole block of symbols (in time), whose length is related to the coherence time of the channel. Due to this feature, this class of precoding schemes is referred to as channel-level precoding.

2.1.1 Communication Model

Let us assume that a base station is equipped with N transmit antennas and wishes to transmit G symbol streams to K single-antenna users, with $N \geq K$ and $K \geq G$. Adopting a baseband discrete memoryless model, the received signal at the kth user for the generic symbol slot n can be written as:

$$y_k[n] = \boldsymbol{h}_k \boldsymbol{x}[n] + z_k[n], \tag{2.1}$$

where $\boldsymbol{h}_k \in \mathbb{C}^{1\times N}$ is a complex vector representing the channel of the kth user, $\boldsymbol{x}[n] \in \mathbb{C}^{N\times 1}$ is a complex vector representing the output signal from the N transmit antennas and $z_k[n]$ is a complex scalar representing the additive white Gaussian noise (AWGN) at receiver k for the symbol slot n, having power σ_z^2. The above communication model can be written in a vector form as follows:

$$\boldsymbol{y}[n] = \boldsymbol{H}\boldsymbol{x}[n] + \boldsymbol{z}[n], \tag{2.2}$$

where $\boldsymbol{y}[n] \in \mathbb{C}^{K\times 1}$ is a complex vector representing the received signal at all K users at time n, $\boldsymbol{H} = [\boldsymbol{h}_1^T \dots \boldsymbol{h}_K^T]^T \in \mathbb{C}^{K\times N}$ is a complex matrix representing the system channel matrix and $\boldsymbol{z}[n] \in \mathbb{C}^{K\times 1}$ is a complex vector representing the AWGN for all K users at instant n.

Let us also assume that each symbol stream is divided into blocks of T symbols, while the channel matrix $\boldsymbol{H}$ remains constant for each block of symbols. In this context, $\boldsymbol{D} = [\boldsymbol{d}_1 \dots \boldsymbol{d}_G]^T \in \mathbb{C}^{G\times T}$ is a complex matrix aggregating the $T \times 1$ input symbol vectors for each symbol stream, which are assumed uncorrelated in time and space and having unit average power. Analogously, the matrix $\boldsymbol{X} \in \mathbb{C}^{N\times T}$ represents the block of output signals. The aim of precoding is to design the output symbols in $\boldsymbol{X}$ in order to counteract the MUI and to efficiently convey the data streams in $\boldsymbol{D}$ to the users. In

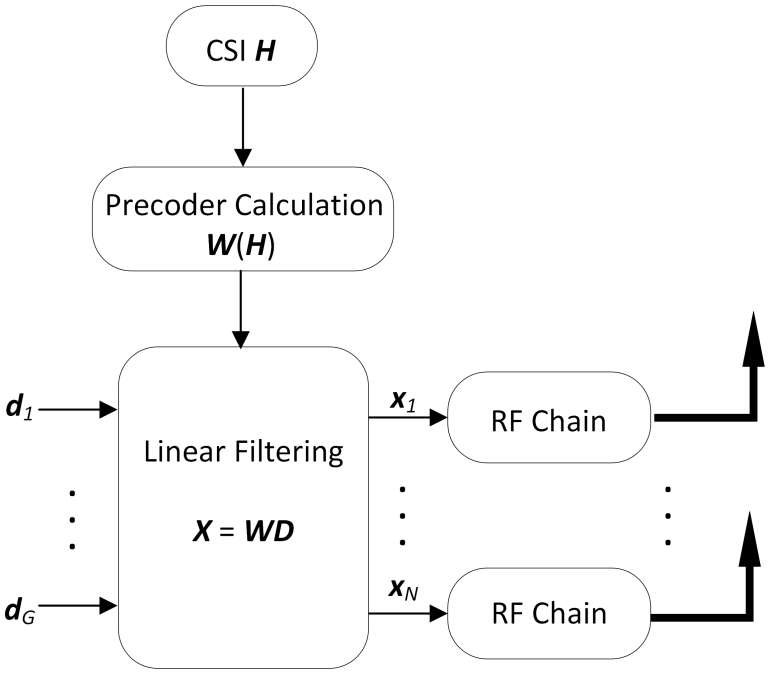

FIGURE 2.1: Schematic diagram of the trasmitter relying on channel-level precoding.

particular, for channel-level precoding the relation between $\boldsymbol{X}$ and $\boldsymbol{D}$ can be written as:

$$\boldsymbol{X} = \boldsymbol{W}\boldsymbol{D}, \tag{2.3}$$

where $\boldsymbol{W} \in \mathbb{C}^{N \times G}$ is the precoding matrix applied to the entire information block $\boldsymbol{D}$. The precoding matrix can be written as $\boldsymbol{W} = [\boldsymbol{w}_1 \dots \boldsymbol{w}_G]$, each column representing a precoding vector for the corresponding stream. From this formalization, it is clear how the problem of channel-level precoding can be reduced to the problem of designing the precoding matrix $\boldsymbol{W}$, using the knowledge of the channel $\boldsymbol{H}$, in order to mitigate the interference. A block scheme of the transmitter relying on channel-level precoding is shown in Fig. 2.1

Regarding the channel estimation, the receivers estimate their respective channel vectors $\boldsymbol{h}_1, \dots, \boldsymbol{h}_K$ by exploiting a training sequence (pilot symbols) included in the framing structure of the communication system, and the resulting CSI is transmitted back to the base station through a feedback channel, in order to be available for the precoding operation. Alternatively, in systems using time-division duplexing (TDD) the channel can be directly estimated at the transmitter based on the uplink-downlink reciprocity principle. The reader is referred to [13, 41] for a more detailed overview of the different channel estimation strategies.

The above formulation considers G independent data streams to be delivered to K users, with $G \leq K$. It is important now to discuss separately the cases when $G = K$, $G < K$, and $G = 1$ as they correspond to different services and, accordingly, to different classes

of channel-level precoding schemes. In the first case, i.e. $G = K$, each data stream is destined to a single intended user, and the related service type is known as unicast. From an information theoretic point of view, this service type has been studied using the broadcast channel [42]. Unicast precoding is the most studied class in the literature, and its aim is to mitigate the interference among the different users. In the second case, i.e. $G < K$, multiple independent messages are transmitted simultaneously but each message is addressed to a group of users. This service is known as multicast, and the related precoding schemes, aimed at mitigating the interference between the different groups, are also referred to as multigroup multicast precoding [18, 19, 43–53]. Finally, the case with $G = 1$ correspond to the broadcast service, in which a transmitter has a common message to be sent to multiple receivers. In physical layer research, this service has been studied under the term of physical layer multicasting [54–61]. Since a single data stream is sent to all receivers, there is no multi-user interference. However, precoding can still be used to improve the Quality-of-Service (QoS) across all users.

Below, an overview of channel-level precoding for the unicast, multicast, and broadcast cases is given.

2.1.2 Channel-level Unicast Precoding

Concerning the class of unicast precoding, the literature provides some closed-form as well as some solutions based on numerical optimization problems. The most relevant closed-form solutions are zero forcing (ZF) precoding [62, 63] and minimum mean square error (MMSE) precoding [64–67]. ZF is one of the simplest suboptimal techniques, which decouples the multi-user channel into parallel single-user channel, thus canceling out the multi-user interference. To this aim, the ZF precoding matrix can be calculated as the pseudo-inverse of the channel matrix, as $\boldsymbol{W} = \boldsymbol{H}^{\dagger}(\boldsymbol{H}\boldsymbol{H}^{\dagger})^{-1}$. The ability of ZF precoding to cancel out the interference makes it more appealing for the high signal-to-noise ratio (SNR) regime. However, since ZF does not take into account the effect of noise, it does not perform well in the low SNR regime (noise limited regime). MMSE precoding, on the other hand, takes into account both the interference and the noise in order to improve the system performance also in the noise limited scenarios [64]. The MMSE precoding matrix can be written as $\boldsymbol{W} = \boldsymbol{H}^{\dagger}(\boldsymbol{H}\boldsymbol{H}^{\dagger} + \alpha\boldsymbol{I})^{-1}$, with α being a regularization parameter inversely proportional to the SNR. Because of its expression, the MMSE precoder is also referred to as regularized ZF [64, 68, 69]. It is worth mentioning also maximum ratio transmission (MRT) precoding [70], aiming at maximizing the received SNR through a precoding matrix as $\boldsymbol{W} = \boldsymbol{H}^{\dagger}$, which however is a suitable technique only in the noise limited regime, where the multi-user interference can be neglected.

The above mentioned closed-form solutions for precoding are effective and easy to implement. However, they do not allow to optimize the system with respect to specific objectives, or respecting specific constraints. In this regard, a number of objective-driven precoding techniques have been devised, so to enhance the flexibility of the transmitter. The literature on channel-level precoding includes different optimization strategies for the precoding design. The two main performance metrics considered in the precoder optimization are the transmitted power and the QoS at the receivers. The usual approach is to optimize one metric while using the other as a constraint, e.g., power minimization under QoS constraints or QoS maximization under power constraints. Concerning the transmitted power, both the average sum power and the average per-antenna power have been considered in the literature. As to the QoS at the receivers, a typical metric considered in the precoder design is the signal-to-interference-plus-noise ratio (SINR), which enables to characterize the ratio of desired to undesired received power levels, but also the rate has been used as a QoS metric. The vast majority of approaches in the area of channel-level precoding consider Gaussian inputs, as a way of allowing the rate to scale logarithmically with the SINR[1].

The optimal precoding strategy for the minimization of the transmitted average sum power, whilst guaranteeing some QoS targets at each user, was given in [14, 74]. For channel-level precoding, it can be shown that the average sum power is $\bar{P} = \sum_{j=1}^{K} \|\boldsymbol{w}_j\|^2$. Accordingly, the related optimization problem, which is optimally solved by semi-definite relaxation (SDR), can be written as follows:

$$\begin{aligned} \boldsymbol{W}(\boldsymbol{H}, \boldsymbol{\gamma}) = \quad & \arg \min_{\boldsymbol{W}} \quad \sum_{j=1}^{K} \|\boldsymbol{w}_j\|^2 \\ & \text{s.t.} \quad \frac{|\boldsymbol{h}_j \boldsymbol{w}_j|^2}{\sum_{k \neq j, k=1}^{K} |\boldsymbol{h}_j \boldsymbol{w}_k|^2 + \sigma_z^2} \geq \gamma_j, \; j = 1, \ldots, K, \end{aligned} \tag{2.4}$$

where the inputs are the channel matrix and a vector $\boldsymbol{\gamma} = [\gamma_1, \gamma_2, \ldots \gamma_K]$ including the target SINR for the different users, and the output is the precoding matrix.

Another relevant precoding strategy aims at maximizing the minimum SINR across the users, under a sum power constraint (SPC). This approach increases the fairness of the system, thus it is known as max-min fair optimization. The related optimization problem was solved in [75] based on the principles of uplink/downlink duality, and can be written as:

[1] It is worth mentioning some notable exceptions ([71–73]).

$$\begin{aligned} \boldsymbol{W}(\boldsymbol{H}, P) = \ \arg \max_{\boldsymbol{W}} \min_{j} \quad & \frac{|\boldsymbol{h}_j \boldsymbol{w}_j|^2}{\sum_{k\neq j, k=1}^{K} |\boldsymbol{h}_j \boldsymbol{w}_k|^2 + \sigma_z^2} \\ \text{s.t.} \quad & \sum_{j=1}^{K} \|\boldsymbol{w}_j\|^2 \leq P. \end{aligned} \tag{2.5}$$

Block-level precoding for unicast systems was extended in [16, 76] accounting for per-antenna power constraints (PACs). In particular, it is worth mentioning that the average per-antenna power (referring to the generic n-th antenna) can be written as $\bar{P}_n = \left[\sum_{j=1}^{K} \boldsymbol{w}_j \boldsymbol{w}_j^{\dagger}\right]_{nn}$. Moreover, further developments have been done considering per-antenna-array power constraints [17] and non-linear power constraints [77].

Unicast multi-user precoding techniques have been proposed to utilize the spatial multiplexing gains of MIMO for different network capabilities such as multicell MIMO [78], cognitive radio [79], physical layer security [80, 81], simultaneous wireless information and power transfer [80, 82].

2.1.3 Channel-level Multicast Precoding

In the framework of channel-level multicast precoding, we assume multiple interfering groups of users. In each group, each user receives a stream of common data. However, independent symbols are addressed to different groups and inter-group interference comes into play. A unified framework for physical layer multicasting to multiple co-channel groups was given in [18, 19, 43]. Therein, the power minimization and the fairness problems were formulated, proven NP-hard and solved for the sum power constrained multicast multigroup case. The sum power minimization problem, solved resorting to SDR, can be written as:

$$\begin{aligned} \boldsymbol{W}(\boldsymbol{H}, \boldsymbol{\gamma}) = \arg \min_{\boldsymbol{W}} \quad & \sum_{k=1}^{G} \|\boldsymbol{w}_k\|^2 \\ \text{s.t.} \quad & \frac{|\boldsymbol{h}_i \boldsymbol{w}_k|^2}{\sum_{l\neq k, l=1}^{G} |\boldsymbol{h}_i \boldsymbol{w}_l|^2 + \sigma_z^2} \geq \gamma_i, \\ & \forall i \in \mathcal{G}_k, k = 1, \ldots, G, \end{aligned}$$

where $\mathcal{G}_k$ denotes the k-th group of users.

The weighted max-min fair problem under SPC has been solved via bisection over the power minimization problem, and can be written as:

$$\begin{aligned}\boldsymbol{W}(\boldsymbol{H},P) = \arg\ \max_{t,\boldsymbol{W}}\quad & t \\ \text{s.t.}\quad & \frac{1}{\gamma_i}\frac{|\boldsymbol{h}_i\boldsymbol{w}_k|^2}{\sum_{l\neq k,l=1}^{G}|\boldsymbol{h}_i\boldsymbol{w}_l|^2+\sigma_z^2}\geq t, \\ & \forall i\in\mathcal{G}_k, k,=1,\ldots,G, \\ & \sum_{k=1}^{G}\|\boldsymbol{w}_k\|^2\leq P.\end{aligned} \tag{2.6}$$

Different service levels among the users can be considered in this weighted formulation. The problem receives as inputs the SPC P and the target SINR vector $\boldsymbol{\gamma}$, and its goal is to maximize the slack variable t while keeping the SINR at each user above this value. Thus, it constitutes a max-min problem that guarantees fairness amongst users.

The weighted max-min fair problem has been addressed also accounting for PACs. In the related optimization problem, analogous to (2.6), the PACs read as $\left[\sum_{k=1}^{G}\boldsymbol{w}_k\boldsymbol{w}_k^{\dagger}\right]_{nn}\leq P_n, \forall n\in\{1\ldots N\}$. The weighted max-min fair problem with PACs has been solved in [45, 46], based on SDR and Gaussian randomization to solve the power minimization problem, and bisection to derive an accurate approximation of the non-convex max-min fair formulation. Further, an alternative derivation of the precoder has been proposed in [47], based on feasible point pursuit (FPP) successive convex approximation (SCA).

The application of multicasting in multi-user MIMO environment has been proposed in different frameworks, such as cognitive radio [83], simultaneous wireless information and power transfer [84], and hybrid analog digital beamforming for millimeter wave [85]. Recently, the combination of multicast precoding with space-time coding through multi-rank transmissions has been studied in [52, 83, 86–88].

2.1.4 Channel-level Broadcast Precoding

Broadcast precoding can be seen as a special case of multicast, where we have a single group of users receiving the same data information. In this scenario, there is no interference since a single stream is sent to all users. Nonetheless, precoding can still be adopted to improve the QoS across all users. In [54], the NP-hard broadcast precoding problem was accurately approximated by SDR and Gaussian randomization. The associated power minimization problem can be written as:

$$\begin{aligned}\boldsymbol{w}(\boldsymbol{H},\boldsymbol{\gamma}) = \arg\ \min_{\boldsymbol{w}}\quad & \|\boldsymbol{w}\|^2 \\ \text{s.t.}\quad & \frac{|\boldsymbol{h}_j\boldsymbol{w}|^2}{\sigma_z^2}\geq\gamma_i,\ j=1,\ldots,K,\end{aligned} \tag{2.7}$$

where $\boldsymbol{w} \in \mathbb{C}^{N\times 1}$ represents the precoding vector for the unique transmitted data stream. Since no interference mitigation is included in the optimization problem (2.7), there are no constraints on the number of simultaneously served users, and the degrees of freedom of the problem are entirely leveraged to transmit information. An information theoretic capacity of broadcast precoding is studied in [55], where the scaling of the capacity as the number of antennas and/or users is taken to infinity is analyzed. Further, robustness for broadcast precoding is studied [56], where the goal is to design a beamformer that minimizes the transmit power while satisfying probabilistic SNR constraints for line of sight environment.

The broadcast transmissions are studied in different contexts such as cognitive radio [89], simultaneous wireless and information power transfer [90], and coordinated multicell networks [91]. Physical-layer transmission techniques that combine multicast, unicast and broadcast have been proposed in [92–99].

2.2 Symbol-level Precoding

The interference among multiple simultaneous transmissions leads to a deviation of the received symbols from their original position within their reference constellation. As previously discussed, channel-level precoding treats the interference as harmful factor that should be mitigated. In this case, precoding cannot tackle the interference suffered by each symbol, and tries to reduce the interference along a whole block of symbols (or codeword) exploiting the knowledge of the CSI. An illustrative example of a received signal corrupted by interference is shown in Fig. 2.2, where a target symbol in the first quadrant of a quadrature phase shift keying (QPSK) modulation is considered. The target signal is the signal dedicated to the intended user and the interfering signals are the ones transmitted towards the other users. The interfering signals tend to deviate the received target symbol in any direction, and the aim of channel-level precoding is to reduce the average power of interference, so as to prevent it from pushing the target symbol outside its detection region.

On the other hand, in SLP the interference can be controlled symbol-by-symbol, therefore the main objective is not an average reduction of the interference power, but rather a rotation of the interfering signals aimed at pushing the target symbol deeper into its detection region. In other words, as illustrated in Fig. 2.3, SLP controls the interference in order to make it constructive at each user and for each symbol. During the past years several symbol-level processing techniques have been utilized in the multi-user multiple-input single-output (MISO) context [20–24, 100–112]. The MUI can be classified into constructive or destructive based on whether it facilitates or deteriorates

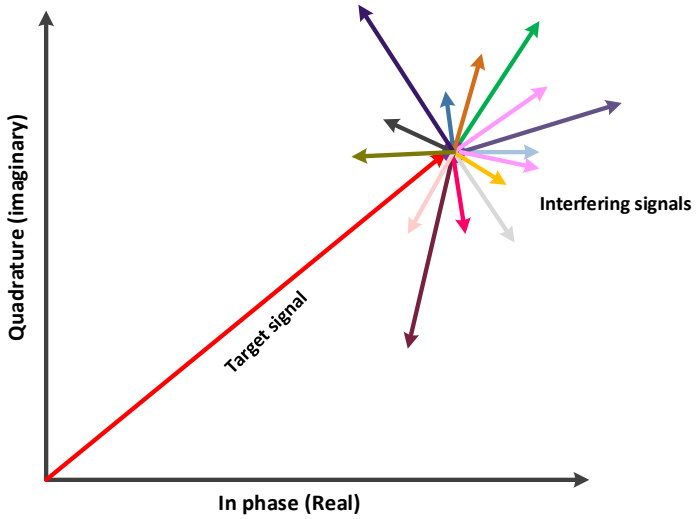

FIGURE 2.2: Received signal corrupted by interference, with channel-level precoding.

the correct detection of the received symbols. Fig. 2.4 illustrates the two scenarios of destructive and constructive interference for the case of a QPSK modulation. A detailed classification of interference is thoroughly discussed in [20], for binary phase shift keying (BPSK) and QPSK modulations, and in [22], for phase shift keying (PSK) modulations. A selective channel inversion scheme was proposed in [20] in order to eliminate the destructive interference, while a more advanced SLP scheme was proposed in [21], based on the rotation of the destructive interference so as to transform it into useful power. Moreover, similarly to the channel-level case, also in SLP different objective-oriented strategies have been considered in the literature. It should be stressed that SLP has been studied only in the context of unicast transmissions, while its application for handling the inter-group interference in multicast scenarios has not been addressed in the literature. Hence, hereinafter the focus is on unicast communications.

Referring to the communication model in (2.1), the aim of SLP is to design the transmitted signal vector $\boldsymbol{x}$ for each symbol slot[2], using the knowledge of both the CSI $\boldsymbol{H}$ and the data information $\boldsymbol{d}$ for achieving constructive interference. A block scheme of the transmitter relying on SLP is shown in Fig. 2.5. It is clear how in SLP the precoding processing takes place on a symbol-by-symbol basis, differently from the channel-level case, where the calculated precoder is fixed as long as the channel $\boldsymbol{H}$ does not change. In the context of SLP, one can directly design the transmitted signal vector $\boldsymbol{x}$, as shown in the provided block scheme, but a model based on a precoding matrix $\boldsymbol{W}$ is still possible (see for instance [22]). In particular, it is possible to design the matrix $\boldsymbol{W} = [\boldsymbol{w}_1 \dots \boldsymbol{w}_K]$

[2]In order to ease the notation, hereafter the time index n is omitted in formulas.

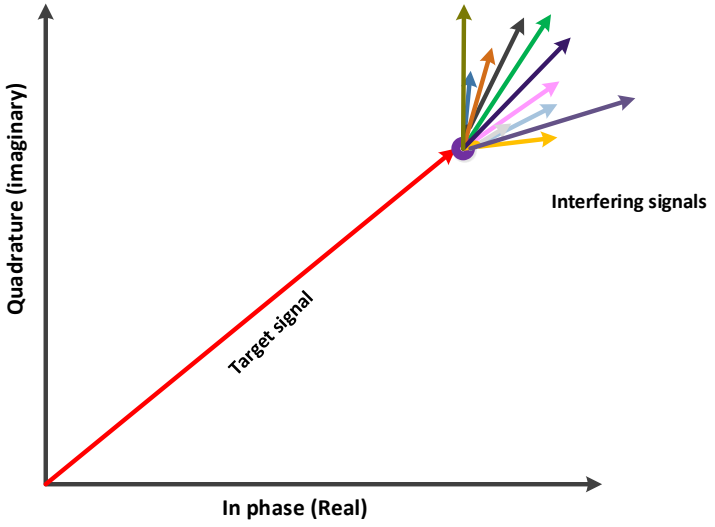

FIGURE 2.3: Constructive interference effect in SLP.

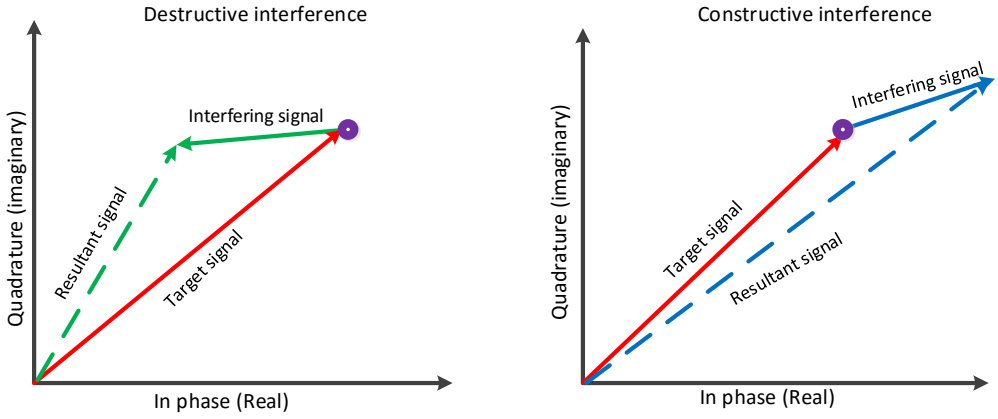

FIGURE 2.4: Illustration of destructive (on the left) and constructive (on the right) interference, considering a single interfering signal and a QPSK modulation.

for each symbol slot, using both the CSI $\boldsymbol{H}$ and the data information $\boldsymbol{d}$, and then calculate the transmitted signal vector as $\boldsymbol{x} = \boldsymbol{W}\boldsymbol{d} = \sum_{k=1}^{K} \boldsymbol{w}_k d_k$. The precoding vectors in the context of SLP have been used in [22] to classify the interference for PSK modulations. Specifically, the normalized interference induced from the k-th data stream onto the j-th user can be formulated as:

$$\psi_{jk} = \frac{\boldsymbol{h}_j \boldsymbol{w}_k}{\|\boldsymbol{h}_j\| \|\boldsymbol{w}_k\|}. \tag{2.8}$$

An M-PSK modulated symbol d_j is said to receive constructive interference from another simultaneously transmitted symbol d_k, which is associated with $\boldsymbol{w}_k$, if and only if the

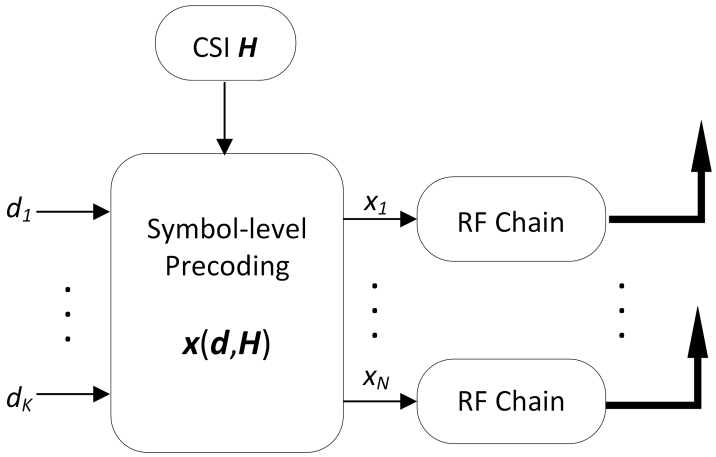

FIGURE 2.5: Schematic diagram of the trasmitter relying on SLP.

following condition holds:

$$\angle d_j - \frac{\pi}{M} \leq \angle(\psi_{jk} d_k) \leq \angle d_j + \frac{\pi}{M}, \tag{2.9}$$

which imposes the received interfering signal, originating from the symbol d_k, to push the target symbol d_j deeper into its detection region. Further, the constructive interference condition has the property of mutuality among pairs of transmitted streams [22].

For constructively interfering symbols, the amplitude of the received signal can be bounded as:

$$\|\boldsymbol{h}_j\| \overset{(a)}{\leq} |y_j| \overset{(b)}{\leq} \|\boldsymbol{h}_j\| \left(1 + \sum_{\forall k, k \neq j}^{K} |\psi_{jk}|\right). \tag{2.10}$$

The inequality (a) holds when all simultaneous users are orthogonal, while (b) holds when all interfering signal are aligned with the intended symbol. On the other hand, in the case of channel-level precoding techniques, the amplitude of the received signal is bounded as:

$$0 \overset{(a)}{\leq} |y_j| \overset{(b)}{\leq} \|\boldsymbol{h}_j\|,$$

with the best case scenario being a complete interference cancellation.

The optimal design for SLP depends on the specific definition of the related optimization problem, and more importantly on how the constraints on constructive interference are defined. The optimal SLP strategy for the minimization of the total transmit power, whilst guaranteeing QoS targets at each user, was given in [22–24, 103–106]. For PSK modulations, the related optimization problem can be written as follows:

$$\begin{aligned} \boldsymbol{W}(\boldsymbol{d},\boldsymbol{\gamma},\boldsymbol{H}) \quad = \quad & \arg\min_{\boldsymbol{W}} \quad \|\sum_{k=1}^{K}\boldsymbol{w}_k d_k\|^2 \\ & s.t. \quad |\boldsymbol{h}_j\sum_{k=1}^{K}\boldsymbol{w}_k d_k|^2 \geq \gamma_j\sigma_z^2,\ j=1,\ldots,K, \\ & \quad \angle(\boldsymbol{h}_j\sum_{k=1}^{K}\boldsymbol{w}_k d_k) = \angle s_j,\ j=1,\ldots,K, \end{aligned} \tag{2.11}$$

where an equality constraint has been imposed on the phase of the received symbols for achieving constructive interference. As already mentioned, the problem can be formulated in order to optimize directly the output vector $\boldsymbol{x}$, by using $\boldsymbol{x} = \sum_{k=1}^{K}\boldsymbol{w}_k d_k$. The direct optimization of $\boldsymbol{x}$ will be considered hereafter (as well as in the remainder of this thesis), since it allows to skip the intermediate step optimizing $\boldsymbol{W}$.

The problem (2.11) has been extended to multi-level modulations, by exploiting the constructive interference on the outermost points of the reference constellation $\mathcal{D}$ while imposing an interference cancellation for the inner points. In particular, for amplitude phase shift keying (APSK) modulations the SLP sum power minimization problem can be formulated as:

$$\begin{aligned} \boldsymbol{x}(\boldsymbol{d},\boldsymbol{\gamma},\boldsymbol{H}) \quad = \quad & \arg\min_{\boldsymbol{x}} \quad \|\boldsymbol{x}\|^2 \\ & s.t. \quad |\boldsymbol{h}_j\sum_{k=1}^{K}\boldsymbol{w}_k d_k|^2 \trianglerighteq \kappa_j^2\gamma_j\sigma_z^2,\ j=1,\ldots,K, \\ & \quad \angle(\boldsymbol{h}_j\sum_{k=1}^{K}\boldsymbol{w}_k d_k) = \angle s_j,\ j=1,\ldots,K, \end{aligned} \tag{2.12}$$

where $\kappa_j = |d_j|/\sqrt{\mathbb{E}_{\mathcal{D}}[|d_j|^2]}$ is a magnitude scaling factor for the symbol d_j , which allows to account for the different amplitudes of the symbols in the multi-level constellation (see [23]), while $\trianglerighteq$ is used as a generalized inequality to be read as $\geq$ or as $=$ depending on whether the constraint is referred to a boundary symbol or to an internal symbol of the constellation, respectively. Further, the optimization can be tailored to exploit the detection regions of quadrature amplitude modulation (QAM) schemes, by referring the constraints to the in-phase and the quadrature components of the received symbols, rather than their magnitude and phase. In this case, the optimization can be formulated

as:

$$\begin{aligned} \boldsymbol{x}(\boldsymbol{d},\boldsymbol{\gamma},\boldsymbol{H}) \quad = \quad & \arg\min_{\boldsymbol{x}} \quad \|\boldsymbol{x}\|^2 \\ & s.t \quad \mathrm{Re}(\boldsymbol{h}_j\boldsymbol{x}) \gtreqless \sigma_z\sqrt{\gamma_j}\,\mathrm{Re}(d_j),\ j=1,\ldots,K, \\ & \qquad\ \ \mathrm{Im}(\boldsymbol{h}_j\boldsymbol{x}) \gtreqless \sigma_z\sqrt{\gamma_j}\,\mathrm{Im}(d_j),\ j=1,\ldots,K, \end{aligned} \tag{2.13}$$

where $\gtreqless$ denotes a generalized inequality, which shall be read as $>$,$<$ or $=$ depending on the position of the data $\boldsymbol{d}_k[i]$ within the QAM constellation and, accordingly, on its detection region.

The optimization problems above have been addressed in [23], where their reformulation into equivalent physical layer multicasting problems has also been discussed. Several different SLP schemes have been proposed in the literature. In [24, 105], the constructive interference precoding design is generalized under the assumption that the received PSK symbol can reside in a relaxed region in order to be correctly detected. Moreover, a weighted maximization of the minimum SNR among all users is studied, taking into account the relaxed detection regions. A symbol error rate (SER) analysis for the proposed schemes is discussed, characterizing the tradeoff between transmit power reduction and SER increase due to the relaxation. These precoding schemes achieve a better energy efficiency in comparison to the techniques in [22, 103]. In [108], a SLP scheme aiming at manipulating both the desired signal and the interfering signals is proposed, such that the desired signal can be superimposed with the interfering signals. In this approach, a Jacobian-based algorithm is applied to enhance the performance. The concept of constructive interference has been further studied in [113], where a systematic definition of optimal and relaxed constructive interference regions is given.

Since the CSI acquisition in most systems is not perfect, a number of works on SLP have also proposed robust schemes accounting for different types of channel errors. In [110], the interference is decomposed into predictable interference, manipulated constructively by the base station, and unpredictable interference, caused by the quantization error. First, an upper bound for the unpredictable interference is derived. Then, the objective is to align the predictable interference at the base station so that its power is much greater than the derived upper bound. During this process, to intensify the received signal power, the base station simultaneously aligns the predictable interference so that it is constructively superimposed with the desired signal. Different approaches aimed at guaranteeing the robustness of SLP have been proposed in [108–110, 114]. These approaches are based on assuming that the errors in CSI is bounded, and the precoding is designed taking into consideration the worst case scenario. The problem in [109] is formulated as second order cone program and can be solved using conventional convex optimization tools.

Recently, hybrid analog-digital schemes have been proposed in the context of SLP, in particular for massive MIMO systems [115]. In fact, in these systems the very large number of antennas hinders the practical application of fully digital precoding schemes, due to the high hardware complexity and power consumption. The utilization of hybrid structures allows to dramatically reduce the power consumption, by reducing the number of radio frequency (RF) chains. In hybrid schemes, the precoding process is divided into the analog domain and digital domain: while phase shifters are applied to provide high dimensional phase-only controls in the analog domain, in the digital domain low-dimensional digital processing is applied to handle the interference. In particular, in [115] a SLP scheme based on constructive interference is proposed for hybrid massive MIMO architecture. In order to further reduce the power consumption, the proposed approach relies on the utilization of 1-bit digital-to-analog converters. Further, the concept of constructive interference has been also exploited in the context of cognitive radio networks in [103], where the focus is on the X-channel, and in [116], focused on the Z-channel. SLP has been applied also in the context of physical layer security in [117], where the concept of constructive interference is exploited to design artificial noise beamformers constructive to the intended receiver but disruptive to possible eavesdroppers.

2.2.1 Directional Modulation

A different research avenue developed in the context of channel and data dependent precoding is known as directional modulation. Directional modulation refers to an analog design strategy where amplitude and phase of each antenna are controlled on a symbol basis, so as to efficiently deliver the intended data to the users. The main difference between directional modulation and SLP is that the former focuses on applying array weights in the analog domain, such that the signals on the receiving antennas have the desired amplitude and phase, while the latter focuses on a digital design at the transmitter, usually aimed to create constructive interference. One of the main application of directional modulation is physical layer security, thus directing the data towards the specific direction of the intended users while hindering the communication towards any possible eavesdropper. In [118], the baseband in-phase and quadrature components of the signals are separately used to excite two different antennas, so that symbols are correctly transmitted only in a specific direction and scrambled in other directions. In another paradigm, [119] uses random and optimized codebook selection, where the optimized selection suppresses large antenna side lobes, in order to improve the security in a millimeter-wave large antenna array system. The authors of [120] derive optimal array weights to get a specific bit error rate (BER) for QPSK modulations in the desired and undesired directions. Further, the Fourier transform is used in [121, 122] to create

the optimal constellation pattern for QPSK directional modulations, while the effect of array structure on the directional modulation performance is investigated in [123]. In particular, the authors have shown that, by increasing the space between the antennas of a two element array, the symbol error rate can be improved for higher order PSK modulation schemes. To overcome imperfect measurements, the authors of [124] propose a robust design for directional modulation in the presence of uncertainty in the estimated direction angle.

In [125, 126], the directional modulation design in a MIMO fading channel has been addressed, considering an arbitrary number of users and symbol streams. Moreover, the necessary conditions for the existence of the precoder for the directional modulation transmitter are derived. The power and SNR minimization precoder design problems are simplified into a linearly-constrained quadratic programming problem. For faster design, an iterative approach as well as non-negative least squares formulation are proposed.

SLP and directional modulation are conceptually similar, since they both exploit the data information and the CSI in order to efficiently deliver the intended messages to specific users. Nonetheless they refer to different contexts and architectures, with SLP being driven by multi-user performance optimization, and directional optimization being driven by implementational aspects. In the remainder of this thesis, the focus will be on SLP, thus assuming a fully digital architecture.

2.3 Non-linear Amplification Stage

The system model described in (2.1)-(2.2) is a linear one. However, as already mentioned, it should be considered that the introduced system model is actually corrupted by the non-linear effects introduced in the per-antenna power amplification stages [26, 27], which affect both the amplitude and the phase of the transmitted waveforms. The input-output characteristics of several typologies of high-power amplifiers (HPAs) are available in the literature [27, 127–131], including the amplitude-to-amplitude (AM-AM) and the amplitude-to-phase (AM-PM) effects. Moreover, analytical models are available for describing the distortion effects of the HPAs, such as Saleh model [132] for traveling-wave tube amplifiers (TWTAs) and a modified version [133] for solid state power amplifiers (SSPAs). To model such non-linear effects, the input signal to the HPA on the generic i-th RF chain of the transmitter can be written in polar coordinates as:

$$x_i = \rho_i \exp(\iota\theta_i), \tag{2.14}$$

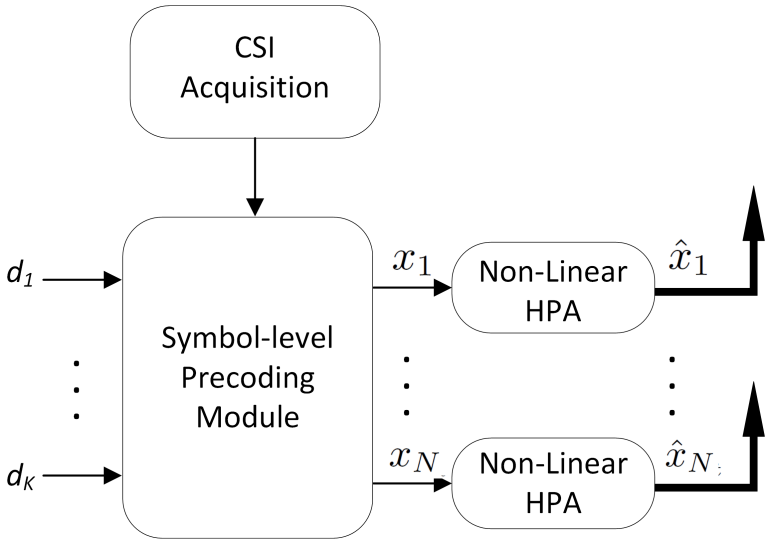

FIGURE 2.6: Block scheme of the transmitter relying on SLP, for a generic symbol slot.

where ρ_i and θ_i are the amplitude and the phase of x_i, respectively. Then, the output signal of the HPA can be written as:

$$\hat{x}_i = f_A(\rho_i)\exp(\iota f_P(\rho_i))\exp(\iota\theta_i), \tag{2.15}$$

with $f_A(\cdot)$ and $f_P(\cdot)$ denoting the AM-AM and the AM-PM conversions, respectively. The resulting system model is shown in Fig. 2.6. A practical example of non-linear HPA is given in Fig. 2.7, where the (normalized) AM-AM and AM-PM characteristics of the non-linearized TWTA model of [130] are represented. Such characteristics clearly show the saturation effect and the introduced phase distortion, respectively. The model of Fig. 2.7 will be used as a practical reference in this thesis, in particular for the numerical results, as it constitutes a highly non-linear model (especially with respect to the AM-PM curve) allowing a proper validation of the proposed SLP schemes. However, it should be stressed that all schemes for non-linear channels proposed in this thesis are applicable to any non-linear AM-AM/AM-PM characteristic, modeled in the form of (2.15).

The importance of taking into account the non-linear effects of the amplification stages in the precoding design lies in the two following considerations.

- In some applications, such as satellite communications [127, 128], the power is a scarce resource that has to be efficiently exploited. As a consequence, the HPAs need to be operated as close as possible to their saturation point, and the consequent AM-AM distortion cannot be neglected.

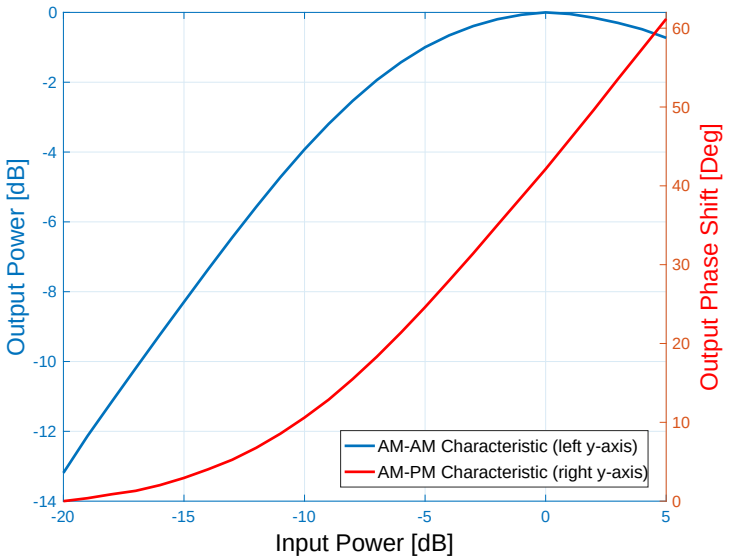

FIGURE 2.7: An example of non-linear amplifier: normalized AM-AM and AM-PM characteristics of the non-linearized TWTA of DVB-S2 standard.

- In other applications the power scarcity is not a crucial issue, therefore stretching the operating region of the HPAs close to saturation is not necessitated. However, there might be the need to employ cheap hardware components for the RF chains, and specifically cheap amplifiers showing more severe non-idealities. This is for example the case of massive-MIMO [134].

In this framework, it is important to control the instantaneous transmitted power and to minimize its peaks, in order to mitigate the performance degradation due to the AM-AM distortion. Furthermore, the use of separate per-antenna HPAs comes with an additional impairment. In fact, as clear from the phase characteristic of the example in Fig. 2.7, the per-antenna amplifiers introduce a phase shift which is considerably different for different instantaneous powers feeding the HPAs. As a consequence, the precoded data streams transmitted on the separate RF chains will experience a different phase shift through the amplification stages, due to the variable power carried out by the symbols. This specific issue, which will be referred to as *differential phase shift*, has not been considered in previous literature, and constitutes an additional source of degradation of the overall system performance.

The SLP strategy, which designs the transmitted signals on a symbol-by-symbol basis, has the potential to control the instantaneous transmit power and in particular to improve the power dynamics accounting for the aforementioned effects. It should be mentioned that this is not possible in the conventional channel-level approach, where the precoder is designed for an entire codeword, including several symbols, hence the

transmitted power can be controlled only in average and not symbol by symbol. Accordingly, this thesis proposes novel SLP schemes coping with the problems of saturation and differential phase shift, arising when non-linear HPAs are used. The main aim is to reduce the power peaks of the transmitted waveforms, firstly accounting only for the spatial dimension (i.e., for the power distribution among the different antennas), and then considering also the waveforms in the temporal dimension. It should be also remarked that a number of works available in the literature have proposed precoding techniques suitable for non-linear channels, especially in the context of massive MIMO systems [29–31]. In particular, these works aim at reducing the peak-to-average power ratio (PAPR) of the transmitted waveforms, or even at designing constant-envelope signals. A fundamental novelty of this thesis with respect to [29–31] lies in the fact that the proposed techniques are able to leverage the constructive interference effect, while at the same time addressing the problem of non-linearities. As a consequence, the exploitation of the MUI as a beneficial factor constitutes an inherent advantage of the proposed schemes. A SLP approach achieving constructive interference and accounting for non-linear channels has also been proposed in [112]. However, the scheme therein proposed aims to a constant envelope precoding design for PSK modulations, thus having a fixed power for each symbol slot and for every antenna. On the other hand, the techniques proposed in this thesis do not perform constant envelope precoding, but they optimize the power dynamics accounting for QoS constraints for the users, following an optimization framework in line with [22, 23] and also accounting for multi-level modulation schemes. Furthermore, in the second part of the thesis, where the temporal dimension is addressed, the waveforms are modeled accounting for oversampling and not only for the symbol-by-symbol power.

2.4 Faster-than-Nyquist Signaling

As mentioned in chapter 1, this thesis is not solely focused on developing SLP schemes for non-linear channels, but also proposes, in its second part, a novel SLP method which enables FTN signaling over multi-user MISO systems. Herein, an overview on FTN signaling and on the related studies is provided, highlighting the novelty of this thesis with repect to them.

FTN signaling is a signal processing strategy which has been studied, in parallel to the full frequency reuse architectures, in order to increase the spectral efficiency of wireless communications [135–141]. The key idea of FTN signaling is a reduction of the time spacing between two adjacent pulses (the symbol period) below the one satisfying the Nyquist condition. In other words, in FTN signaling the data rate is increased

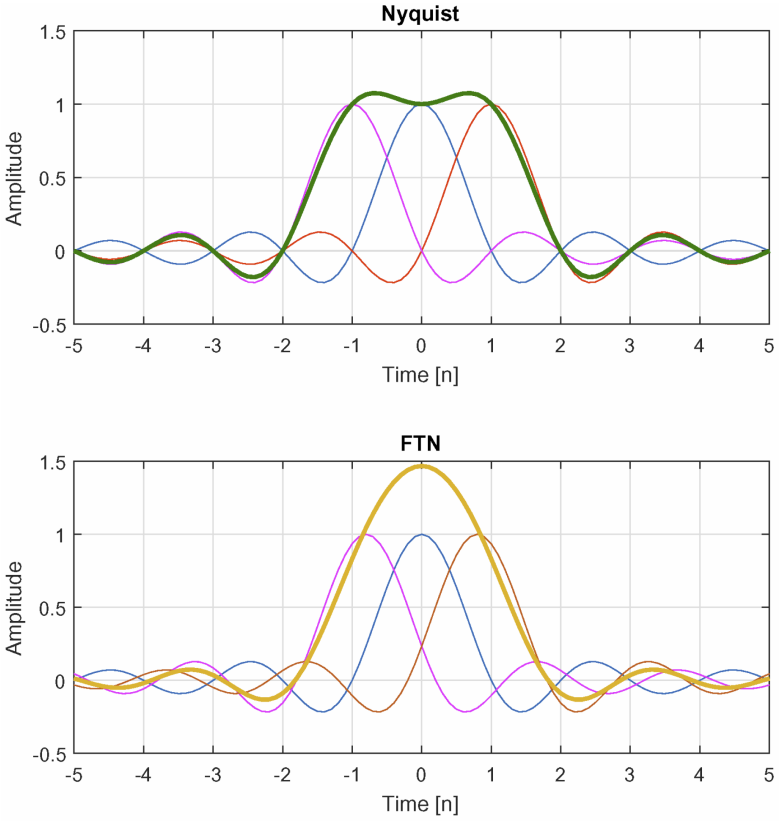

FIGURE 2.8: Nyquist vs. Faster-than-Nyquist for a sinc pulse, in the time domain.

by accelerating the transmitted pulses in the temporal dimension (time packing), thus introducing controlled inter-symbol interference (ISI) which needs to be handled. This is graphically shown in Fig. 2.8 for the case of a sinc pulse, where it can be seen how in the FTN case the subsequent pulses are not orthogonal, and therefore the increased data rate comes with ISI that has to be tackled.

The FTN concept was firstly introduced in the mid 70s by Mazo in [135], where it was shown that, given a fixed bandwidth, it is possible to accelerate binary sinc pulses up to a factor of 0.802 with respect to the Nyquist[3] limit without damaging the error rate. Although this result was initially received with skepticism and was not developed for many years, the interest in FTN has grown in the last decade. In [136] it was shown that the FTN concept applies also with squared root raised cosine (SRRC) pulses, which allow a higher acceleration thanks to their excess bandwidth. In [137] the achievable rate regions for FTN broadcast were investigated, considering SRRC pulses. Further, FTN has also been extended in the frequency domain, by squeezing the signals together in frequency just as they were accelerated in time [138]. The FTN principle has also been applied jointly in two dimensions, time and frequency, for multi-carrier systems

[3]This means considering a symbol period equal to 0.802 times the one allowed by the Nyquist condition.

[139, 140], showing improved achievable rate performance. A review of the work on FTN signaling can be found in [141]. The main problem of FTN signaling is the need to cope with the introduced ISI, which in turn results in complex receivers relying on trellis decoders as well as ad hoc equalization schemes, which are often prohibitive in practical applications.

In this thesis, a novel transmission method is proposed which allows to merge the aggressive frequency reuse relying on precoding and the FTN signaling. Considering a generic multi-user MISO system, the main idea is to extend the concept of symbol-level precoding in order to tackle at the transmitter side not only the interference in the spatial dimension (the MUI), but also the interference in the temporal dimension (the ISI), using the pulse shaping filters as additional side information. The novelty with respect to the state of the art in FTN signaling is, on one hand, the application of FTN in a multi-user MISO framework and, on the other hand, the ability to completely handle the ISI at the transmitter side, which solve the problem of having highly complex receivers for FTN. Furthermore, it is important to highlight that this approach allows to exploit in a constructive fashion the interference both in the temporal and in the spatial dimensions, thus gleaning benefits from both the domains.

2.5 Main Assumptions in the Thesis

The main assumptions considered in this thesis are the following:

- Unicast transmissions are considered, i.e., each data stream is destined to a single user. As mentioned, the extension to SLP to multicast scenarios is not straightforward and has not been addressed in the literature so far.
- Perfect knowledge of the CSI is assumed in the formulation of the proposed techniques, thus the robustness to channel errors is out of the scope of this thesis. Nonetheless, when specified so, channel uncertainties are considered in the numerical results.
- Only quasi-static flat fading channels are considered, in a single-carrier scenario. The extension to frequency selective channels, which comes with the need to tackle the related ISI, is part of the future work. Concerning the channel model, the presented SLP schemes apply to any full-rank channel matrix. For numerical results, the main considered channel model is a Rayleigh fading channel, but also satellite channel models are considered (the simulated channel model is always specified throughout the thesis).

- Single-antenna users are considered. Moreover, the problem of optimal user scheduling is not addressed, as the main focus is on optimizing the transmitted waveforms accounting for QoS constraints.
- The design of the proposed SLP schemes does not take into account the application of forward error correction (FEC) schemes. However, when specified so, FEC has been considered for the numerical results.
- The proposed approaches consider different modulation schemes for the data information, however no adaptive coding and modulation (ACM) scheme is considered.
- The considered models for non-linear HPAs are memoryless. Moreover, the inter-symbol interference created by the non-linear amplification stages is not modeled in the proposed optimization schemes (although accounted for in the numerical evaluation).
- A fully digital architecture is assumed, as the focus is on the design of the transmitted baseband waveforms.

2.6 Thesis Contributions

The main contributions of this thesis are discussed hereafter, for each of the presented chapters.

2.6.1 Chapter 3: Symbol-level Precoding for Per-antenna Power Limited Systems

In this chapter, novel SLP schemes are proposed in order to account for the per-antenna power limitations of multi-user MISO systems, while constructively exploiting the interference. In fact, a common practice in multi-antenna systems is the use of separate per-antenna amplifiers, thus considering the power constraints individually for each transmitting antenna is particularly important. First, the problem of per-antenna power minimization in SLP is formulated and solved, under QoS constraints given in the form of per-user target SINR. Then, the SLP max-min fair problem under per-antenna power constraints is formulated and tackled through a bisection procedure over the previous power minimization problem. This precoding design optimizes the system performance at the receiver side in terms of SINR, whilst guaranteeing the system fairness and allowing a control over the power transmitted by each antenna. Besides accounting for individual per-antenna power limitations, the proposed schemes allow a reduction of the power peaks in the spatial dimension. Numerical results are presented to show the

effectiveness of the proposed schemes, which outperform the existing state of the art techniques in terms of reduction of the power peaks and of the PAPR across the transmitting antennas. The contributions of this chapter have been published in [129, 142, 143].

2.6.2 Chapter 4: Symbol-level Precoding for the Non-linear multi-user MISO Downlink Channel

This chapter presents more advanced SLP strategies, which exploit the potential of SLP not only to achieve constructive interference but also to control the per-antenna instantaneous transmit power. In particular, the power peaks amongst the transmitting antennas and the instantaneous power imbalances across the different transmitted streams are minimized. These objectives are particularly relevant with respect to the non-linear amplitude and phase distortions induced by the per-antenna amplifiers, which are important sources of performance degradation in practical systems. More specifically, this work proposes two different SLP approaches. The first approach performs a weighted per-antenna power minimization, under QoS constraints and under a lower bound constraint on the per-antenna transmit power. The related optimization problem is solved through an iterative procedure relying on SCA. The second strategy performs a minimization of the spatial PAPR, evaluated amongst the transmitting antennas, under QoS constraints. The related optimization problem is tackled by resorting jointly to parametric programming and SCA. Numerical results are presented in a comparative fashion to show the effectiveness of the proposed techniques, which outperform the state of the art SLP schemes in terms of spatial PAPR and spatial dynamic range. Moreover, a simulation accounting for the oversampled transmitted waveform and for a non-linear HPA model is considered, in order to assess the enhanced robustness of the introduced schemes to non-linear effects, based on SER results. The contributions of this chapter have been published in [144, 145].

2.6.3 Chapter 5: PAPR Minimization through Spatio-temporal Symbol-level Precoding

In this chapter, a novel precoding method is proposed, referred to as spatio-temporal SLP, which allows to optimize the transmitted waveforms not only in the spatial dimension but also in the temporal dimension, accounting for the pulse shaping at each antenna. In particular, this new strategy is used for minimizing the PAPR of the transmitted waveform both in space and time, while at the same time exploiting the constructive interference effect. The related optimization problem can be formulated similarly to the spatial PAPR minimization of chapter 4, therefore it is addressed resorting once more

to parametric programming and SCA. By accounting also for the temporal dimension of the waveforms, the spatio-temporal SLP strategy further improves the robustness of the signals to non-linear channels with respect to the previous methods. Numerical results are presented to highlight the enhanced performance in terms of power distribution and SER over non-linear channels. The contributions of this chapter have been published in [146].

2.6.4 Chapter 6: Faster-than-Nyquist Signaling through Spatio-temporal Symbol-level Precoding

In this chapter, the concept of spatio-temporal SLP is applied in order to go beyond the classical precoding paradigm aimed at handling the MUI. In particular, spatio-temporal SLP is used to enable FTN signaling over multi-user MISO systems, by constructively exploiting the interference both in the spatial dimension (MUI) and in the temporal dimension (ISI). By merging aggressive frequency reuse relying on precoding and FTN signaling, the proposed method enhances the rate performance without imposing additional complexity at the user terminals. Two different optimization strategies are considered: a first approach splits the data streams in blocks of symbols and tackles the interference (MUI and ISI) within each block; a second approach performs a sequential optimization and handles also the inter-block interference. Numerical results are presented in a comparative fashion to show the effectiveness of the proposed techniques, which outperform the state of the art symbol-level precoding schemes in terms of SER, effective rate, and energy efficiency. The contributions of this chapter have been published in [147, 148].

Part I

Space-only Symbol-level Precoding

Chapter 3

Symbol-level Precoding for Per-antenna Power Limited Systems

In this chapter, novel symbol-level precoding (SLP) schemes are proposed in order to account for the per-antenna power limitations of practical multi-user multiple-input single-output (MISO) systems, while constructively exploiting the interference. As previously discussed, the motivation for such schemes is twofold. A first consideration, valid for any precoding technique, is that in many cases there is a lack of flexibility in sharing the energy resources amongst the multiple transmitting antennas, since it is common to have individual per-antenna amplifiers. This justifies the need to consider power limitations independently for each transmitter. In addition to this, the instantaneous variation of the per-antenna transmit power need to be controlled in order to limit the performance degradation due to non-linear high-power amplifiers (HPAs). In this regard, the proposed schemes allow a reduction of the power peaks in the spatial dimension, i.e., amongst the different antennas, for each symbol slot. More specifically, the contributions of this chapter can be summarized as follows:

- The problem of SLP for per-antenna power minimization is formulated and solved for phase shift keying (PSK) modulations, under Quality-of-Service (QoS) constraints in the form of per-user target signal-to-interference-plus-noise ratio (SINR). The problem is tackled by reformulating it as a second-order cone program (SOCP).
- The SLP max-min fair problem, under per-antenna power constraints, is formulated for PSK modulations, and solved through a bisection procedure over the previous power minimization problem. This scheme is discussed in the context

of a multi-beam satellite scenario. Nonetheless, it can be applied to any general channel model.

3.1 Symbol-level Precoding for Per-antenna Power Minimization

This section focuses on the SLP per-antenna power minimization scheme.

3.1.1 System and Signals Model

Let us consider a single-cell multiple-antenna downlink scenario, where a single base station is equipped with N transmit antennas that serve K user terminals, with $K \leq N$, each one equipped with a single receiving antenna. The adopted modulation is PSK, and a block fading channel $\boldsymbol{h}_j \in \mathbb{C}^{1\times N}$ is assumed between the transmit base station antennas and the j-th user. The received signal at the j-th user in the symbol slot n can be written as:

$$y_j[n] = \boldsymbol{h}_j \boldsymbol{x}[n] + z_j[n], \tag{3.1}$$

where $\boldsymbol{x}[n] \in \mathbb{C}^{N\times 1}$ represents the transmitted signal vector from the N transmit antennas, and $z_j[n]$ is a complex circular symmetric random variable, modeling the zero mean additive white Gaussian noise (AWGN) measured at the j-th user's receiving antenna. Without loss of generality, the noise variance is assumed to be 1.

By collecting the received signals by all the users in a vector $\boldsymbol{y}[n] \in \mathbb{C}^{K\times 1}$, the above model can be rewritten in a compact form as:

$$\boldsymbol{y}[n] = \boldsymbol{H}\boldsymbol{x}[n] + \boldsymbol{z}[n], \tag{3.2}$$

where $\boldsymbol{H} = [\boldsymbol{h}_1^T \dots \boldsymbol{h}_K^T]^T \in \mathbb{C}^{K\times N}$ represents the system channel matrix, and $\boldsymbol{z}[n] \in \mathbb{C}^{K\times 1}$ collects the AWGN components for all the users.

According to the SLP approach [22], the transmitted signal vector $\boldsymbol{x}[n]$ is obtained as output of a precoding module, which directly designs $\boldsymbol{x}[n]$ using the channel state information (CSI), which is an estimate of $\boldsymbol{H}$, and the input data symbols $\boldsymbol{d}[n] \in \mathbb{C}^{K\times 1}$, namely the data information that the base station wants to convey to the users. The data symbols, drawn from a PSK constellation, are assumed to be uncorrelated and having unit power.

3.1.2 SLP for Peak Power Minimization (PPM)

Following the definition of constructive interference provided in [22], the objective is to design the transmitted vector $\boldsymbol{x}$ (to ease the notation, hereafter the time index n is omitted), based on the CSI and the data information, assuring that the received signal lies in the detection region of the desired symbol, for each user. In other words, the interfering signals should be forced to constructively contribute to the useful received power. Moreover, unlike [22], where the total transmit power is minimized, here the aim is to minimize the per-antenna transmit power. To this end, the proposed approach is to minimize the maximum power among the different transmitters. Such minimization can be seen as the minimization of the peak power between the antennas, thus the proposed scheme is referred to as SLP for peak power minimization (PPM). The resulting optimization problem can be written as:

$$\begin{aligned} \boldsymbol{x}(\boldsymbol{d},\boldsymbol{H},\boldsymbol{\gamma}) = \arg\min_{\boldsymbol{x}} \max_{i=1,\dots,N} \quad & \{|x_i|^2\} \\ \text{s.t.} \quad \mathcal{C}1: \quad & |\boldsymbol{h}_j\boldsymbol{x}|^2 \geq \gamma_j,\ j=1,\dots,K, \\ \mathcal{C}2: \quad & \angle \boldsymbol{h}_j\boldsymbol{x} = \angle d_j,\ j=1,\dots,K, \end{aligned} \tag{3.3}$$

where γ_j is the target SINR that should be granted for the j-th user, and $\boldsymbol{\gamma} = [\gamma_1 \dots \gamma_K]^T \in \mathbb{C}^{K\times 1}$ contains the target SINR for all the users. The set of constraints $\mathcal{C}1$ is a QoS constraint for each user. The set of constraints $\mathcal{C}2$ represents the constructive interference condition, guaranteeing that each user receives the desired data symbol.

Following the method of [126], the following steps are carried out in order to write the problem (3.3) in a more tractable form. The equality constraint in (3.3) can be rewritten, by applying the tangent operator[1], as:

$$\frac{\mathrm{Im}(\boldsymbol{h}_j\boldsymbol{x})}{\mathrm{Re}(\boldsymbol{h}_j\boldsymbol{x})} = \alpha_j,\ j=1,\dots,K, \tag{3.4}$$

where $\alpha_j = \tan(\angle d_j)$. However, since the tangent is not a one-to-one function, the following conditions should be added, in order to ensure that the received symbol and the intended one lie in the same quadrant:

$$\begin{aligned} \mathrm{Re}(d_j)\,\mathrm{Re}(\boldsymbol{h}_j\boldsymbol{x}) \geq 0,\ j=1,\dots,K, \\ \mathrm{Im}(d_j)\,\mathrm{Im}(\boldsymbol{h}_j\boldsymbol{x}) \geq 0,\ j=1,\dots,K. \end{aligned} \tag{3.5}$$

[1]This does not apply for data symbols laying on the imaginary axis, since the tangent is not defined in such case. Although this case can be easily handled, it is not considered herein, since a phase offset preventing this situation can be always assumed.

Concerning the inequality constraint in the problem (3.3), it can be rewritten referring to the amplitude levels of the in-phase and quadrature components of the corresponding symbols, as follows:

$$\begin{aligned} |\operatorname{Re}(\boldsymbol{h}_j\boldsymbol{x})| &\geq \sqrt{\gamma_j}|\operatorname{Re}(d_j)|,\ j=1,\dots,K, \\ |\operatorname{Im}(\boldsymbol{h}_j\boldsymbol{x})| &\geq \sqrt{\gamma_j}|\operatorname{Im}(d_j)|,\ j=1,\dots,K, \end{aligned} \tag{3.6}$$

where the absolute value is necessary for accounting negative components. By multiplying both the members of the above equations by $\operatorname{Re}(d_j)$ and $\operatorname{Im}(d_j)$ respectively, and by taking into account the conditions in (3.5), the above constraints become:

$$\begin{aligned} \operatorname{Re}(d_j)\operatorname{Re}(\boldsymbol{h}_j\boldsymbol{x}) &\geq \sqrt{\gamma_j}\operatorname{Re}^2(d_j),\ j=1,\dots,K, \\ \operatorname{Im}(d_j)\operatorname{Im}(\boldsymbol{h}_j\boldsymbol{x}) &\geq \sqrt{\gamma_j}\operatorname{Im}^2(d_j),\ j=1,\dots,K. \end{aligned} \tag{3.7}$$

Modeling the constraints as shown in (3.4) and (3.7), and resorting to the concept of l_∞ norm, the PPM problem can be rewritten as:

$$\begin{aligned} \boldsymbol{x}(\boldsymbol{d},\boldsymbol{H},\boldsymbol{\gamma}) = \ & \arg\min_{\boldsymbol{x}} \quad ||\boldsymbol{x}||_\infty \\ \text{s.t.} \quad \mathcal{C}1: \quad & \operatorname{Re}(d_j)\operatorname{Re}(\boldsymbol{h}_j\boldsymbol{x}) \geq \sqrt{\gamma_j}\operatorname{Re}^2(d_j),\ j=1,\dots,K, \\ \mathcal{C}2: \quad & \operatorname{Im}(d_j)\operatorname{Im}(\boldsymbol{h}_j\boldsymbol{x}) \geq \sqrt{\gamma_j}\operatorname{Im}^2(d_j),\ j=1,\dots,K, \\ \mathcal{C}3: \quad & \frac{\operatorname{Im}(\boldsymbol{h}_j\boldsymbol{x})}{\operatorname{Re}(\boldsymbol{h}_j\boldsymbol{x})} = \alpha_j,\ j=1,\dots,K. \end{aligned} \tag{3.8}$$

Ultimately, the problem can be rewritten in a more compact form as:

$$\begin{aligned} \boldsymbol{x}(\boldsymbol{d},\boldsymbol{H},\boldsymbol{\gamma}) = & \arg\min_{\boldsymbol{x}} \quad ||\boldsymbol{x}||_\infty \\ \text{s.t.} \quad \mathcal{C}1: \quad & \operatorname{Re}(\boldsymbol{D})\operatorname{Re}(\boldsymbol{H}\boldsymbol{x}) \geq \boldsymbol{\beta_r} \\ \mathcal{C}2: \quad & \operatorname{Im}(\boldsymbol{D})\operatorname{Im}(\boldsymbol{H}\boldsymbol{x}) \geq \boldsymbol{\beta_i} \\ \mathcal{C}3: \quad & \boldsymbol{A}\operatorname{Re}(\boldsymbol{H}\boldsymbol{x}) - \operatorname{Im}(\boldsymbol{H}\boldsymbol{x}) = \boldsymbol{0}, \end{aligned} \tag{3.9}$$

where $\boldsymbol{D} = \operatorname{diag}(\boldsymbol{d})$, $\boldsymbol{A} = \operatorname{diag}(\alpha_1,\dots,\alpha_K)$, $\boldsymbol{\beta_r} = \sqrt{\boldsymbol{\gamma}} \circ \operatorname{Re}(\boldsymbol{d})^{\circ 2}$, $\boldsymbol{\beta_i} = \sqrt{\boldsymbol{\gamma}} \circ \operatorname{Im}(\boldsymbol{d})^{\circ 2}$.

A way to tackle the problem (3.9) is to write it as a SOCP [149] in the stacked variable $\tilde{\boldsymbol{x}} = [\operatorname{Re}(\boldsymbol{x})^T, \operatorname{Im}(\boldsymbol{x})^T]^T \in \mathbb{R}^{2N\times 1}$. To this end, the objective function, as well as the constraints, should be written in terms of $\tilde{\boldsymbol{x}}$.

Concerning the objective function, it is not difficult to see that:

$$||\boldsymbol{x}||_\infty = \max_{i=1,\dots,N}\{|x_i|\} = \max_{i=1,\dots,N}||\boldsymbol{B}_i\tilde{\boldsymbol{x}}||, \tag{3.10}$$

where $\boldsymbol{B}_i \in \mathbb{R}^{2\times 2N}$ is a matrix used for selecting $\mathrm{Re}(x_i)$ and $\mathrm{Im}(x_i)$ in the stacked vector $\tilde{\boldsymbol{x}}$ and, $\forall i = 1,\ldots,N$, is defined as:

$$\begin{bmatrix} \boldsymbol{e}_i & \boldsymbol{0}_N \\ \boldsymbol{0}_N & \boldsymbol{e}_i \end{bmatrix}, \tag{3.11}$$

with $\boldsymbol{e}_i$ being a the i-th row of an identity matrix with size N, and $\boldsymbol{0}_N$ being the all zero entries vector in $\mathbb{R}^{1\times N}$.

For writing also the constraints of (3.9) in terms of $\tilde{\boldsymbol{x}}$, it is convenient to split the vector $\boldsymbol{Hx}$ into its real and imaginary parts:

$$\begin{aligned} \boldsymbol{Hx} = &\,\mathrm{Re}(\boldsymbol{H})\,\mathrm{Re}(\boldsymbol{x}) - \mathrm{Im}(\boldsymbol{H})\,\mathrm{Im}(\boldsymbol{x}) + \\ &+ \iota[\mathrm{Re}(\boldsymbol{H})\,\mathrm{Im}(\boldsymbol{x}) + \mathrm{Im}(\boldsymbol{H})\,\mathrm{Re}(\boldsymbol{x})], \end{aligned} \tag{3.12}$$

which leads straightforwardly to:

$$\mathrm{Re}(\boldsymbol{Hx}) = \boldsymbol{H_1}\tilde{\boldsymbol{x}}, \quad \mathrm{Im}(\boldsymbol{Hx}) = \boldsymbol{H_2}\tilde{\boldsymbol{x}}, \tag{3.13}$$

where $\boldsymbol{H_1} = [\mathrm{Re}(\boldsymbol{H}), -\mathrm{Im}(\boldsymbol{H})]$, $\boldsymbol{H_2} = [\mathrm{Im}(\boldsymbol{H}), \mathrm{Re}(\boldsymbol{H})]$. Hence, the optimization problem (3.9) becomes:

$$\begin{aligned} \tilde{\boldsymbol{x}}(\boldsymbol{d},\boldsymbol{H},\boldsymbol{\gamma}) = \arg\min_{\tilde{\boldsymbol{x}}} \max_{i=1,\ldots,N} \quad & ||\boldsymbol{B}_i\tilde{\boldsymbol{x}}|| \\ \text{s.t.} \quad \mathcal{C}1: \quad & \mathrm{Re}(\boldsymbol{D})\boldsymbol{H_1}\tilde{\boldsymbol{x}} \geq \boldsymbol{\beta_r}, \\ \mathcal{C}2: \quad & \mathrm{Im}(\boldsymbol{D})\boldsymbol{H_2}\tilde{\boldsymbol{x}} \geq \boldsymbol{\beta_i}, \\ \mathcal{C}3: \quad & (\boldsymbol{AH_1} - \boldsymbol{H_2})\tilde{\boldsymbol{x}} = \boldsymbol{0}. \end{aligned} \tag{3.14}$$

Finally, by introducing a slack variable r, the PPM problem can be formulated as a SOCP as follows:

$$\begin{aligned} \tilde{\boldsymbol{x}}(\boldsymbol{d},\boldsymbol{H},\boldsymbol{\gamma}) = \arg\min_{r,\tilde{\boldsymbol{x}}} \quad & r \\ \text{s.t.} \quad \mathcal{C}1: \quad & ||\boldsymbol{B}_i\tilde{\boldsymbol{x}}|| \leq r,\ i = 1,\ldots,N, \\ \mathcal{C}2: \quad & \mathrm{Re}(\boldsymbol{D})\boldsymbol{H_1}\tilde{\boldsymbol{x}} \geq \boldsymbol{\beta_r} \\ \mathcal{C}3: \quad & \mathrm{Im}(\boldsymbol{D})\boldsymbol{H_2}\tilde{\boldsymbol{x}} \geq \boldsymbol{\beta_i} \\ \mathcal{C}4: \quad & (\boldsymbol{AH_1} - \boldsymbol{H_2})\tilde{\boldsymbol{x}} = \boldsymbol{0}. \end{aligned} \tag{3.15}$$

The global optimum of this optimization problem can be obtained using the standard convex optimization tools [149].

3.1.3 Numerical Results

In this section some numerical results are presented, to show the effectiveness of the proposed PPM approach. Before discussing the results, let us define the considered performance metrics. The symbol-level average power transmitted by each antenna is defined as $P_{\text{av}} = \frac{||\boldsymbol{x}||^2}{N}$, whilst the symbol-level peak power among the antennas will be $P_{\text{peak}} = ||\boldsymbol{x}||_\infty^2$. By taking an average of such quantities over a large number of symbol slots, the frame-level average power and peak power are obtained, which are used as performance metric hereafter. Furthermore, the spatial peak-to-average power ratio (SPAPR), intended as the ratio of the introduced power metrics, is also considered to quantify the relative weight of the power peaks.

The numerical results of the proposed scheme are compared with the ones obtained with the approach of [22], which we can refer to as constructive interference for sum power minimization (SPM). The corresponding optimization problem is the following:

$$\begin{aligned} \boldsymbol{x}(\boldsymbol{d}, \boldsymbol{H}, \boldsymbol{\gamma}) = \arg\min_{\boldsymbol{x}} \quad & ||\boldsymbol{x}||^2 \\ \text{s.t.} \quad \mathcal{C}1: \quad & |\boldsymbol{h}_j \boldsymbol{x}|^2 \geq \gamma_j, \ j = 1, \ldots, K, \\ \mathcal{C}2: \quad & \angle \boldsymbol{h}_j \boldsymbol{x} = \angle d_j, \ j = 1, \ldots, K. \end{aligned} \tag{3.16}$$

The presented results in Figs. 3.1-3.4 have been obtained by averaging over 500 frames of $N = 100$ symbol slots each. The quasi-static block fading channel coefficients have been generated, for the generic user j, as $\boldsymbol{h}_j \sim \mathcal{CN}(0, \sigma_h^2 \boldsymbol{I})$, with $\sigma_h^2 = 1$. Each fading block is assumed to correspond to a frame. Moreover, the assumed modulation scheme is quadrature phase shift keying (QPSK). Finally, the number of transmit antennas N is assumed to be equal to the number of users K, and such number will be hereafter referred to as system size.

Fig. 3.1 shows the introduced power metrics, in dBW, as a function of the target SINR, assumed the same for all the users for the sake of simplicity. The system size is fixed to 10. As expected, it can be seen how the required transmit power increases with the target SINR, and how the proposed PPM approach attains better performance in terms of peak power with respect to the SPM approach. This gain on the peak power, close to 1 dB, comes with the sacrifice of a higher average transmit power. As a result, we have a lower SPAPR (3.1 dB) with the proposed PPM approach, with respect to the SPM one (4.7 dB).

Fig. 3.2 shows the transmit power, in dBW, as a function of the system size, for a target SINR fixed to 3 dB. Besides the fact that the PPM approach outperforms the SPM one in terms of peak power, it is worth noticing how the power has a decreasing trend

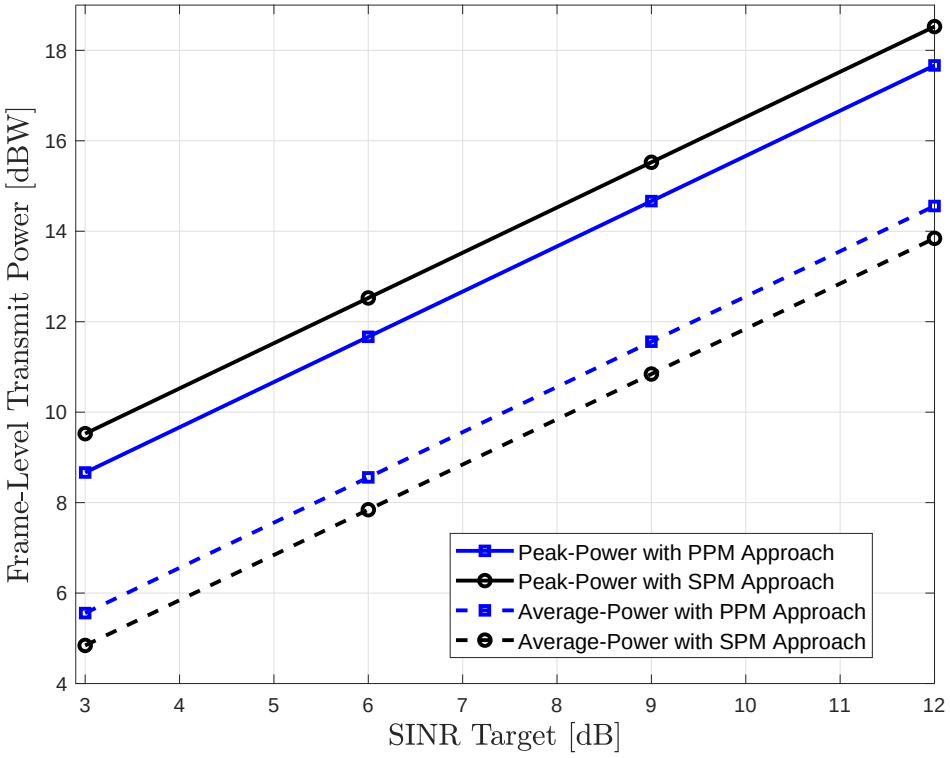

FIGURE 3.1: Frame-level transmit power in dBW vs. SINR target in dB.

with the system size. This can be intuitively explained considering that, for a higher numbers of transmitting antennas, the stronger effect of constructive interference allows to achieve the target SINR with a lower required power. Moreover, it is important to notice how the performance gap between the two compared techniques increases with the system size. This implies that much higher gains can be expected for very high system size value. This is the case of large antenna arrays in massive multiple-input multiple-output (MIMO) [150] and of multi-beam satellite systems [128]. Further insights can be given by the SPAPR curves shown in Fig. 3.3. In fact, with the proposed approach the SPAPR is remarkably lower when the system size increases.

Fig. 3.4 shows the transmit power as a function of the effective user rate, assuming the system size fixed to 10. The effective user rate is clearly related to the target SINR and, for a generic user j, can be defined as:

$$\bar{R}_j = R_j(1 - \text{SER}), \tag{3.19}$$

where R_j denotes the maximum rate, in bits per symbol, supported by the adopted modulation, and SER is the symbol error rate. It can be seen how the maximum

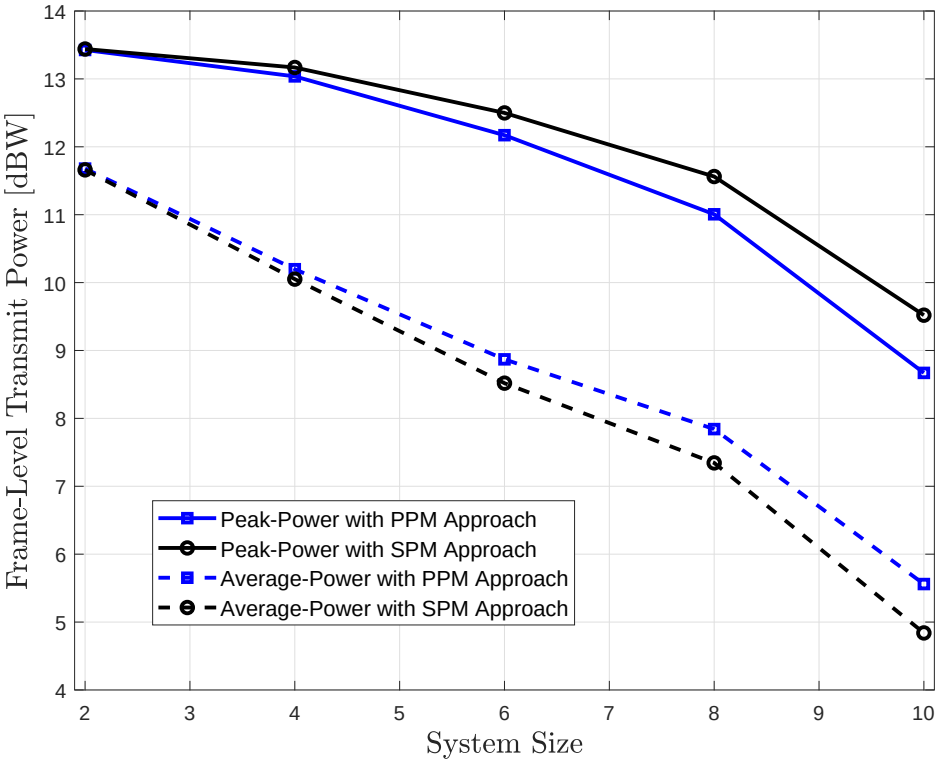

FIGURE 3.2: Frame-level transmit power in dBW vs. system size.

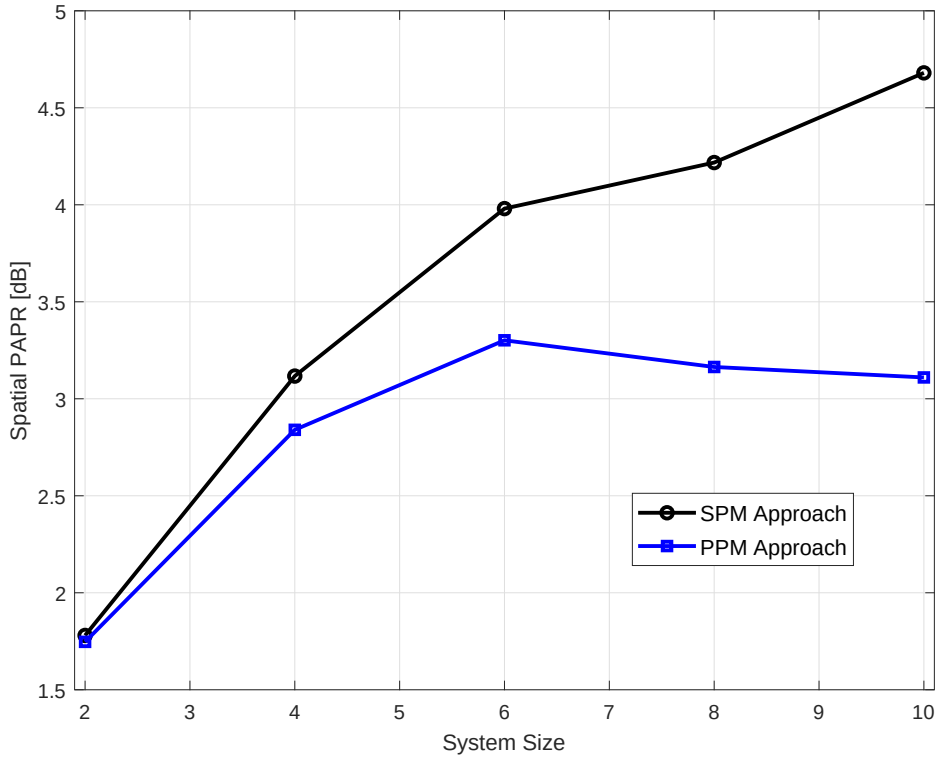

FIGURE 3.3: SPAPR in dB vs. system size.

$$\boldsymbol{H} = \begin{bmatrix} -0.123+0.524\imath & 0.706+0.273\imath & 0.825-0.188\imath & -1.411-0.598\imath & -1.351+0.925\imath \\ -0.792-0.615\imath & 0.210+0.543\imath & 0.607+1.892\imath & -0.258-0.544\imath & -0.735-0.710\imath \\ 0.779-1.338\imath & -0.598+1.069\imath & 0.769+0.947\imath & -0.566-1.004\imath & 0.253+0.512\imath \\ 0.783+0.013\imath & 0.313+0.476\imath & -0.339+0.238\imath & -0.858+1.292\imath & 0.065+0.053\imath \\ -0.347-1.000\imath & 0.697-0.227\imath & -0.183+0.557\imath & 1.331-0.422\imath & -0.145-0.265\imath \end{bmatrix}, \tag{3.17}$$

$$\boldsymbol{d} = [0.707+0.707\imath \quad 0.707+0.707\imath \quad 0.707+0.707\imath \quad -0.707+0.707\imath \quad -0.707-0.707\imath]^T \tag{3.18}$$

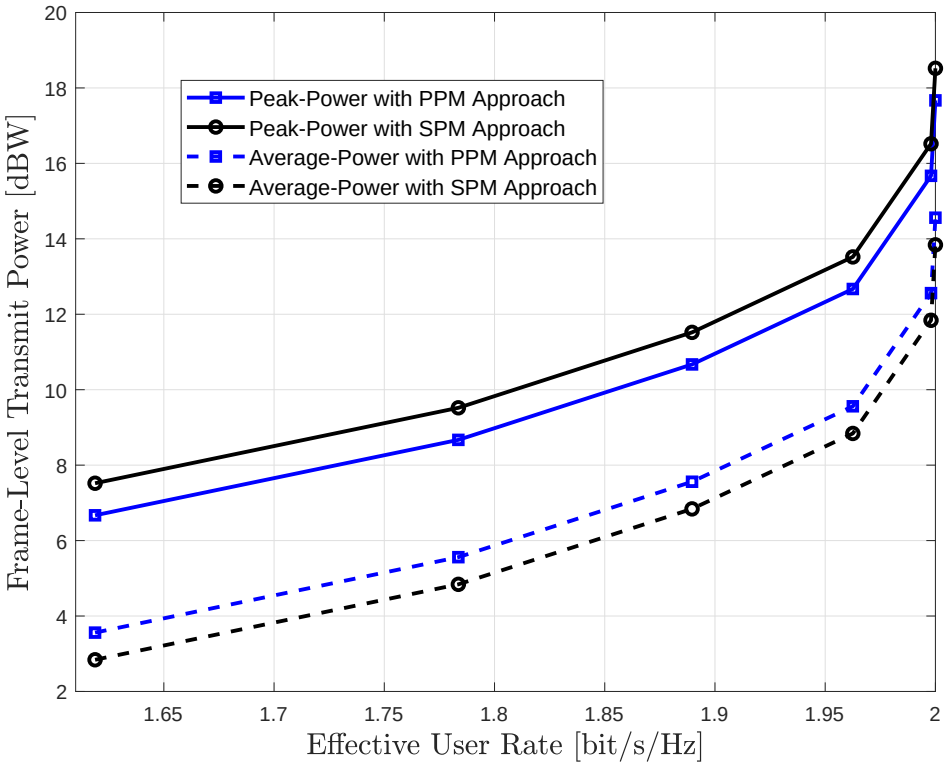

FIGURE 3.4: Frame-level transmit power in dBW vs. effective user rate in bit/s/Hz.

supported user rate of 2 bits/s/Hz is attained with a lower peak power with the proposed approach.

Finally, Fig. 3.5 shows the instantaneous power utilization, in linear scale, for each transmit antenna, with the PPM and the SPM approaches, for a 5×5 system and a target SINR of 3 dB. The channel matrix and the data information vector are fixed to the values reported in (3.17), (3.18). Such representation clearly shows how, sacrificing some average power, the proposed approach leads to a more uniform distribution of the power between the antennas, resulting in a lower peak power.

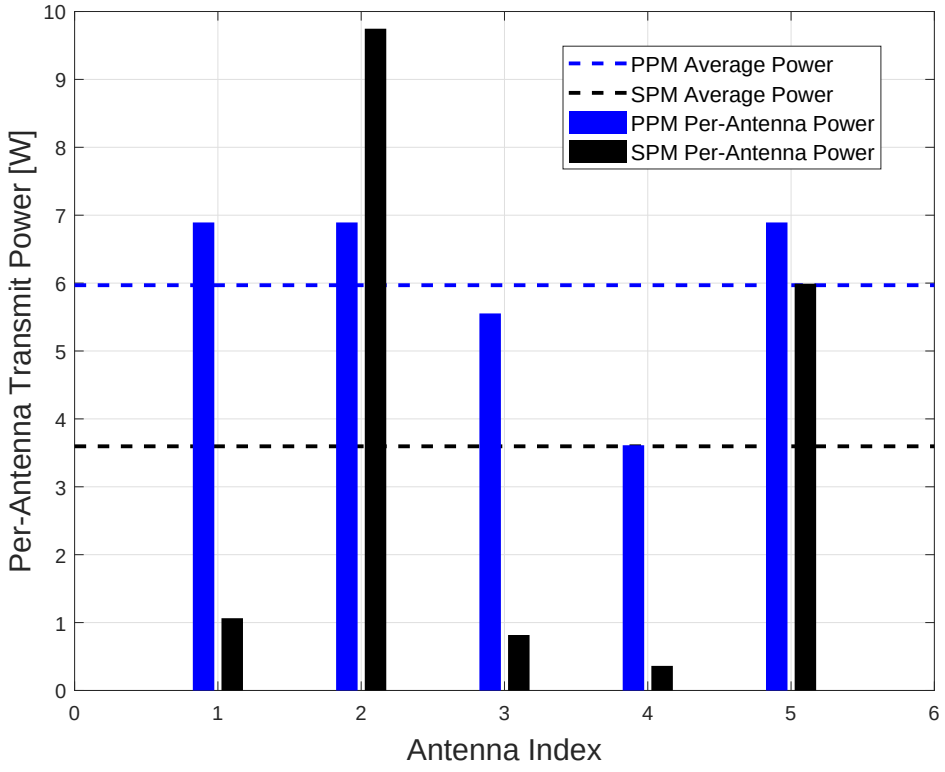

FIGURE 3.5: Per-antenna power utilization in Watts for a 5×5 system.

3.2 Symbol-level Precoding with Per-antenna Power Constraints

In this section the SLP max-min fair problem, under per-antenna power constraints (PACs), is addressed, considering a multi-beam satellite scenario.

3.2.1 System and Signals Model

We focus on a multi-user MISO satellite system. Let N denote the number of transmitting elements of the transmitter and K the number of users, with $K \leq N$, each one equipped with a single receiving antenna. The adopted modulation is PSK, and a channel vector $\boldsymbol{h}_j \in \mathbb{C}^{1\times N}$ is assumed between the transmitting antennas and the j-th user. The received signal at the j-th user in the symbol slot n can be written as:

$$y_j[n] = \boldsymbol{h}_j \boldsymbol{x}[n] + z_j[n], \tag{3.20}$$

where $\boldsymbol{x}[n] \in \mathbb{C}^{N\times 1}$ represents the transmitted signal vector from the N transmit antennas, and $z_j[n]$ is a complex circular symmetric random variable, modeling the zero

mean AWGN measured at the j-th user's receiving antenna. Without loss of generality, the noise variance is assumed to be 1.

By collecting the received signals by all the users in a vector $\boldsymbol{y}[n] \in \mathbb{C}^{K\times 1}$, the above model can be rewritten in a compact form as:

$$\boldsymbol{y}[n] = \boldsymbol{H}\boldsymbol{x}[n] + \boldsymbol{z}[n], \tag{3.21}$$

where $\boldsymbol{H} = [\boldsymbol{h}_1^T \dots \boldsymbol{h}_K^T]^T \in \mathbb{C}^{K\times N}$ represents the system channel matrix, and $\boldsymbol{z}[n] \in \mathbb{C}^{K\times 1}$ collects the AWGN components for all the users.

As regard to the channel model, assuming fixed users with highly directive antennas, we consider real channel gains depending only on the multi-beam antenna pattern and on the users position[2]. Considering the i-th beam and the k-th user, the corresponding entry of the channel matrix $\boldsymbol{H}$ can be calculated resorting to the well accepted method of Bessel functions, thus it will be the square root of the following power gain [151]:

$$g_{ik}(\theta_{ik}) = G_{\max}\left(\frac{J_1(u)}{2u} + 36\frac{J_3(u)}{u^3}\right)^2, \tag{3.22}$$

where θ_{ik} is the off-axis angle of the user with respect to the boresight of the beam, $u = 2.07123 \sin\theta_{ik}/\sin\theta_{3\text{dB}}$, with $\theta_{3\text{dB}}$ being the one-sided half-power angular beamwidth, $G_{\max}$ is the maximum on-axis power gain of the antenna, and J_1, J_3 are the Bessel functions of the first kind, of order one and three respectively.

As discussed in the previous section, SLP directly designs the vector $\boldsymbol{x}[n]$ using the CSI and the input data symbols $\boldsymbol{d}[n] \in \mathbb{C}^{K\times 1}$. The data symbols, drawn from a PSK constellation, are assumed to be uncorrelated and having unit power. It should be noticed that, after the precoding operation, the constellation diagram of the transmitted signals is completely different from the PSK one associated to the original data information, because of the correlation between the multiple data streams induced by the precoding module. To better illustrate this, referring to an example with 7 beams and a 8-PSK modulation for the data information, Figs. 3.6-3.7 show the scatter plot of a large number of symbols associated to one of the transmitting antennas, before and after the application of precoding (the max-min fair symbol-level scheme with sum power constraint - SPC of [22] is used), respectively. The effect of precoding is clearly visible, in particular with respect to the transmitted power, which is far from being constant for the various symbols and actually presents some peaks.

[2]However, the main conclusions of this work are still valid if a random phase is incorporated in the channel model.

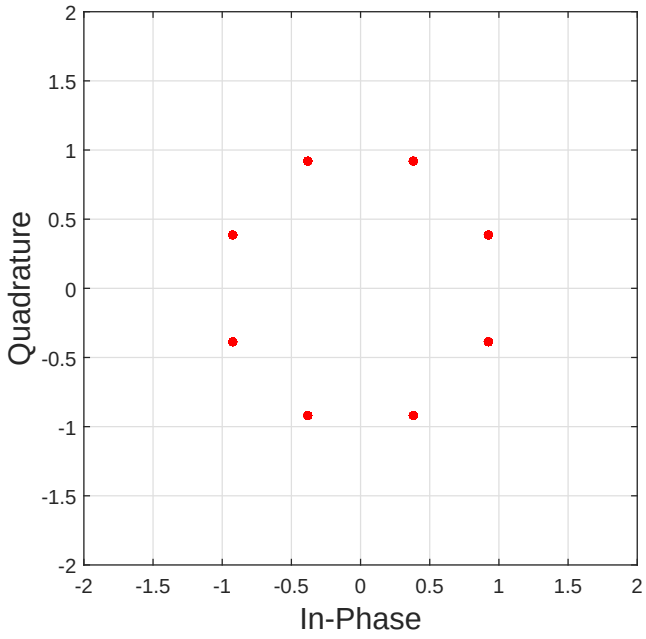

FIGURE 3.6: Scatter plot of the symbols (8-PSK) associated to one antenna, before precoding.

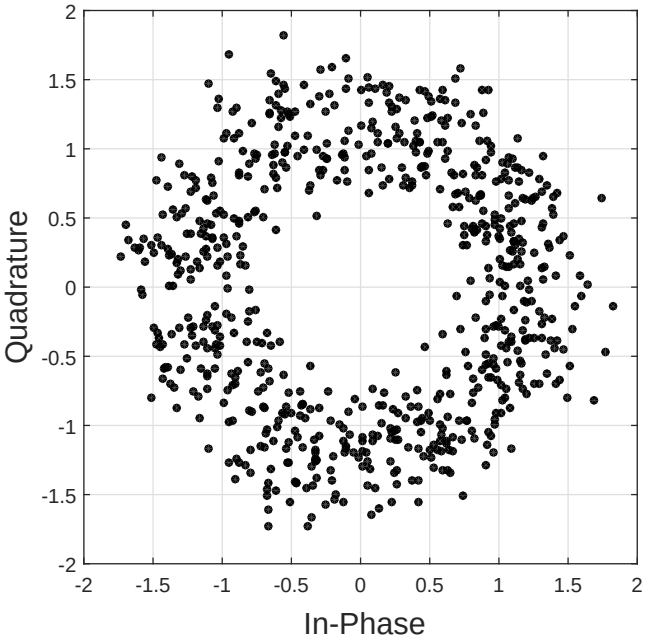

FIGURE 3.7: Scatter plot of the symbols associated to one antenna, after SLP with SPC.

As already mentioned, it should be considered that the system model of (3.21) is actually corrupted by the non-linear effects introduced by the on-board per-antenna traveling-wave tube amplifiers (TWTAs), which affect both the amplitude and the phase of the transmitted waveforms. Different models describing the relationship between the input and the output signals of the on-board amplifiers are provided in [130, 131]. The common non-linearized TWTA model of [130] will be taken as a reference. The related amplitude-to-amplitude (AM-AM) and amplitude-to-phase (AM-PM) characteristics have been shown in Fig. 2.7, where the saturation effect introduced by the amplifier can be noticed. The on-board TWTAs need to be operated as close as possible to saturation, to efficiently exploit the scarce available power. As a consequence, the need of controlling the power level of the transmitted waveforms is pivotal in order to reduce the detrimental effect of the non-linearities of the satellite channel, which is critical in presence of precoding, because of the complex structure of the transmitted constellations. In particular, the transmitted power should be kept below the saturation point of the amplifiers.

3.2.2 SLP for Max-Min Fair with Per-antenna Power Constraints (Max-Min-PAC)

The aim is to design the transmitted vector $\boldsymbol{x}$ (to ease the notation, hereafter the time index n is omitted), based on the CSI and the data information, in order to achieve constructive interference. More specifically, the proposed approach aims to maximize the minimum SINR amongst the users (max-min fair), while satisfying per-antenna constraints for the transmitted power, in addition to the constructive interference condition. The use of PACs is the novel aspect of the work, with respect to the max-min fair problem solved in [22], where the imposed constraints are over the total transmitted power (hence a SPC is considered). The resulting optimization problem, which is referred to as max-min fair with PACs (Max-Min-PAC), is the following:

$$\begin{aligned} \boldsymbol{x}(\boldsymbol{d},\boldsymbol{H}) = \arg\max_{\boldsymbol{x}} \min_{j=1,\dots,K} \quad & |\boldsymbol{h}_j\boldsymbol{x}|^2 \\ \text{s.t.} \quad \mathcal{C}1: \quad & |x_i|^2 \leq P_{\text{Th}},\ i=1,\dots,N, \\ \mathcal{C}2: \quad & \angle \boldsymbol{h}_j\boldsymbol{x} = \angle d_j,\ j=1,\dots,K. \end{aligned} \tag{3.23}$$

The set of constraints $\mathcal{C}1$ represent the PACs, imposing that the power transmitted by each antenna should be not larger than a predefined threshold power P_{Th}. The set of constraints $\mathcal{C}2$ represents the constructive interference condition, guaranteeing that each user receives the desired data symbol.

With respect to the max-min fair problem with SPC of [22] (which hereafter will be referred to as Max-Min-SPC), we can expect worse performance in terms of attained

SINR for a linear system, because of the tighter constraints. However, if the non-linearities of the satellite channel are taken into account, the proposed scheme with PACs can present some advantages. In particular, a wise choice of the value of P_{Th}, in relation to the saturation power of the on-board TWTAs, can guarantee that even the power peaks of the transmitted waveforms (visible in the example of Fig. 3.7) lie in the linear region of the amplifiers. For instance, denoting by P_{Sat} the saturation power of the amplifiers, a possible choice for the PACs could be $P_{\mathrm{Th}}^{\mathrm{dB}} = P_{\mathrm{Sat}}^{\mathrm{dB}} - \Delta^{\mathrm{dB}}$, where the values are in dB and Δ denotes an imposed minimum separation interval.

The problem (3.23) can be solved, in the same fashion of [22], based on a bisection procedure on the solution of the equivalent power minimization problem. The related per-antenna power minimization problem has been addressed in the previous section. It is convenient now to reformulate it as follows:

$$\begin{aligned} \boldsymbol{q}(\boldsymbol{d},\boldsymbol{H},\boldsymbol{\gamma}) = \arg\min_{\boldsymbol{q}} \max_{i=1,\dots,N} \quad & |q_i|^2 \\ \text{s.t.} \quad \mathcal{C}1: \quad & |\boldsymbol{h}_j\boldsymbol{q}|^2 \geq \gamma_j,\ j=1,\dots,K, \\ \mathcal{C}2: \quad & \angle \boldsymbol{h}_j\boldsymbol{q} = \angle d_j,\ j=1,\dots,K, \end{aligned} \tag{3.24}$$

where $\boldsymbol{q}$ denotes the transmitted signal vector[3].

The relation between the power minimization problem and the max-min fair problem at hand is discussed below.

3.2.3 Relation between the Max-Min-PAC and the PPM Problems

The relation between the max-min fair and the power minimization problems can be established, in the same fashion of [22], rewriting the Max-Min-PAC problem (3.23) as follows, where the slack variable t is introduced:

$$\begin{aligned} \boldsymbol{x}(\boldsymbol{d},\boldsymbol{H}) = \arg\max_{t,\boldsymbol{x}} \quad & t \\ \text{s.t.} \quad \mathcal{C}1: \quad & |x_i|^2 \leq P_{\mathrm{Th}},\ i=1,\dots,N, \\ \mathcal{C}2: \quad & \angle \boldsymbol{h}_j\boldsymbol{x} = \angle d_j,\ j=1,\dots,K, \\ \mathcal{C}3: \quad & |\boldsymbol{h}_j\boldsymbol{x}|^2 \geq t,\ j=1,\dots,K. \end{aligned} \tag{3.25}$$

Denoting by t^* the optimal value of t in the problem (3.25), it turns out that the relation between the Max-Min-PAC and the PPM problems can be described as $\boldsymbol{x}(\boldsymbol{d},\boldsymbol{H}) =$

[3] To avoid ambiguity, a different notation is used for the solution to the PPM problem ($\boldsymbol{q}$) and for the solution to the Max-Min-PAC problem ($\boldsymbol{x}$).

$\boldsymbol{q}(\boldsymbol{d}, \boldsymbol{H}, t^*\mathbf{1}_K)$, where $\mathbf{1}_K$ denotes the all one entries vector in $\mathbb{R}^{K\times 1}$. In other words, the max-min fair solution is a scaled version of minimum power solution. This implies that the solution to the Max-Min-PAC problem can be found applying a simple bisection procedure [149] over the solution of the equivalent PPM problem, as in [22].

3.2.4 Numerical Results

In this section some numerical results are presented, in order to validate the proposed Max-Min-PAC approach. For the sake of comparison, we consider also numerical results related to the Max-Min-SPC scheme of [22], whose corresponding optimization problem is the following:

$$\begin{aligned} \boldsymbol{x}(\boldsymbol{d}, \boldsymbol{H}) = \arg\max_{\boldsymbol{x}} \min_{j=1,\dots,K} \quad & |\boldsymbol{h}_j \boldsymbol{x}|^2 \\ \text{s.t.} \quad \mathcal{C}1: \quad & ||\boldsymbol{x}||^2 \leq P_{\text{Tot}}, \\ \mathcal{C}2: \quad & \angle \boldsymbol{h}_j \boldsymbol{x} = \angle d_j, \ j = 1, \dots, K, \end{aligned} \tag{3.26}$$

where P_{Tot} represents the total available power at the transmitter.

The presented results are obtained assuming a 7-beam satellite channel based on the radiation pattern described by (3.22), with a maximum power gain $G_{\max} = 10$ dB. The number of users K is assumed to be equal to the number of transmitting antennas N, and the position of each user is fixed in the center of the respective beam. A picture of the considered beam pattern, together with the users position, is given in Fig. 3.8. The considered modulation is 8-PSK.

In Fig. 3.9 the attained minimum SINR (across the users) is shown as a function of the total available transmit power, for the proposed PAC approach and for the SPC approach. For fair comparison, the total available power is equally distributed amongst the transmit antennas when the PACs are considered, thus the value of P_{Th} is set equal to $\frac{P_{\text{Tot}}}{N}$ (this assumption is kept for all the following comparisons). Moreover, the result is obtained by averaging over a large number of transmitted symbols. It is clearly visible how the attained SINR over a linear channel is lower with the proposed approach, showing a worse performance with respect to the SPC case. This could be expected considering that the use of PACs implies a more restrained exploitation of the available power, with a resulting lower SINR. In this regard, in Fig. 3.10 the instantaneous power utilization for each transmit antenna is shown for the two approaches at hand, for a specific symbol slot. The total available power is fixed to 10 Watts. It is evident how the available power is not fully utilized with the proposed Max-Min-PAC approach, since the PACs are not attained for each transmit antenna.

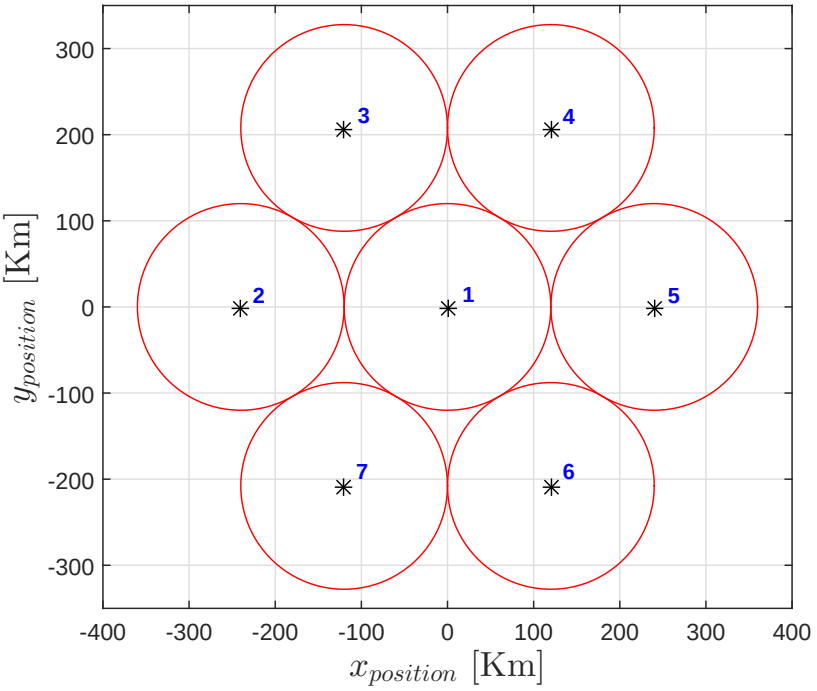

FIGURE 3.8: Beam pattern (circles) considered in the simulations, together with the position of the users (marked with the stars).

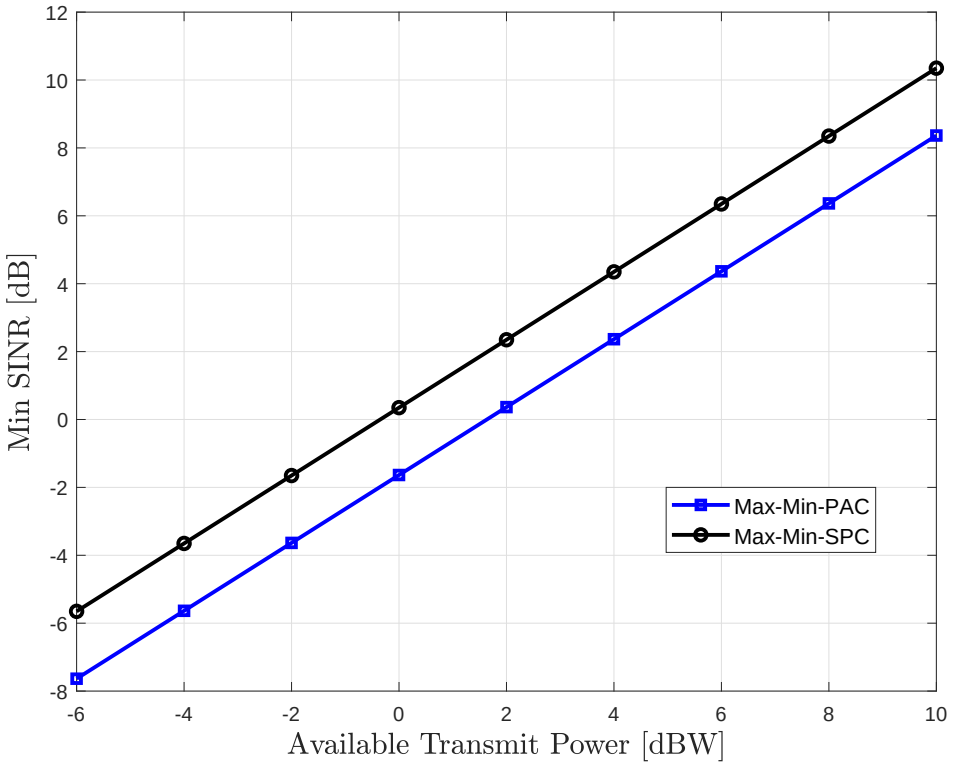

FIGURE 3.9: Minimum SINR amongst the users, in dB, vs. available transmit power, in dBW.

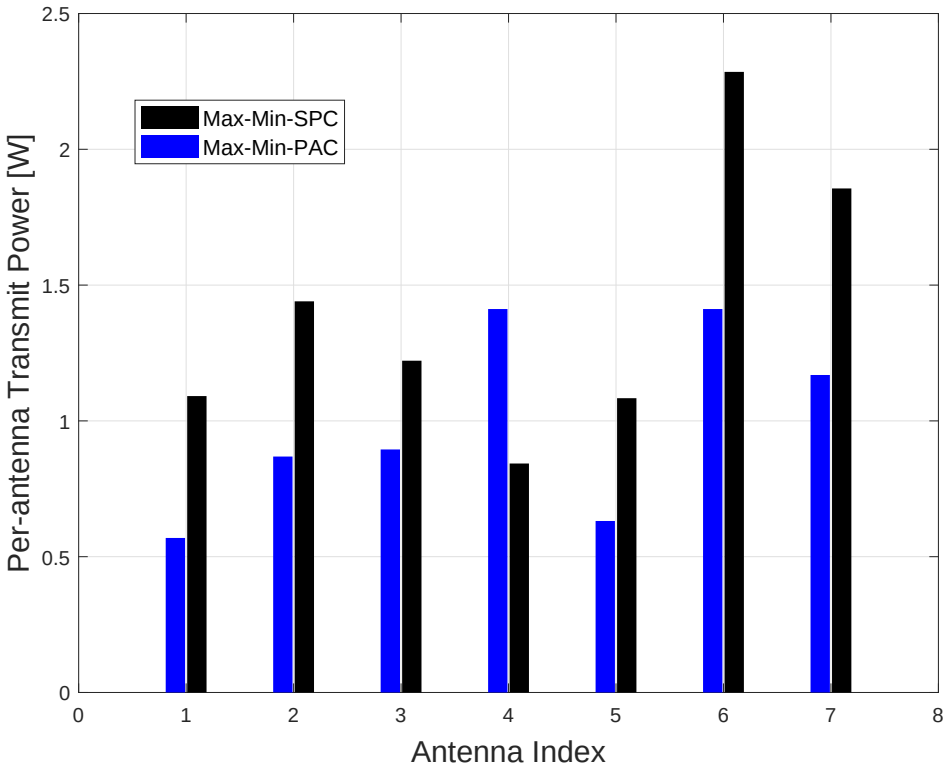

FIGURE 3.10: Per-antenna power utilization in Watts for a specific data information vector.

Although this can be seen as a disadvantage of the proposed technique, it should be highlighted how the PACs are not avoidable in per-antenna power limited systems, where the energy sharing between the different transmission chains is not possible. Furthermore, the advantages of the Max-Min-PAC technique can be noticed focusing on non-linear satellite channels, accounting the non-linear characteristic of the TWTAs, as shown in Fig. 2.7. In fact, as already mentioned, in this case the existence of power peaks in the transmitted waveforms can determine a distortion effect with a considerable loss in performance. Focusing on this aspect, we show now how the proposed scheme affects the power distribution of the transmitted waveforms.

First of all, it is worth comparing the scatter plots of the symbols transmitted by one of the antennas, with the SPC approach, as shown in Fig. 3.7, and with the proposed PAC approach, as shown in Fig. 3.11. In both cases, a total available power of 10 dBW is assumed. It is evident how the proposed Max-Min-PAC scheme prevents the power peaks, which are observable in the Max-Min-SPC case, where the per-antenna power cannot be controlled. The proposed scheme, by imposing the PACs in the design of the transmitted symbols, results in a constellation lying inside a circle, and this clearly constitutes a relevant advantage with respect to the non-linearities of the satellite

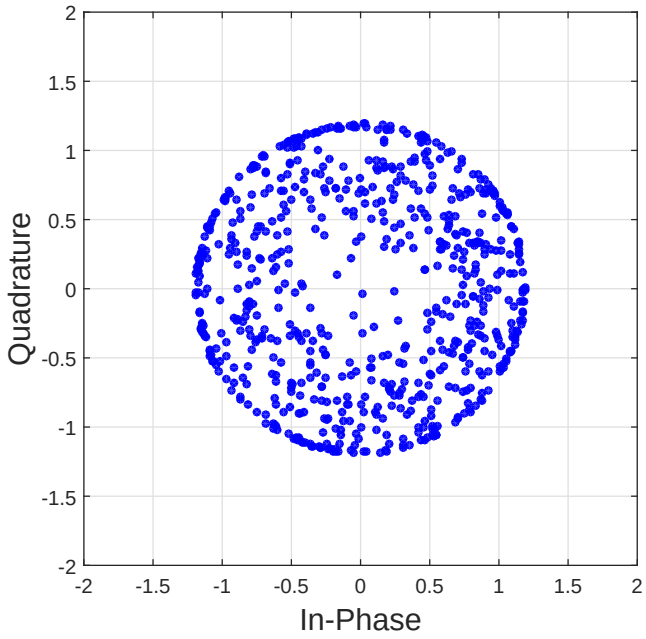

FIGURE 3.11: Scatter plot of the symbols associated to one antenna, after SLP with PACs.

channel.

In Fig. 3.12 the power transmitted by one of the antennas is considered (we take, without loss of generality, the antenna with indexed by 1, whose transmit power is $P_1 = |x_1|^2$), and the empirical evaluation of its complementary cumulative distribution function (CCDF) is drawn for the Max-Min-PAC and the Max-Min-SPC approaches, assuming a total available power of 10 dBW in both cases. The CCDF of the power P_1 is a function of a variable z defined as the probability of P_1 being larger than z, i.e., $\text{CCDF}_{P_1}(z) = \Pr(P_1 > z)$. With respect to the SPC case, where a long tail is visible in the curve, in the proposed approach the power results to be more bounded. The difference between the maximum value of P_1 in the two cases is over 4 dBW, which is considerable taking into account the saturation effects of non-linear TWTAs.

Another interesting figure of merit for evaluating the dynamic properties of the transmitted waveforms, with respect to the non-linear satellite channel, is the instantaneous-to-average power ratio (IAPR). This quantity, referring again to the antenna indexed by 1, is defined as:

$$\text{IAPR}_1 = \frac{|x_1|^2}{\mathbb{E}_n|x_1|^2}, \tag{3.27}$$

and its maximum value over a certain time interval is the more common peak-to-average power ratio (PAPR). The IAPR distribution over time gives an information about the

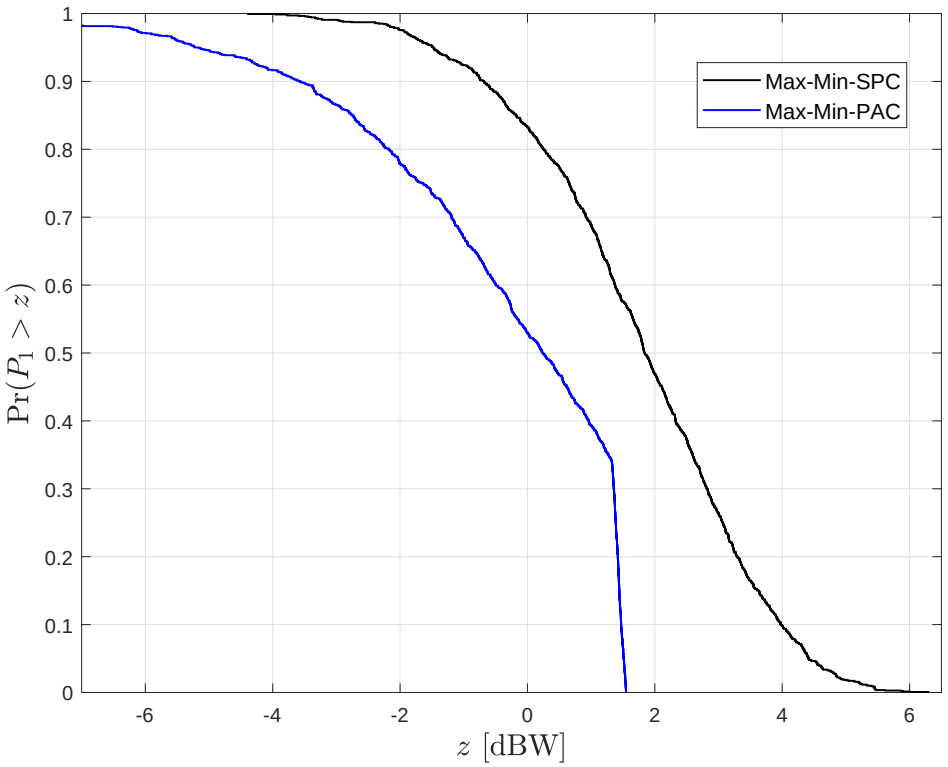

FIGURE 3.12: CCDF of the transmitted power by a single antenna.

power variation around its average value, and thus about the power peaks. In Fig. 3.13, the empirical evaluation of the CCDF of the IAPR, for a single transmit antenna, is shown, considering the PAC and SPC cases. The total available power is again fixed to 10 dBW. The result shows how, with the proposed Max-Min-PAC approach, also the IAPR is more bounded. This implies smaller variations of the transmitted power in time, and this property is very important for non-linear systems. A considerable difference of over 2 dB in the PAPR between the two techniques is observable.

3.3 Conclusions

In this chapter, novel SLP techniques have been proposed, taking into account the per-antenna power limitations that arise typically in practical multi-user MISO systems. First, the problem of minimization of the peak power amongst the transmitting antenna, under QoS constraints, has been formulated and solved for PSK modulations, in order to have a more uniform distribution of the transmitted power with respect to the state of the art symbol-level techniques. Then, the related max-min fair scheme, under per-antenna power constraints, is addressed, with specific regard to a multi-beam satellite scenario. The max-min fair optimization problem is tackled through a bisection procedure over the

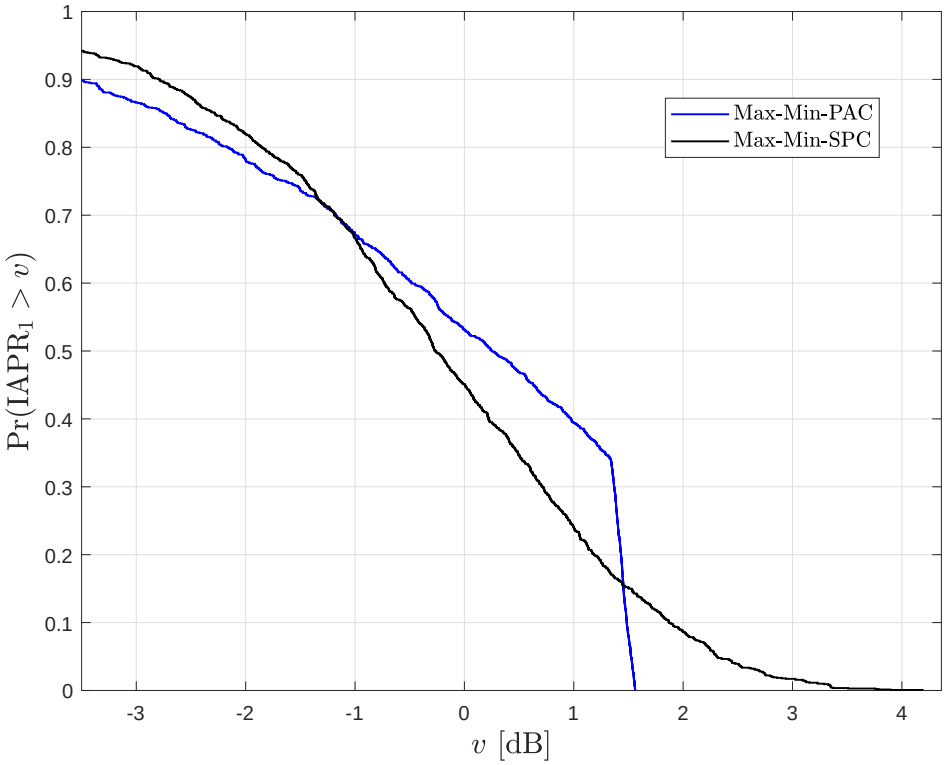

FIGURE 3.13: CCDF of the IAPR for a single transmit antenna.

previous power minimization problem. The proposed schemes allow a reduction of the power peaks amongst the transmit antennas, and therefore they are particularly suitable for systems corrupted by non-linear effects. Numerical results have been presented to show the effectiveness of the proposed schemes, which outperform the existing state of the art techniques in terms of reduction of the power peaks and of the peak-to-average power ratio across the transmitting antennas.

Chapter 4

Symbol-level Precoding for the Non-linear Multiuser MISO Downlink Channel

This chapter presents novel symbol-level precoding (SLP) schemes for multi-level modulations, aimed at exploiting the constructive interference effect and, at the same time, controlling the instantaneous per-antenna power levels. Specifically, the contributions of the chapter can be summarized as follows:

- Two different SLP strategies are proposed, with the objective of reducing the power imbalances between the multiple transmit antennas, in order to have improved performance over non-linear channels with respect to the symbol-level schemes of the literature. In both the proposed approaches Quality-of-Service (QoS) constraints are considered to guarantee a per-user required signal-to-interference-plus-noise ratio (SINR), and a multi-level modulation scheme is assumed for the data information.
- The first presented algorithm minimizes the per-antenna transmit power, and imposes a lower bound to the power carried by each transmitted signal. In this approach, the imbalances between the different RF chains are reduced by constraining the per-antenna transmit power within a specific range. The related optimization problem is solved through an iterative procedure relying on successive convex approximation (SCA).
- The second proposed scheme directly tackles a minimization of the spatial peak-to-average power ratio (SPAPR) amongst the multiple transmit antennas. The

related optimization problem is tackled by resorting jointly to parametric programming and SCA.

The main novelty of the proposed techniques with respect to the state of the art on SLP for constructive interference [20–25] is their ability to exploit the potential of the symbol-level design for producing more robust waveforms to the harmful effects of non-linear channels. A first step in this direction has already been taken in chapter 3. Nevertheless, the scheme therein introduced performs just a peak power minimization (and the related max-min fair formulation), without imposing any lower bound nor optimizing the SPAPR. On the other hand, the techniques proposed herein directly aim at a reduction of the power imbalances across the different antennas, thus they are able to tackle the problem of differential phase shift discussed in chapter 2, and therefore to achieve enhanced performance.

4.1 System and Signals Model

We consider a single-cell multiple-antenna downlink scenario, where a single base-station is equipped with N transmit antennas serving K user terminals, with $N \geq K$, each one equipped with a single receiving antenna. We assume a block fading channel $\boldsymbol{h}_j \in \mathbb{C}^{1\times N}$ between the transmit base-station antennas and the j-th user. The received signal at the j-th user in the symbol slot n can be written as:

$$y_j[n] = \boldsymbol{h}_j \boldsymbol{x}[n] + z_j[n], \tag{4.1}$$

where $\boldsymbol{x}[n] \in \mathbb{C}^{N\times 1}$ represents the transmitted signal vector from the N transmit antennas, and $z_j[n]$ is a random variable distributed as $\mathcal{CN}(0, \sigma_z^2)$, modeling the zero mean additive white Gaussian noise (AWGN) measured at the j-th user's receiving antenna.

By collecting the received signals by all the users in a vector $\boldsymbol{y}[n] \in \mathbb{C}^{K\times 1}$, the above model can be rewritten in a compact form as:

$$\boldsymbol{y}[n] = \boldsymbol{H}\boldsymbol{x}[n] + \boldsymbol{z}[n], \tag{4.2}$$

where $\boldsymbol{H} = [\boldsymbol{h}_1^T \dots \boldsymbol{h}_K^T]^T \in \mathbb{C}^{K\times N}$ represents the system channel matrix, and $\boldsymbol{z}[n] \in \mathbb{C}^{K\times 1}$ collects the AWGN components for all the users.

The transmitted signal vector $\boldsymbol{x}[n]$ is obtained as output of a precoding module, which takes as input the channel state information (CSI), which is an estimate of $\boldsymbol{H}$, and the data information $\boldsymbol{d}[n] \in \mathbb{C}^{K\times 1}$, namely the data symbols to be conveyed to the users. A

framing structure including a preamble of pilot symbols is assumed in the transmission scheme. As discussed in chapter 2, such pilots are exploited by each user to estimate the related channel vector, and the resulting CSI is fed back to the base station in order to be available for the precoding operation. The data symbols are assumed to be uncorrelated and taken from a generic multi-level constellation represented by the symbol set $\mathcal{D}$, having unit average power, i.e., $\mathbb{E}_{\mathcal{D}}[|d_j|^2] = 1$.

The system model described in (4.2) is a linear one. However, as discussed in section 2.3 of chapter 2, it should be kept in mind that the introduced system model is actually corrupted by the non-linear effects introduced in the per-antenna power amplification stages, which affect both the amplitude and the phase of the transmitted waveforms. The resulting system model can be represented as in Fig. 2.6. Although the SLP schemes proposed in this chapter are applicable to any non-linear model, the traveling-wave tube amplifier (TWTA) model introduced in Fig. 2.7 will be used as a practical reference. The SLP schemes herein proposed aim at improving the power distribution of the transmitted signals in the spatial dimension, in order to counteract the distortion and the differential phase shift introduced by the amplification stages[1]. In the following sections, these novel precoding strategies are further explained, and the related optimization problems are formalized and solved.

4.2 Symbol-level Precoding for Weighted Peak Power Minimization with Lower Bound (WPPMLB)

In this section a novel symbol-level precoding scheme is presented, which performs a weighted per-antenna power minimization and imposes a lower bound on the transmit power on each radio frequency (RF) chain. According to the general framework of symbol-level precoding, the main objective of the proposed scheme is to design the transmitted vector $\boldsymbol{x}$ by assuring a constructive interference effect at the users' side, following the definition in [22]. In other words, $\boldsymbol{x}$ should be optimized so that the superposition of the multiple streams through the channel forces the received signal to the detection region of the desired symbol, for each user. The novelty of the proposed scheme, with respect to the work on constructive interference carried out in [22, 23], lies in the different optimization of the transmitted power. While the available literature focuses on minimizing the total transmitted power while guaranteeing some QoS targets at the users, here the focus is on the per-antenna transmitted power. Taking into

[1]It should be noted that the inter-symbol interference created by the non-linear amplification stages is not modeled in the proposed optimization schemes, as they design the transmit signals only in the spatial dimension, for each symbol slot. However, this effect is taken into account in the numerical evaluation stage of section 4.4.3.

account the non-linear effects of the channel, the goal is to minimize the maximum power among the different antennas and, at the same time, to put a lower bound constraint on such power. This would guarantee a reduction of the power peaks and a reduced variation of the instantaneous power transmitted by the different antennas, granting better properties with respect to the non-linear amplification stages and, in particular, limiting the differential phase shift. Lastly, the per-antenna transmit power is considered in a weighted fashion, so as to account possible asymmetries in the different RF chains. The resulting problem, referred to as weighted peak power minimization with lower bound (WPPMLB), can be written as follows[2]:

$$\begin{aligned} \boldsymbol{x}(\boldsymbol{d},\boldsymbol{H},\boldsymbol{\gamma},\boldsymbol{p}) = \arg\min_{r,\boldsymbol{x}} \quad & r \\ \text{s.t.} \quad \mathcal{C}1: \quad & \alpha r^2 \leq \frac{|x_i|^2}{p_i} \leq r^2,\ i=1,\dots,N, \\ \mathcal{C}2: \quad & |\boldsymbol{h}_j\boldsymbol{x}|^2 \ \trianglerighteq \kappa_j^2\gamma_j\sigma_z^2,\ j=1,\dots,K, \\ \mathcal{C}3: \quad & \angle\boldsymbol{h}_j\boldsymbol{x} = \angle d_j,\ j=1,\dots,K, \end{aligned} \tag{4.3}$$

where r is a non-negative slack variable used for bounding the power, α is a parameter determining the lower bound (which is better characterized afterwards), γ_j is the target SINR that should be granted for the j-th user, p_i is the power weight for the i-th antenna, and $\kappa_j = |d_j|/\sqrt{\mathbb{E}_{\mathcal{D}}[|d_j|^2]}$ is a magnitude scaling factor for the symbol d_j, which allows to account the different amplitudes of the symbols in the multi-level constellation $\mathcal{D}$. The assumption to have symbols with unit average power implies that $\kappa_j = |d_j|$. Moreover, the vector $\boldsymbol{\gamma} = [\gamma_1 \dots \gamma_K]^T \in \mathbb{C}^{K\times 1}$ stacks the target SINR for all the users, while $\boldsymbol{p} = [p_1 \dots p_N]^T \in \mathbb{C}^{N\times 1}$ stacks the power weights for all the antennas. Further, the notation $\trianglerighteq$ represents a generalized inequality: it shall be read as $\geq$ or $=$ depending whether the constraint is referred to a boundary symbol or to an inner symbol of the constellation $\mathcal{D}$, respectively (generalized inequalities related to the different detection regions can be also found in [23]).

The set of constraints $\mathcal{C}1$ in (4.3) gathers two different kinds of constraints. In particular, such constraints impose an upper bound on the per-antenna weighted transmit power (through the slack variable r, so to have a peak power minimization), and a lower bound at the same time. The lower bound is defined through the design parameter α. This parameter shall be chosen such that $0 \leq \alpha \leq 1$ and, if considered in dB, represents the width of the region where the transmit power is constrained. The closer to 1 is α, the more the power variations will be limited. Nonetheless, the choice of a high value for

[2]It should be mentioned that this formulation of the optimization problem is referred to circular constellations, such as phase shift keying (PSK) and amplitude phase shift keying (APSK). A similar formulation for rectangular constellations, such as quadrature amplitude modulation (QAM), can be straightforwardly given but it is not shown for the sake of brevity. This consideration applies to the optimization problems formulated in the remainder of this chapter.

α comes with a reduction of the degrees of freedom of the optimization problem, whose feasibility is not guaranteed, as discussed afterwards. Concerning the power weights, they are positive parameters affecting the loading of the different RF chains: a higher value for p_i implies as higher power loading for the i-th antenna with respect to the other ones. The set of constraints $\mathcal{C}2$ represents a QoS constraint for each user. The set of constraints $\mathcal{C}3$ represents the constructive interference condition, guaranteeing that each user receives the desired data symbol with the correct phase.

The problem (4.3) appears to be complex and hard to tackle. However, it is possible to reformulate it in a more tractable form. More specifically, the following theorem holds, whose proof is reported in the Appendix A:

Theorem 4.1. *The optimization problem* (4.3) *is equivalent to the following one:*

$$\begin{aligned}
\tilde{\boldsymbol{x}}(\boldsymbol{d},\boldsymbol{H},\boldsymbol{\gamma},\boldsymbol{p}) = \arg\min_{r,\tilde{\boldsymbol{x}}} \quad & r \\
\text{s.t.} \quad \mathcal{C}1: \quad & \|\boldsymbol{B}_i\tilde{\boldsymbol{x}}\| \leq r,\ i=1,\dots,N, \\
\mathcal{C}2: \quad & \tilde{\boldsymbol{x}}^{\dagger}(\boldsymbol{A}_i)\tilde{\boldsymbol{x}} \leq -\alpha r^2,\ i=1,\dots,N, \\
\mathcal{C}3: \quad & \mathrm{Re}(\boldsymbol{D})\boldsymbol{H_1}\tilde{\boldsymbol{x}} \trianglerighteq \boldsymbol{\beta_R}, \\
\mathcal{C}4: \quad & \mathrm{Im}(\boldsymbol{D})\boldsymbol{H_2}\tilde{\boldsymbol{x}} \trianglerighteq \boldsymbol{\beta_I}, \\
\mathcal{C}5: \quad & (\boldsymbol{T}\boldsymbol{H_1}-\boldsymbol{H_2})\tilde{\boldsymbol{x}} = \boldsymbol{0},
\end{aligned} \tag{4.4}$$

where the optimization variable $\tilde{\boldsymbol{x}}$ is a stacked version of $\boldsymbol{x}$, namely $\tilde{\boldsymbol{x}} = [\mathrm{Re}(\boldsymbol{x})^T, \mathrm{Im}(\boldsymbol{x})^T]^T \in \mathbb{R}^{2N\times 1}$, and the other introduced quantities are defined as functions of the input parameters only[3]*, with the matrices $\boldsymbol{A}_i$ being negative semi-definite (NSD) $\forall i = 1,\dots,N$.*

In particular, the sets of constraints $\mathcal{C}1$ and $\mathcal{C}2$ in (4.4) *correspond to the upper and lower bounding of the per-antenna transmit power, respectively, while the remaining constraints are related to the attained SINR and the received symbol phases at the different users*[4]*.*

□

In the problem in (4.4), it can be seen how all the constraints are convex, with the exception of $\mathcal{C}2$, imposing the lower bound. Indeed, the upper bound constraint is a second order cone constraint, the QoS constraints and the phase constraints are affine, whilst the lower bound constraint is a non-convex, since the matrices $\boldsymbol{A}_i$ are NSD.

Hereafter an approach to solve the non-convex problem (4.4), based on a successive convex approximation (SCA) procedure [152, 153], is proposed.

[3]The definition of the introduced vectors and matrices can be found in the proof, and is not reported here for the sake of brevity.

[4]The generalized inequalities $\trianglerighteq$ applied to vectors in the constraints shall be considered element-wise.

4.2.1 FPP-SCA Algorithm

The main idea of the SCA algorithm is to iteratively approximate the non-convex problem at hand into a convex one, so to converge to the solution of the original problem. More specifically, assuming a random point $\boldsymbol{z} \in \mathbb{R}^{2N\times 1}$, it is always true that $(\tilde{\boldsymbol{x}}-\boldsymbol{z})^{\dagger}(\boldsymbol{A}_i)(\tilde{\boldsymbol{x}}-\boldsymbol{z}) \leq 0$, being $\boldsymbol{A}_i$ NSD. Hence, the following inequality holds:

$$\tilde{\boldsymbol{x}}^{\dagger}(\boldsymbol{A}_i)\tilde{\boldsymbol{x}} \leq 2\boldsymbol{z}^{\dagger}(\boldsymbol{A}_i)\tilde{\boldsymbol{x}} - \boldsymbol{z}^{\dagger}(\boldsymbol{A}_i)\boldsymbol{z}, \tag{4.5}$$

which represents a linear restriction of $\tilde{\boldsymbol{x}}^{\dagger}(\boldsymbol{A}_i)\tilde{\boldsymbol{x}}$ around the point $\boldsymbol{z}$. By using the above inequality, the non-convex constraint can be replaced by the following, which is affine in $\tilde{\boldsymbol{x}}$:

$$2\boldsymbol{z}^{\dagger}(\boldsymbol{A}_i)\tilde{\boldsymbol{x}} - \boldsymbol{z}^{\dagger}(\boldsymbol{A}_i)\boldsymbol{z} \leq -\alpha r^2. \tag{4.6}$$

By using the above linear restriction, the problem (4.4) can be written in the following approximated form, to be tackled iteratively:

$$\begin{aligned}
\tilde{\boldsymbol{x}}(\boldsymbol{d},\boldsymbol{H},\boldsymbol{\gamma},\boldsymbol{p}) = \arg\min_{r,\tilde{\boldsymbol{x}}} \quad & r \\
\text{s.t.} \quad \mathcal{C}1: \quad & \|\boldsymbol{B}_i\tilde{\boldsymbol{x}}\| \leq r,\ i=1,\dots,N, \\
\mathcal{C}2: \quad & 2\boldsymbol{z}_k^{\dagger}(\boldsymbol{A}_i)\tilde{\boldsymbol{x}} - \boldsymbol{z}_k^{\dagger}(\boldsymbol{A}_i)\boldsymbol{z}_k \leq -\alpha r^2, \\
& i=1,\dots,N, \\
\mathcal{C}3: \quad & \mathrm{Re}(\boldsymbol{D})\boldsymbol{H_1}\tilde{\boldsymbol{x}} \succeq \boldsymbol{\beta_R}, \\
\mathcal{C}4: \quad & \mathrm{Im}(\boldsymbol{D})\boldsymbol{H_2}\tilde{\boldsymbol{x}} \succeq \boldsymbol{\beta_I}, \\
\mathcal{C}5: \quad & (\boldsymbol{T}\boldsymbol{H_1} - \boldsymbol{H_2})\tilde{\boldsymbol{x}} = \boldsymbol{0},
\end{aligned} \tag{4.7}$$

where $\boldsymbol{z}_k$ is the introduced auxiliary variable at the k-th iteration, which is updated as $\boldsymbol{z}_{k+1} = \tilde{\boldsymbol{x}}$ until convergence, i.e., until $\|\tilde{\boldsymbol{x}} - \boldsymbol{z}_k\|$ is smaller than a predefined threshold.

The introduced approach resorts to the SCA procedure [152–154], which requires the initial point $\boldsymbol{z}_0$ to be a feasible one for the original problem. However, since the feasibility of (4.4) is not guaranteed, it is not easy to find such feasible initial point. To solve the issue, we can rely on the feasible point pursuit (FPP) SCA algorithm [153]. In particular, the problem can be made always feasible by introducing an additional slack penalty term $\boldsymbol{s}$ as follows:

$$
\begin{aligned}
\tilde{\boldsymbol{x}}(\boldsymbol{d}, \hat{\boldsymbol{H}}, \boldsymbol{\gamma}) = \arg \min_{r, \tilde{\boldsymbol{x}}, \boldsymbol{s}} \quad & r + \lambda \|\boldsymbol{s}\| \\
\text{s.t.} \quad \mathcal{C}1: \quad & \|\boldsymbol{B}_i \tilde{\boldsymbol{x}}\| \leq r + s_i, \; i = 1, \ldots, N, \\
\mathcal{C}2: \quad & 2\boldsymbol{z}_k^{\dagger}(\boldsymbol{A}_i)\tilde{\boldsymbol{x}} - \boldsymbol{z}_k^{\dagger}(\boldsymbol{A}_i)\boldsymbol{z}_k \leq -\alpha r^2 + s_{i+N}, \\
& i = 1, \ldots, N, \\
\mathcal{C}3: \quad & \mathrm{Re}(\boldsymbol{D})\boldsymbol{H_1}\tilde{\boldsymbol{x}} \succeq \boldsymbol{\beta_R}, \\
\mathcal{C}4: \quad & \mathrm{Im}(\boldsymbol{D})\boldsymbol{H_2}\tilde{\boldsymbol{x}} \succeq \boldsymbol{\beta_I}, \\
\mathcal{C}5: \quad & (\boldsymbol{T}\boldsymbol{H_1} - \boldsymbol{H_2})\tilde{\boldsymbol{x}} = \boldsymbol{0},
\end{aligned}
\tag{4.8}
$$

with $\boldsymbol{s} \in \mathbb{R}^{2N \times 1}$, and λ being a trade-off term between the original objective function and the new penalty one. The modified problem in (4.8) is always feasible for any choice of $\boldsymbol{z}_0$ and the convergence is guaranteed [152, 153]. Therefore, the initial point $\boldsymbol{z}_0$ can be randomly chosen. If the converged slack penalty variables turn out being all zero, then the related solution solves the original problem (4.4). In general, the FPP-SCA algorithm can be applied by using different starting points $\boldsymbol{z}_0$, and then choosing the best solution, namely the one resulting in the lowest-norm penalty term. Concerning the trade-off term λ, in the fashion of [153] we consider $\lambda \gg 1$, in order to force the penalty terms toward zero, hence pushing the iterates towards the feasible region of the original problem (4.4), when it is non-empty.

4.3 Spatial Peak-to-Average Power Ratio Reduction

In this section, a different symbol-level precoding scheme is proposed, with the objective of directly minimizing the SPAPR amongst the transmit antennas. A metric usually considered in the literature, in the context of non-linear systems, is the peak-to-average power ratio (PAPR) evaluated over time. For example, the temporal PAPR has been tackled for orthogonal frequency-division multiplexing (OFDM) systems [30, 155, 156]. Here the focus is instead on the SPAPR which, in light of the impairments described in section 2.3 of chapter 2, is also important in order to utilize the multiple amplifiers in a more homogeneous way. The SPAPR can be defined as:

$$
\mathrm{SPAPR} = \frac{\|\boldsymbol{x}\|_{\infty}^2}{\|\boldsymbol{x}\|^2/N}. \tag{4.9}
$$

In the direction of designing the transmit waveforms controlling their instantaneous power, the opportunity to have low SPAPR allows a reduction of the per-antenna power

imbalances across the different high-power amplifiers (HPAs), thus limiting the related differential phase shift.

4.3.1 Spatial PAPR Optimization

The SPAPR minimization (SPAPR-Min) problem can be formulated as non-linear fractional program, as:

$$\begin{aligned} \boldsymbol{x}(\boldsymbol{d},\boldsymbol{H},\boldsymbol{\gamma}) = \arg\min_{\boldsymbol{x}} \quad & \frac{\|\boldsymbol{x}\|_\infty^2}{\|\boldsymbol{x}\|^2} \\ \text{s.t.} \quad \mathcal{C}1: \quad & |\boldsymbol{h}_j\boldsymbol{x}|^2 \ \trianglerighteq \kappa_j^2\gamma_j\sigma_z^2, \ j=1,\dots,K, \\ \mathcal{C}2: \quad & \angle\boldsymbol{h}_j\boldsymbol{x} = \angle d_j, \ j=1,\dots,K. \end{aligned} \tag{4.10}$$

It is possible to reformulate the problem (4.10), as shown in the following theorem, whose proof is reported in the Appendix B:

Theorem 4.2. *The optimization problem* (4.10) *is equivalent to the following one:*

$$\begin{aligned} \boldsymbol{x}(\boldsymbol{d},\boldsymbol{H},\boldsymbol{\gamma}) = \arg\min_{\boldsymbol{x}} \quad & \frac{\|\boldsymbol{x}\|_\infty^2}{\|\boldsymbol{x}\|^2} \\ \text{s.t.} \quad \mathcal{C}1: \quad & \mathrm{Re}(d_j)\frac{\boldsymbol{h}_j\boldsymbol{x}+\boldsymbol{x}^\dagger\boldsymbol{h}_j^\dagger}{2} \trianglerighteq \sigma_z\sqrt{\gamma_j}\,\mathrm{Re}^2(d_j), \\ & j=1,\dots,K, \\ \mathcal{C}2: \quad & \mathrm{Im}(d_j)\frac{\boldsymbol{h}_j\boldsymbol{x}-\boldsymbol{x}^\dagger\boldsymbol{h}_j^\dagger}{2\iota} \trianglerighteq \sigma_z\sqrt{\gamma_j}\,\mathrm{Im}^2(d_j), \\ & j=1,\dots,K, \\ \mathcal{C}3: \quad & t_j(\iota t_j-1)\boldsymbol{h}_j\boldsymbol{x}+(\iota t_j+1)\boldsymbol{x}^\dagger\boldsymbol{h}^\dagger = 0, \\ & j=1,\dots,K. \end{aligned} \tag{4.11}$$

where $t_j = \tan(\angle d_j)$.

□

In the reformulated problem (4.11), the challenging part is in the non-linear fractional objective function. Dinkelbach suggests a parametric way of solving the non-linear fractional problems [157, 158], whose basic idea is to tackle the fractional problem by solving a sequence of easier problems which converges to the global solution. Nevertheless, Dinkelbach's algorithm can be applied only if the numerator and denominator are convex and concave, respectively. Therefore, it cannot be directly applied to the

problem at hand, since the numerator $\|\boldsymbol{x}\|_\infty^2$ and denominator $\|\boldsymbol{x}\|^2$ are both convex functions. In order to solve the problem, we can again resort to a SCA approach [152–154]. In particular, the quadratic function can be approximated around a certain vector $\boldsymbol{z} \in \mathbb{C}^{N\times 1}$ by a concave (affine) function as:

$$\begin{aligned}(\boldsymbol{x}-\boldsymbol{z})^\dagger(\boldsymbol{x}-\boldsymbol{z}) &= \boldsymbol{x}^\dagger\boldsymbol{x} - 2\,\mathrm{Re}(\boldsymbol{z}^\dagger\boldsymbol{x}) + \boldsymbol{z}^\dagger\boldsymbol{z} \geq 0 \\ &\boldsymbol{x}^\dagger\boldsymbol{x} \geq 2\,\mathrm{Re}(\boldsymbol{z}^\dagger\boldsymbol{x}) - \boldsymbol{z}^\dagger\boldsymbol{z} \\ &\boldsymbol{x}^\dagger\boldsymbol{x} \approx 2\,\mathrm{Re}(\boldsymbol{z}^\dagger\boldsymbol{x}) - \boldsymbol{z}^\dagger\boldsymbol{z}. \end{aligned} \tag{4.12}$$

Using this lower bound approximation, the problem in (4.10) can be rewritten as:

$$\begin{aligned}\boldsymbol{x}(\boldsymbol{d},\boldsymbol{H},\boldsymbol{\gamma}) = \arg\min_{\boldsymbol{x}} \quad & \frac{\|\boldsymbol{x}\|_\infty^2}{(2\,\mathrm{Re}(\boldsymbol{z}^\dagger\boldsymbol{x}) - \boldsymbol{z}^\dagger\boldsymbol{z})} \\ \text{s.t.} \quad \mathcal{C}1: \quad & \mathrm{Re}(d_j)\frac{\boldsymbol{h}_j\boldsymbol{x} + \boldsymbol{x}^\dagger\boldsymbol{h}_j^\dagger}{2} \trianglerighteq \sigma_z\sqrt{\gamma_j}\,\mathrm{Re}^2(d_j), \\ & j = 1,\ldots,K, \\ \mathcal{C}2: \quad & \mathrm{Im}(d_j)\frac{\boldsymbol{h}_j\boldsymbol{x} - \boldsymbol{x}^\dagger\boldsymbol{h}_j^\dagger}{2\iota} \trianglerighteq \sigma_z\sqrt{\gamma_j}\,\mathrm{Im}^2(d_j), \\ & j = 1,\ldots,K, \\ \mathcal{C}3: \quad & t_j(\iota t_j - 1)\boldsymbol{h}_j\boldsymbol{x} + (\iota t_j + 1)\boldsymbol{x}^\dagger\boldsymbol{h}^\dagger = 0, \\ & j = 1,\ldots,K. \end{aligned} \tag{4.13}$$

Now the problem can be solved by applying parametric programming on the approximated formulation in (4.13). To this aim, it is possible to define the optimization function $F(\eta,\boldsymbol{z}) = \min_{\boldsymbol{x}\in\mathcal{S}}\{\|\boldsymbol{x}\|_\infty^2 - \eta(2\,\mathrm{Re}(\boldsymbol{z}^\dagger\boldsymbol{x}) - \boldsymbol{z}^\dagger\boldsymbol{z})\}$, where $\mathcal{S}$ represents the sets of constraints $\mathcal{C}_1$, $\mathcal{C}_2$, $\mathcal{C}_3$ and η is an auxiliary variable to apply parametric programming techniques. Therefore, the problem can be formulated as:

$$\begin{aligned}\boldsymbol{x}(\boldsymbol{d},\boldsymbol{H},\boldsymbol{\gamma}) = \arg\min_{\boldsymbol{x},\eta} \quad & \|\boldsymbol{x}\|_\infty^2 - \eta(2\,\mathrm{Re}(\boldsymbol{z}^\dagger\boldsymbol{x}) - \boldsymbol{z}^\dagger\boldsymbol{z}) \\ \text{s.t.} \quad \mathcal{C}1: \quad & \mathrm{Re}(d_j)\frac{\boldsymbol{h}_j\boldsymbol{x} + \boldsymbol{x}^\dagger\boldsymbol{h}_j^\dagger}{2} \trianglerighteq \sigma_z\sqrt{\gamma_j}\,\mathrm{Re}^2(d_j), \\ & j = 1,\ldots,K, \\ \mathcal{C}2: \quad & \mathrm{Im}(d_j)\frac{\boldsymbol{h}_j\boldsymbol{x} - \boldsymbol{x}^\dagger\boldsymbol{h}_j^\dagger}{2\iota} \trianglerighteq \sigma_z\sqrt{\gamma_j}\,\mathrm{Im}^2(d_j), \\ & j = 1,\ldots,K, \\ \mathcal{C}3: \quad & t_j(\iota t_j - 1)\boldsymbol{h}_j\boldsymbol{x} + (\iota t_j + 1)\boldsymbol{x}^\dagger\boldsymbol{h}^\dagger = 0, \\ & j = 1,\ldots,K. \end{aligned} \tag{4.14}$$

TABLE 4.1: Proposed Successive Linear Approximation for Non-linear Fractional Programming

1. Initialization: Set ϵ, $k = 0$, $\eta = 0$ in (4.14), which results in solving $F(0)$.
2. Evaluate $\eta_0 = \frac{\|\boldsymbol{x}\|_\infty^2}{\|\boldsymbol{x}\|^2}$, $\boldsymbol{z}_0 = \boldsymbol{x}$.
3. Solve the following optimization:

$$\begin{aligned} \boldsymbol{x} = \arg\min_{\boldsymbol{x}} \quad & \|\boldsymbol{x}\|_\infty^2 - \eta_k(2\,\mathrm{Re}(\boldsymbol{z}_k^\dagger \boldsymbol{x}) - \boldsymbol{z}_k^\dagger \boldsymbol{z}_k) \\ \text{s.t.} \quad \mathcal{C}1: \quad & \mathrm{Re}(d_j)\frac{\boldsymbol{h}_j\boldsymbol{x} + \boldsymbol{x}^\dagger \boldsymbol{h}_j^\dagger}{2} \trianglerighteq \sigma_z\sqrt{\gamma_j}\,\mathrm{Re}^2(d_j),\ j = 1,\dots,K, \\ \mathcal{C}2: \quad & \mathrm{Im}(d_j)\frac{\boldsymbol{h}_j\boldsymbol{x} - \boldsymbol{x}^\dagger \boldsymbol{h}_j^\dagger}{2\iota} \trianglerighteq \sigma_z\sqrt{\gamma_j}\,\mathrm{Im}^2(d_j),\ j = 1,\dots,K, \\ \mathcal{C}3: \quad & t_j(\iota t_j - 1)\boldsymbol{h}_j\boldsymbol{x} + (\iota t_j + 1)\boldsymbol{x}^\dagger \boldsymbol{h}^\dagger = 0,\ j = 1,\dots,K. \end{aligned} \tag{4.15}$$

4. Evaluate $|F(\eta_k, \boldsymbol{z}_k)|$ and $\|\boldsymbol{x} - \boldsymbol{z}_k\|$; if $|F(\eta_k, \boldsymbol{z}_k)| \geq \epsilon$ or $\|\boldsymbol{x} - \boldsymbol{z}_k\| \geq \epsilon$ go to step 5.
5. Set $\eta_{k+1} = \frac{\|\boldsymbol{x}\|_\infty^2}{\|\boldsymbol{x}\|^2}$, $\boldsymbol{z}_{k+1} = \boldsymbol{x}$, $k = k + 1$, go to step 3.

Ultimately, to efficiently solve (4.11) using the formulation in (4.14), the algorithm in Table 4.1 is proposed. The theoretical lower bound occurs when all the antennas have the same power (i.e., $\|\boldsymbol{x}\|^2/N$), with an achieved unit SPAPR.

4.3.2 Convergence of the Algorithm

It is proven in [157] that the parametric programming scheme applied to concave/linear fractional programs converge to a global optimum (if the objective is to maximize the concave/linear function). In our case this holds, since the objective is to minimize a convex/linear function.

On the other hand, considering the SCA approach, it is proven convergent [152] to a Karush-Kuhn-Tucker (KKT) point, provided that the approximation is a concave lower bound having the same first order behavior of the original function. This is the case of the approximation in (4.12), as stated in the following proposition.

Proposition 4.3. *Given the convex function $f(\boldsymbol{x}) = \|\boldsymbol{x}\|^2$, and its concave (affine) approximation around $\boldsymbol{z}$ $\tilde{f}(\boldsymbol{x}, \boldsymbol{z}) = 2\,\mathrm{Re}(\boldsymbol{z}^\dagger \boldsymbol{x}) - \boldsymbol{z}^\dagger \boldsymbol{z}$, the following properties hold:*

$$\tilde{f}(\boldsymbol{x}, \boldsymbol{z}) \leq f(\boldsymbol{x}), \tag{4.16}$$

$$\tilde{f}(\boldsymbol{x}, \boldsymbol{x}) = f(\boldsymbol{x}), \tag{4.17}$$

$$\frac{\partial}{\partial \boldsymbol{x}} \tilde{f}(\boldsymbol{x}, \boldsymbol{z})\bigg|_{\boldsymbol{z}=\boldsymbol{x}} = \frac{\partial}{\partial \boldsymbol{x}} f(\boldsymbol{x}), \tag{4.18}$$

$$\frac{\partial}{\partial \boldsymbol{x}^*} \tilde{f}(\boldsymbol{x}, \boldsymbol{z})\bigg|_{\boldsymbol{z}=\boldsymbol{x}} = \frac{\partial}{\partial \boldsymbol{x}^*} f(\boldsymbol{x}), \tag{4.19}$$

where the gradient is considered with respect to $\boldsymbol{x}$ and $\boldsymbol{x}^*$, and these variable are treated as independent, in the fashion of [159].

Proof. The properties (4.16) and (4.17) come straightforwardly from (4.12). In order to prove (4.18) and (4.19), we derive hereafter the gradient of $f(\boldsymbol{x})$ and $\tilde{f}(\boldsymbol{x}, \boldsymbol{z})$ with respect to $\boldsymbol{x}$ and $\boldsymbol{x}^*$, based on [159]:

$$\frac{\partial}{\partial \boldsymbol{x}} f(\boldsymbol{x}) = \frac{\partial}{\partial \boldsymbol{x}} \{\boldsymbol{x}^\dagger \boldsymbol{x}\} = \boldsymbol{x}^\dagger, \tag{4.20}$$

$$\frac{\partial}{\partial \boldsymbol{x}^*} f(\boldsymbol{x}) = \frac{\partial}{\partial \boldsymbol{x}^*} \{\boldsymbol{x}^\dagger \boldsymbol{x}\} = \boldsymbol{x}^T, \tag{4.21}$$

$$\frac{\partial}{\partial \boldsymbol{x}} \tilde{f}(\boldsymbol{x}, \boldsymbol{z}) = \frac{\partial}{\partial \boldsymbol{x}} \{\boldsymbol{z}^\dagger \boldsymbol{x} + \boldsymbol{x}^\dagger \boldsymbol{z}\} = \boldsymbol{z}^\dagger, \tag{4.22}$$

$$\frac{\partial}{\partial \boldsymbol{x}^*} \tilde{f}(\boldsymbol{x}, \boldsymbol{z}) = \frac{\partial}{\partial \boldsymbol{x}^*} \{\boldsymbol{z}^\dagger \boldsymbol{x} + \boldsymbol{x}^\dagger \boldsymbol{z}\} = \boldsymbol{z}^T. \tag{4.23}$$

By evaluating (4.22) and (4.23) in $\boldsymbol{z} = \boldsymbol{x}$, the properties (4.18) and (4.19) follows, and the proposition is proved. □

Although the parametric programming and the SCA approaches have been shown convergent individually, it shall be noticed how the formulation (4.14), and accordingly the algorithm proposed in Table 4.1, employs these schemes in a joint fashion, and it is not straightforward to prove the convergence of the final algorithm. However, the proposed scheme has been shown convergent through numerical simulations. This is shown in Fig. 4.1 for two instances of the algorithm, with $K = 5$ and N set to 10 and 8, respectively. The figure shows, for both the cases, how the SCA error $\|\boldsymbol{x} - \boldsymbol{z}_k\|$ and the parametric programming error $|F(\eta_k)|$ vary with respect to the iteration index, going to zero in a few iterations.

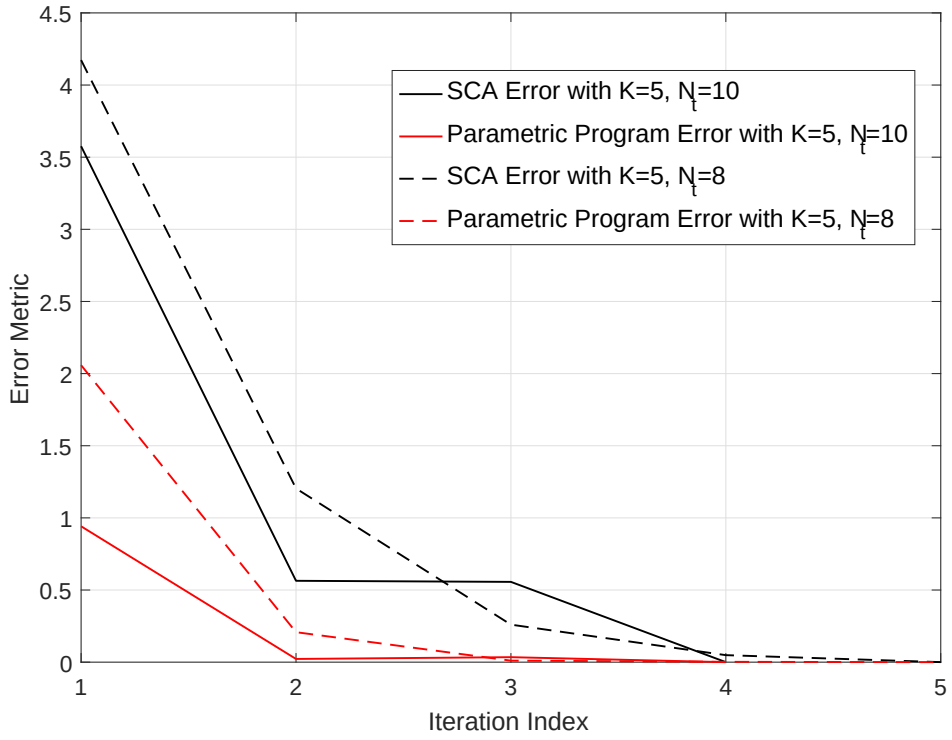

FIGURE 4.1: Error metrics of the algorithm of 4.1, versus iteration index, for two instances of the algorithm.

4.4 Numerical Results

In this section some numerical results are presented, to show the effectiveness of the proposed approaches, in particular the WPPMLB scheme and the SPAPR-Min sheme. Before discussing the results, let us introduce the considered performance metrics. The most prominent metrics with respect to the problem of non-linearities, which is the main object of this contribution, are the SPAPR and the spatial dynamic range. The former has been already defined in equation (4.9), while the latter is defined, for a specific symbol slot, as the ratio between the maximum and the minimum transmit power amongst the antennas, i.e., as $\frac{\|\boldsymbol{x}\|_\infty^2}{\min_i |x_i|^2}$. Moreover, the total transmit power and the average achieved SINR are also considered for the performance evaluation. The introduced quantities, which are symbol dependent by definition, are considered at a frame level by averaging over a large number of symbol slots. An additional performance metric used in this section is the symbol error rate (SER), which is useful to quantify the effectiveness of the proposed techniques when a non-linear channel is applied in the communication chain.

All the results presented in the remainder of this section are obtained assuming a 16-APSK modulation scheme for the data symbols, while the number of users is fixed to

$K = 5$. The quasi-static block fading channel coefficients have been generated, for the generic user j, as $\boldsymbol{h}_j \sim \mathcal{CN}(0, \sigma_h^2 \boldsymbol{I})$, with $\sigma_h^2 = 1$. The results have been obtained averaging over 30 fading blocks of 20 symbol slots each, for a total of 600 realizations. Moreover, the noise variance σ_z^2 is assumed unitary. Finally, the target SINR is assumed the same for all the users for the sake of simplicity, and it is fixed to 12 dB for all the results[5].

In the following, the performance of the WPPMLB and SPAPR-Min schemes are analyzed with respect to some parameters, such as the number of transmit antennas and the input α (for the WPPMLB case). Then, some comparative results are presented, in order to compare the proposed techniques to the benchmarks, i.e., the sum power minimization approach of [22, 23], the peak power minimization scheme presented in chapter 3, and the constant envelope precoder of [29].

4.4.1 Performance of WPPMLB Scheme with respect to the Parameters

Hereafter, the performance of the WPPMLB scheme is investigated with respect to the number of transmit antennas and to the value of the design parameter α in the problem (4.3). Concerning this, it is worth noticing that the value $1/\alpha$ represents the imposed spatial dynamic range for the transmit signal. Nevertheless, it has been mentioned how the imposition of a tight spatial dynamic range (i.e., α close to 1) may compromise the feasibility of the problem, since it implies a reduction in the degrees of freedom. As a consequence, it is imperative to study to which extent it is possible to constraint the WPPMLB problem, and how this is affected by the number of transmit antennas N. The presented results are obtained by running the FPP-SCA algorithm using two random starting points and then choosing the best solution, as discussed in section 4.2.1. Moreover, the power weights are assumed equal to one, for simplicity.

In Fig. 4.2 the attained spatial dynamic range is displayed as a function of the imposed one (i.e. $1/\alpha$), in dB, for different values of N. It is apparent how, when the number of transmit antennas is equal to the number of users (fixed to 5), the attained spatial dynamic range is larger than the required one for almost all the simulated values. In other words, in this case the WPPMLB problem (4.3) turns out not to be feasible for all the symbols and channel realizations[6], unless the imposed spatial dynamic range is very large (over 7 dB). It can be also noticed how, due to the infeasibility of the optimization problem, the attained spatial dynamic range shows even a decreasing trend with $1/\alpha$

[5] This does not apply for the results in Figs. 4.6, 4.8, where the power-SINR dependence is studied.

[6] This implies that the lower bound constraints on the power are not met in average, as clear from the displayed result.

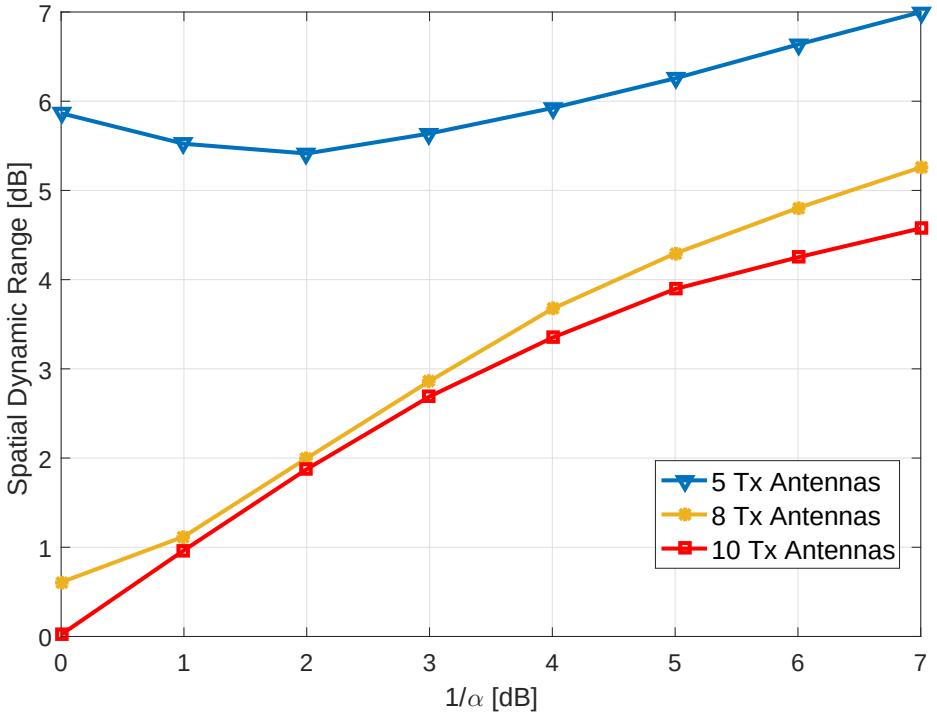

FIGURE 4.2: Attained spatial dynamic range, in dB, versus imposed one in dB.

when the latter is below 2 dB. This means that, in the case of 5 antennas, reducing too much the imposed spatial dynamic range can even worsen the performance. On the other hand, by increasing N the optimization problem is relaxed, and it is possible to respect the imposed constraints also with a reduced spatial dynamic range, as it is visible from the results obtained with $N = 8$ and $N = 10$. Remarkably, in the latter case the problem is feasible even when a unit spatial dynamic range (0 dB) is imposed. The dependency of the problem feasibility on the imposed spatial dynamic range and on the number of antennas is further shown in Fig. 4.3, where the probability of success in solving the WPPMLB problem is shown. This quantity, which is the probability of respecting the imposed constraint on the spatial dynamic range, is calculated through a Monte Carlo simulation over the multiple channel and symbols realizations. This figure shows how the probability of success is low for $N = 5$, and how it strongly decreases when $1/\alpha$ is reduced. This explains the decreasing trend observed in Fig. 4.2 for $1/\alpha$ below 2 dB. Increasing the number of transmit antennas the probability of success increases considerably, becoming basically 1 for any imposed spatial dynamic range when $N = 10$.

In Fig. 4.4 the total transmit power, in dBW, is shown as a function of the imposed spatial dynamic range, for 8 and 10 transmit antennas. The case with only 5 antennas is not considered, since the problem is not feasible for basically all the values of $1/\alpha$, as previously discussed. It can be seen how the configuration with $1/\alpha = 0$ dB requires a

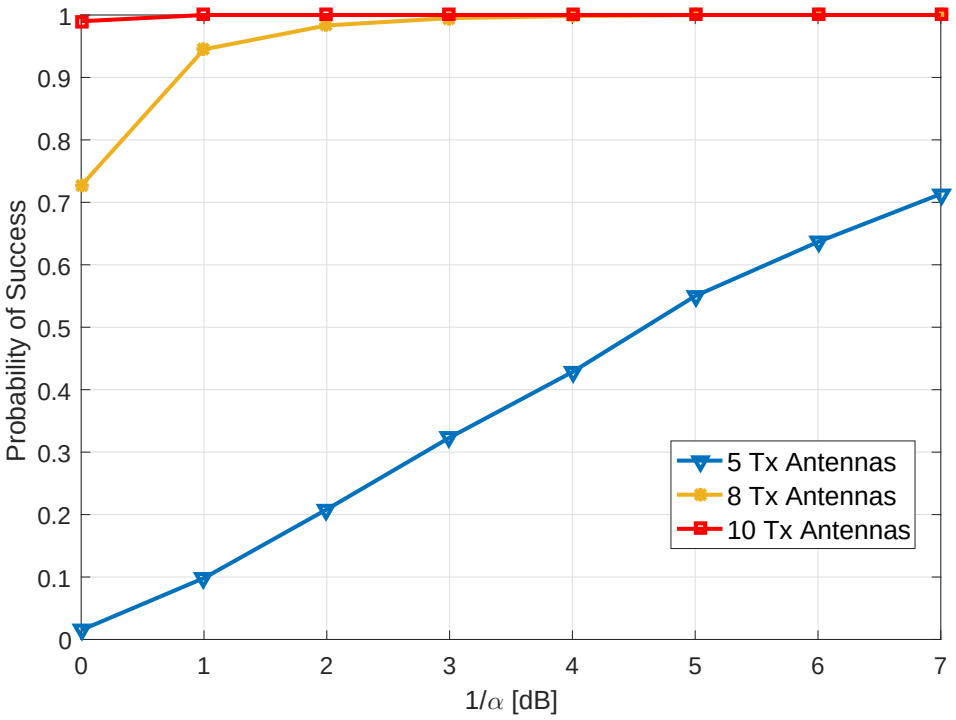

FIGURE 4.3: Probability of success versus imposed spatial dynamic range in dB.

high transmit power[7], because of the very tight constraint, especially in the case with 8 antennas. Nevertheless, the result shows how a relaxation of the constraint on the imposed spatial dynamic range, as well as an increase in the number of antennas, allows to reduce the transmit power. Such behavior is due to an increase of the degrees of freedom of the optimization problem when the constraint is relaxed or more antennas are used.

4.4.2 Performance of SPAPR-Min Scheme with respect to the Number of Tx Antennas

Herein, the dependency of the performance of the SPAPR-Min scheme on the number of transmit antennas N is examined. This dependency can be seen in Fig. 4.5, which displays the attained SPAPR and the total transmit power as functions of N. Similarly to the previous problem, also here we can observe how increasing the number of transmit antennas implies better performance. In particular, the attained SPAPR decreases when N increases, reaching the theoretical lower bound of 0 dB for $N \geq 9$. Moreover, the total transmit power sensibly decreases when N increases.

[7]However, it should be kept in mind that a reference scenario with unit noise variance at the receivers' side is assumed, so the results in terms of transmit power shall be interpreted more in a comparative fashion than in an absolute way.

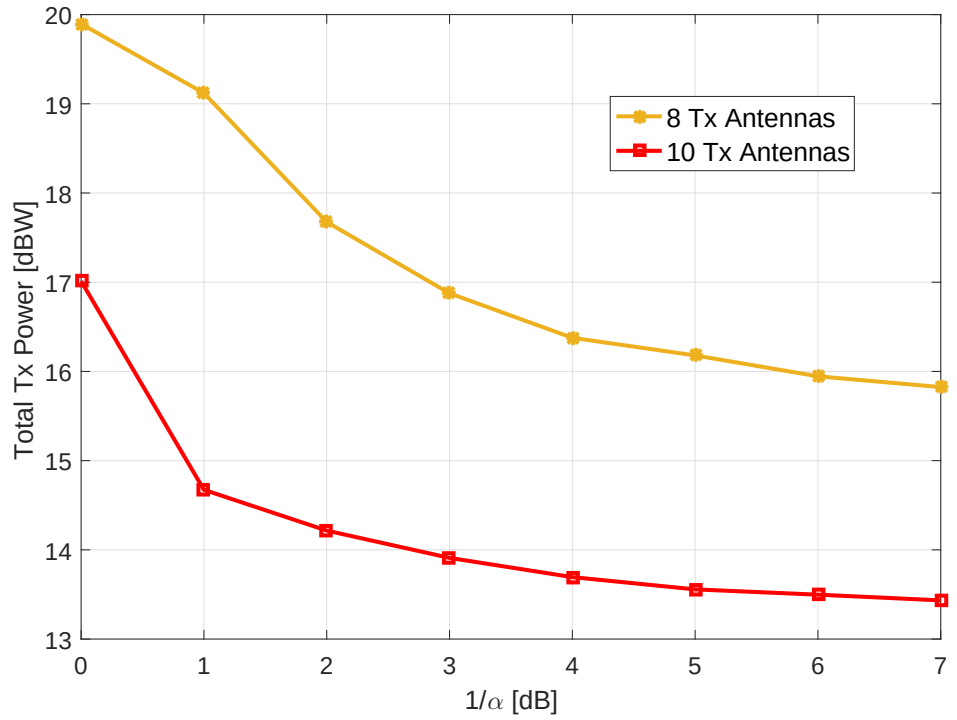

FIGURE 4.4: Total transmit power, in dBW, versus imposed spatial dynamic range in dB.

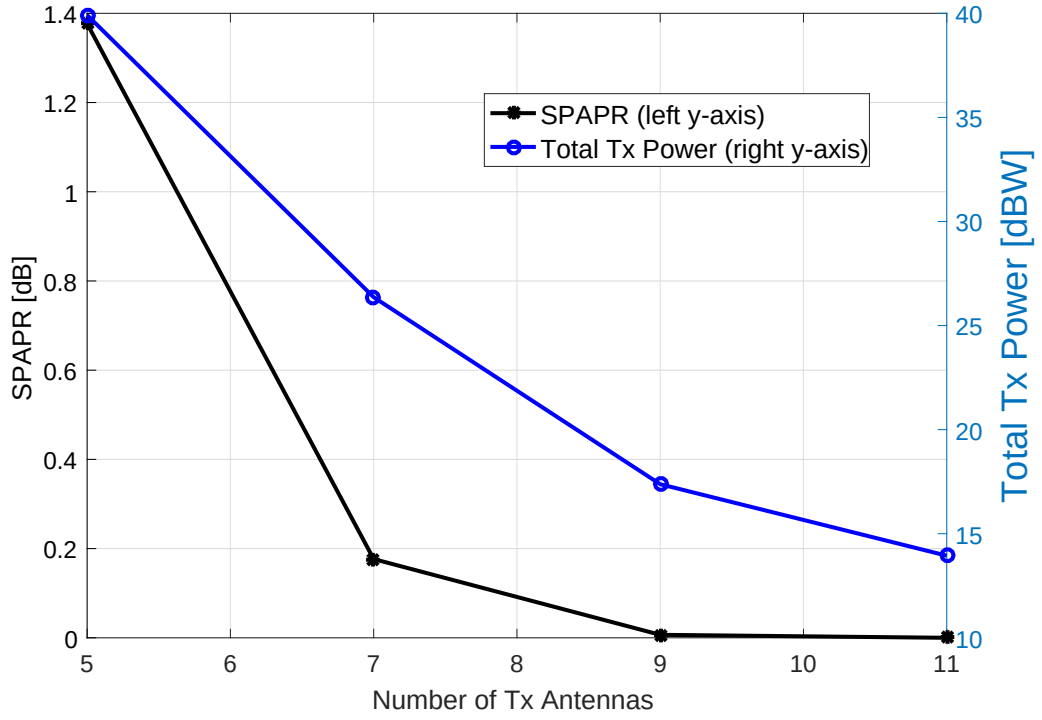

FIGURE 4.5: Attained SPAPR, in dB, versus number of transmit antennas.

TABLE 4.2: Summary of the considered SLP techniques.

Technique Acronym	Extended Name	Problem Ref.
WPPMLB	Weighted Peak Power Minimization with Lower Bound	(4.3)
SPAPR-Min	Spatial Peak-to-Average Power Ratio Minimization	(4.10)
PPM	Peak Power Minimization	(4.25)
SPM	Sum Power Minimization	(4.24)

4.4.3 Comparative Performance Analysis

Hereafter, some comparative simulation results are discussed for the proposed techniques, i.e. WPPMLB and SPAPR-Min. Unless specified otherwise, the number of transmit antennas is fixed to 10, allowing additional degrees of freedom in the optimization problems to be exploited, and the imposed spatial dynamic range in the WPPMLB approach is fixed to 1 dB (i.e., $\alpha = -1$ dB)[8].

In the context of symbol-level precoding, the considered benchmarks are the sum power minimization (SPM) scheme [22, 23] and the peak power minimization (PPM) of chapter 3. For the sake of completeness, a multi-level formulation for the SPM and the PPM optimization problems, respectively, is provided in the following:

$$\begin{aligned} \boldsymbol{x}(\boldsymbol{d},\boldsymbol{H},\boldsymbol{\gamma}) = \arg\min_{\boldsymbol{x}} \quad & \|\boldsymbol{x}\|^2 \\ \text{s.t.} \quad \mathcal{C}1: \quad & |\boldsymbol{h}_j\boldsymbol{x}|^2 \ \trianglerighteq \kappa_j^2\gamma_j\sigma_z^2, \ j=1,\ldots,K, \\ \mathcal{C}2: \quad & \angle\boldsymbol{h}_j\boldsymbol{x} = \angle d_j, \ j=1,\ldots,K, \end{aligned} \tag{4.24}$$

$$\begin{aligned} \boldsymbol{x}(\boldsymbol{d},\boldsymbol{H},\boldsymbol{\gamma}) = \arg\min_{\boldsymbol{x}} \max_{i=1,\ldots,N} \quad & \{|x_i|^2\} \\ \text{s.t.} \quad \mathcal{C}1: \quad & |\boldsymbol{h}_j\boldsymbol{x}|^2 \ \trianglerighteq \kappa_j^2\gamma_j\sigma_z^2, \ j=1,\ldots,K, \\ \mathcal{C}2: \quad & \angle\boldsymbol{h}_j\boldsymbol{x} = \angle d_j, \ j=1,\ldots,K. \end{aligned} \tag{4.25}$$

For the sake of clarity, all the considered SLP schemes are summarized in Table 4.2, with their acronyms and the reference to the respective optimization problems.

First of all, let us focus on the achieved performance in terms of spatial dynamic range and SPAPR, which are summarized in Table 4.3. The displayed values show a substantial gain of the proposed schemes with respect to the benchmarks, especially in terms of

[8] However, it may be set to any value depending on the specific non-linear scenario at hand.

TABLE 4.3: Comparison of the spatial dynamic range and SPAPR values for the different schemes.

	SPAPR-Min	WPPMLB	PPM	SPM
Spatial Dynamic Range [dB]	0	1	5.1	14.4
SPAPR [dB]	0	0.2	0.6	4.7

spatial dynamic range, which turns out extremely high when the SPM scheme is used. As already observed, the SPAPR-Min approach is able to reach the lower bound for the spatial dynamic range and the SPAPR. It should be highlighted that this is also possible with the WPPMLB approach by properly setting α to 0 dB, which would come of course with a higher transmit power required, according to the trade-off shown in Fig. 4.4. Actually, the strength of the WPPMLB approach lies in its flexibility which allows to cope with systems having different requirements, realizing a trade-off between imposed spatial dynamic range and consumed power.

In Fig. 4.6 the total transmit power, in dBW, is shown as a function of the target SINR, in dB, for the considered techniques. As expectable, the power requirements of the proposed schemes are higher with respect to the benchmarks. In particular, the SPAPR-Min scheme requires a higher total power than the WPPMLB one. Moreover, Fig. 4.7 displays the average power transmitted by each antenna for the different schemes at hand, for a fixed channel realization. This result allows to better visualize the trade-off of the proposed precoding approaches, which produce a more uniform power distribution amongst the antennas at the expense of a higher consumed power. It shall be highlighted how the more uniform power distribution attained by the proposed approaches implies better performance with respect to the benchmarks (SPM and PPM), over a generic non-linear channel. This is clearly quantified in SER analysis presented later on in this section.

In order to give further insights on the proposed symbol-level precoding schemes, let us also consider herein a comparison with the constant envelope precoding of [29]. By construction, this approach designs waveforms with 0 dB dynamic range (both in space and in time), but it does not achieve the constructive interference effect of the symbol-level schemes at hand. This can be seen in Fig. 4.8, where the achieved average SINR at the users, in dB, is compared between the different approaches, as a function of the total transmit power in dBW. In fact, it can be noted that an increase in the transmit power, which in turn implies an increase in the interference level, enhances the constructive interference effect in the symbol-level schemes, and results in a considerable gain in the attained SINR. On the other hand, in the scheme of [29] the interference is harmful,

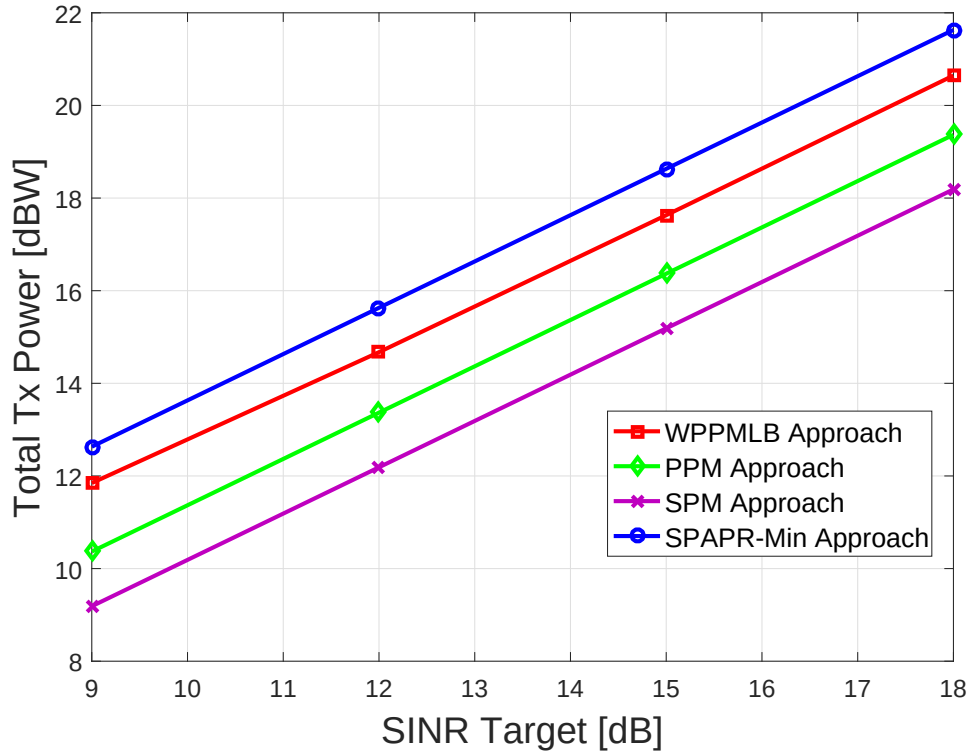

FIGURE 4.6: Total transmit power, in dBW, versus target SINR, in dB.

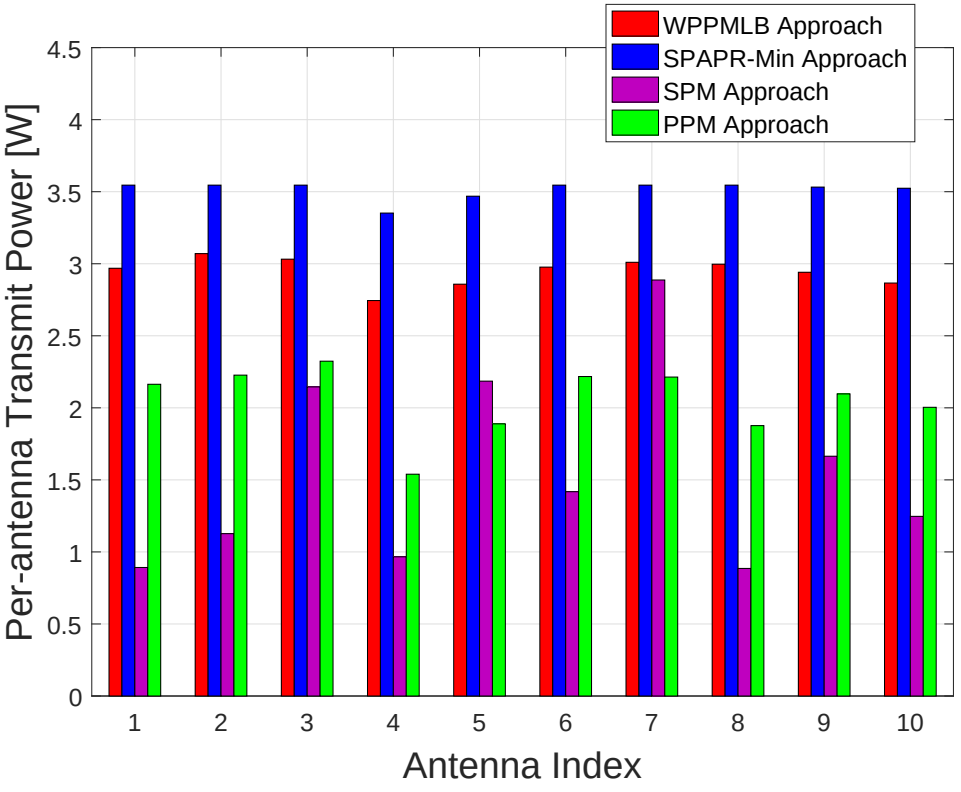

FIGURE 4.7: Per-antenna average power, in W, for a fixed channel realization.

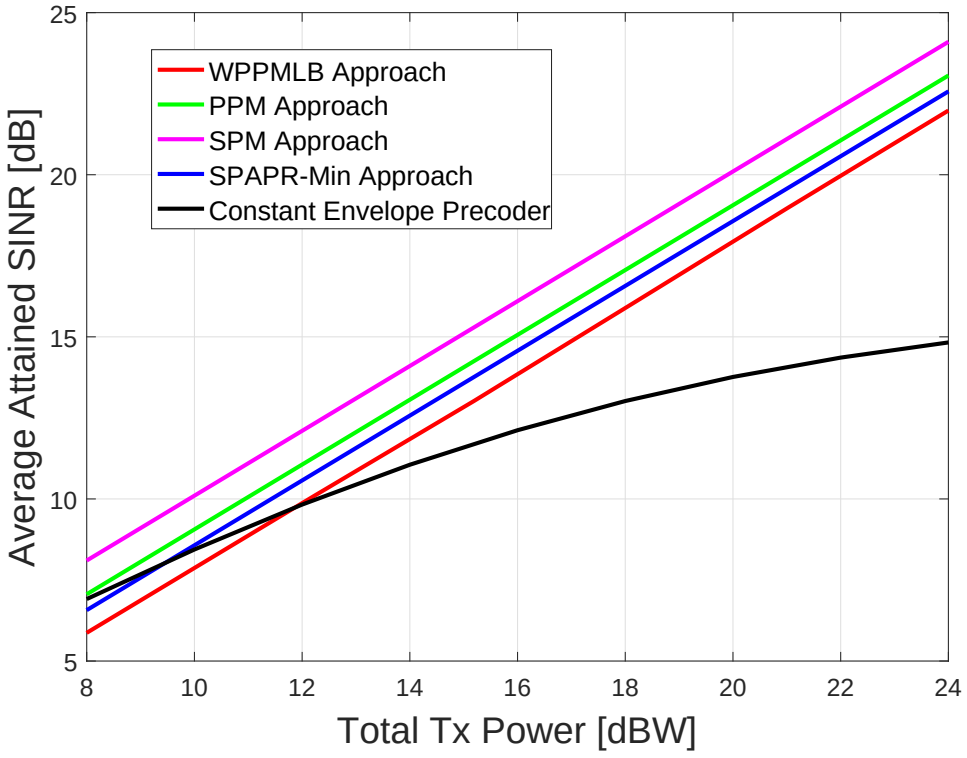

FIGURE 4.8: Average achieved SINR, in dB, versus total transmit power, in dBW.

thus the SINR has a slower growth when the transmit power increases. In particular, in the case of [29] one can observe a saturation effect of the SINR curve for high transmit power, which results in a maximum achievable SINR. In the remainder of this section, the comparison with the scheme of [29] is also presented in term of SER over a non-linear channel.

In Figs. 4.9-4.10 a comparative result in terms of SER is given. In particular, these results present the SER achieved at the users' side when the schemes at hand are applied over a channel corrupted by non-linearities (besides the MUI and the AWGN), considering a case with 8 transmit antennas and a case with 10 transmit antennas, respectively. This analysis allows to evaluate the overall effectiveness of the proposed techniques with respect to the differential phase shift effect. The results have been obtained by simulating $S = 3000$ symbol slots and considering, for both cases, a fixed realization for the channel matrix and a target SINR of 12 dB[9]. The non-linear model of Fig. 2.7 has been considered for the simulations[10]. In order to apply the non-linear characteristics,

[9]This target SINR is also considered for the approach of [29], although in this case it is not always guaranteed that this threshold is achieved, because of the saturation effect of the SINR with the increasing power.

[10]It should be mentioned that the absolute average phase rotation, given by the PM characteristic of the amplifiers, is assumed estimated and compensated at the receiver side, based on pilot symbols. This phase recovery and compensation is a necessary operation, without which the detection process cannot proceed, and is normally easy to perform, since it is referred to the average phase shift.

the transmitted waveforms have been modeled by oversampled discrete sequences, by applying a pulse shaping operation to the generated symbols, for each antenna. The pulse shaping operation is performed using a unit energy symmetric pulse waveform $g(t)$. Denoting by T the symbol period and by ξ the oversampling factor, the transmitted waveform for the generic i-th antenna can be represented through its discrete samples spaced by $t_s = \frac{T}{\xi}$, as follows:

$$x_i^{\text{ovs}}[lt_s] = \sum_{n=0}^{S-1} x_i[n] g[lt_s - nT], \quad l = 0, \ldots, \xi S - 1, \tag{4.26}$$

where n indexes the S symbols while l indexes the samples. At the generic j-th user, in order to obtain the received signal in the symbol domain, a matched filtering and downsampling operation is applied to the oversampled received waveform $y_j^{\text{ovs}}[lt_s]$, as follows:

$$y_j[n] = \sum_{l=0}^{\xi S-1} y_j^{\text{ovs}}[lt_s] g[lt_s - nT], \quad n = 0, \ldots, S - 1. \tag{4.27}$$

The pulses $g(t)$ considered for the simulations are square-root-raised-cosine (SRRC) with a roll-off factor of 0.25, and the oversampling factor ξ has been set to 10.

The figures show the obtained SER as a function of the input back-off (IBO), in dB, applied to the signal feeding the non-linear amplifiers. The shape of the obtained curves can be explained by considering that, in general, rescaling the average power of the transmit signals (i.e., applying a back-off with respect to the saturation point of the amplifiers) allows to mitigate the non-linear effects, and therefore to improve the SER performance. On the other hand, the back-off operation reduces the SINR, hence a very high IBO tends to increase the achieved SER. Ultimately there is a trade-off, and the optimal IBO can be identified as the one minimizing the SER.

In both the cases with 8 and 10 antennas, it is visible how the proposed approaches allow to achieve an improved SER with respect to the symbol-level precoding benchmarks, i.e., the PPM approach and the SPM approach[11]. Furthermore, it can be noted that, in most of the simulated cases, the proposed techniques allow the non-linear amplifiers to operate with a lower IBO in the optimal operating point. Interestingly, it turns out that the SPAPR-Min scheme slightly outperforms the WPPMLB one, even when a spatial dynamic range of 0 dB is imposed in the latter. It is conjectured that this is due to

[11] The attained SER values can be reduced by increasing the SINR target. Moreover, although channel coding is out of the scope of this work, it should be noted that a forward error correction (FEC) scheme can strongly boost the overall performance in terms of bit error rate. A study of the proposed schemes including FEC is foreseen in future work.

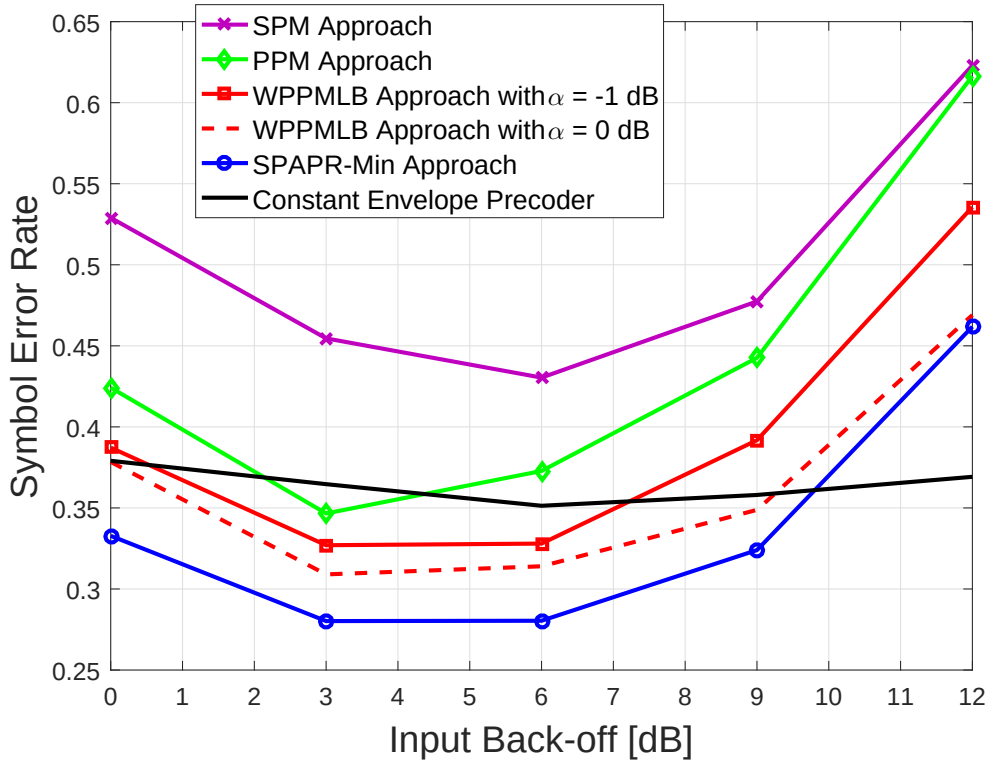

FIGURE 4.9: Achieved SER versus IBO, in dB, for a channel with 5 users and 8 antennas.

a better constructive interference effect taking place with the SPAPR-Min scheme, or even to an improved dynamic in the temporal dimension experienced in such scheme.

The comparison of the proposed schemes with the constant envelope precoder of [29] needs a separate discussion. Remarkably, in the case with 8 antennas of Fig. 4.9, the proposed approaches outperform the constant envelope precoder in terms of achieved SER. As a matter of fact, the numerical analysis has revealed that the maximum SINR achievable by [29] in this scenario is around 9 dB, due to the aforementioned saturation effect of the SINR. Therefore, the constant envelope precoder cannot guarantee the target SINR of 12 dB. However, the symbol level schemes are able to achieve the guaranteed SINR target. As a result, a better SER performance is attained by the proposed schemes. The situation changes in the case with 10 antennas of Fig. 4.10. In fact, in turns out that in this scenario the constant envelope scheme can guarantee the target SINR of 12 dB, as well as the proposed schemes. As a consequence, the advantage of [29] in terms of dynamic range of the waveforms (it achieves constant envelope waveforms in space and time) dominates, and a better SER performance is obtained. It can be concluded that the number of antennas is an important factor in the choice of one scheme over the other. Further, the target SINR is also a relevant factor in the choice, since the scheme in [29] presents a saturation effect (as also shown in Fig. 4.8).

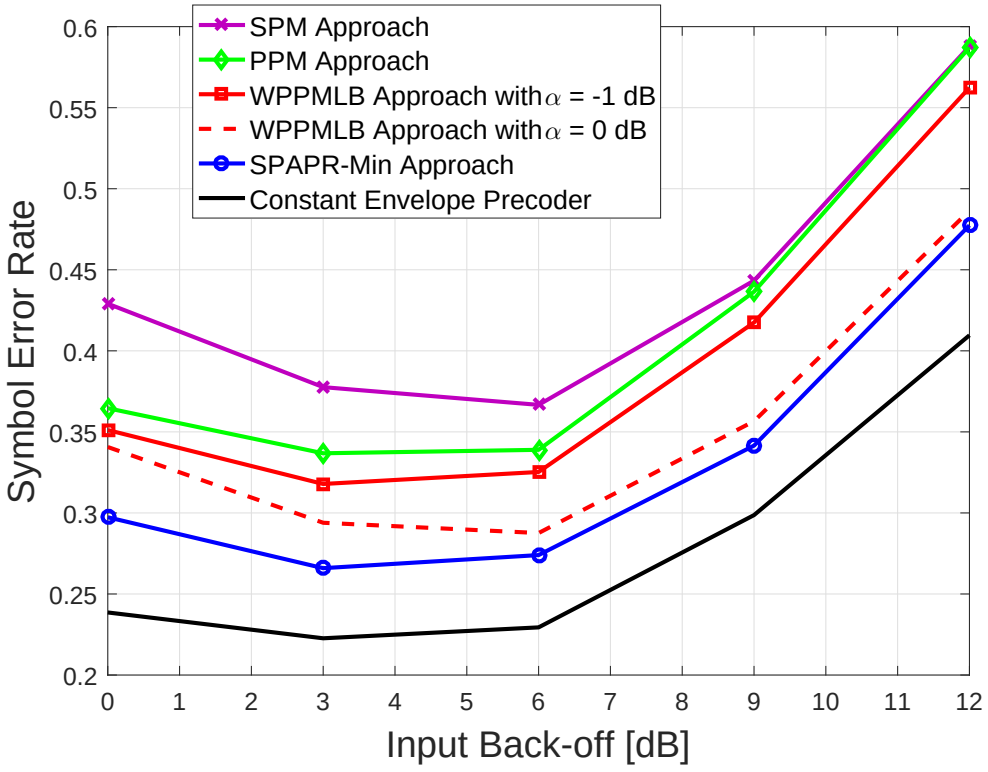

FIGURE 4.10: Achieved SER versus IBO, in dB, for a channel with 5 users and 10 antennas.

4.4.4 Out-of-band Radiation

A final remark about the proposed precoding schemes is related to the out-of-band radiation. In fact, it is well known that the non-linear relation (2.15) widens the spectrum of the amplified waveforms, determining the transmission of power outside the pulse bandwidth. Considering the signal transmitted by one of the antennas when a 3 dB IBO is applied, Fig. 4.11 compares the related power spectral density at the output of the non-liner amplifier, for the symbol-level precoding approaches at hand, together with the case of a non-precoded waveform. Interestingly, it emerges how the proposed approaches (WPPM, WPPMLB and SPAPR-Min) determine a moderately higher out-of-band radiation with respect to the SPM precoding case and the non-precoded one. This can be explained by considering that the introduced techniques are not improving the signals dynamic properties in the time dimension. Accordingly, a reduction of the out-of-band radiation was out of the scope of this work. Nonetheless, it shall be noted how the relative level of the out-of-band radiation with respect to the in-band radiation for the proposed techniques is comparable with the non-precoded case. Finally, the DC level observable in the WPPMLB case reveals an asymmetric shape for the transmit constellations produced by this approach.

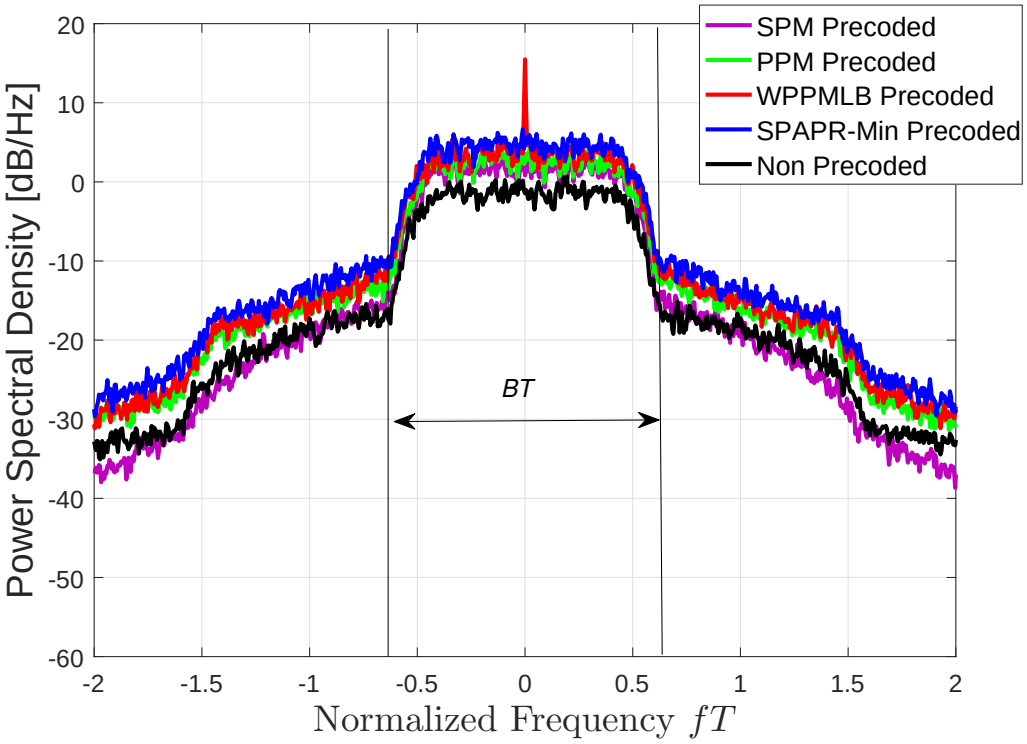

FIGURE 4.11: Power spectral density of the output signals with the proposed approaches for a 3 dB IBO; the normalized frequency fT is considered, with T being the symbol period; the pulse bandwidth is $BT = 1.25$.

4.4.5 Numerical Evaluation of the Complexity

This section is concluded by providing a numerical evaluation of the complexity of the proposed algorithms[12]. First of all, Table 4.4 quantifies the average number of iterations required for convergence in the WPPMLB scheme and in the SPAPR-Min one, considering the cases with 8 and 10 transmit antennas. Moreover, the symbol-level precoding algorithms are compared in Fig. 4.12 in terms of average total running time, based on simulations over the same machine, as a function of the number of transmit antennas. The WPPMLB technique is considered with $\alpha = 0$ dB, -1 dB, and -3 dB. The most evident outcome is the impressive increase in the running time of the proposed schemes with respect to the benchmarks, which is clearly due to the increased complexity and to the fact that multiple iterations have to be performed. It is also worth noticing how in the SPAPR-Min scheme the number of iterations and the total running time decrease when the number of antennas is increased, while in the WPPMLB scheme such numbers increase with N, for $\alpha = -1$ dB and $\alpha = -3$ dB[13]. Interestingly, the case with $\alpha = 0$ has a different behavior. It is conjectured that this is due to the reduced number of

[12]The complexity of the SPM scheme is also discussed in [22].

[13]A possible explanation of this fact is that a higher N gives more degrees of freedom to the SPAPR-Min optimization problem (4.13), without increasing the number of its constraints, which depends only

TABLE 4.4: Avg. Number of Iterations.

	$N = 8$	$N = 10$
WPPMLB $\alpha = 0$ dB	15.4	10.4
WPPMLB $\alpha = -1$ dB	10.9	11.9
WPPMLB $\alpha = -3$ dB	8.8	10.1
SPAPR-Min	14.4	5.9

feasible instances of the optimization problem in this edge case, which depends on N as discussed in section 4.4.1 and, in turn, affects the running time.

Overall, it turns out that the proposed techniques are suitable for systems that can afford to use a considerable computing capability to have improved performance over non-linear channels. For systems with a very high number of transmitting elements, e.g. large-scale antenna arrays, the SPAPR-Min scheme should be preferred to the WPPMLB one if the affordable computing capability is limited, since in the former strategy the number of required iterations, and accordingly the running time, results much lower. Whenever the computational complexity is a major limitation, the proposed PPM scheme can be considered in order to cope with the non-linear effects in a simpler fashion.

4.5 Conclusions

In this chapter, two novel strategies for SLP have been proposed, aiming at controlling the per-antenna instantaneous transmit power and at limiting the power imbalances across the different RF chains. A first proposed scheme (WPPMLB) performs a weighted per-antenna power minimization, imposing a lower bound to the power carried by each transmitted stream. A second scheme (SPAPR-Min) performs the minimization of the spatial peak-to-average power ratio. Both the approaches allow to reduce the spatial dynamic of the transmitted waveforms, besides exploiting the constructive interference as in other symbol-level strategies available in the literature. Such feature, which is novel in the context of symbol-level precoding, makes these techniques particularly relevant in systems affected by non-linear impairments. More specifically, they allow to deal with the problem of differential phase shift, which is characterized in the contribution. The performance of the proposed schemes has been assessed through numerical results in terms of spatial dynamic range, spatial peak-to-average power ratio and symbol error rate, in comparison with state of the art symbol-level precoding techniques. The results

on K. On the other hand, in the case of the WPPMLB optimization problem (4.8), a higher N increases also the number of constraints, besides allowing more degrees of freedom.

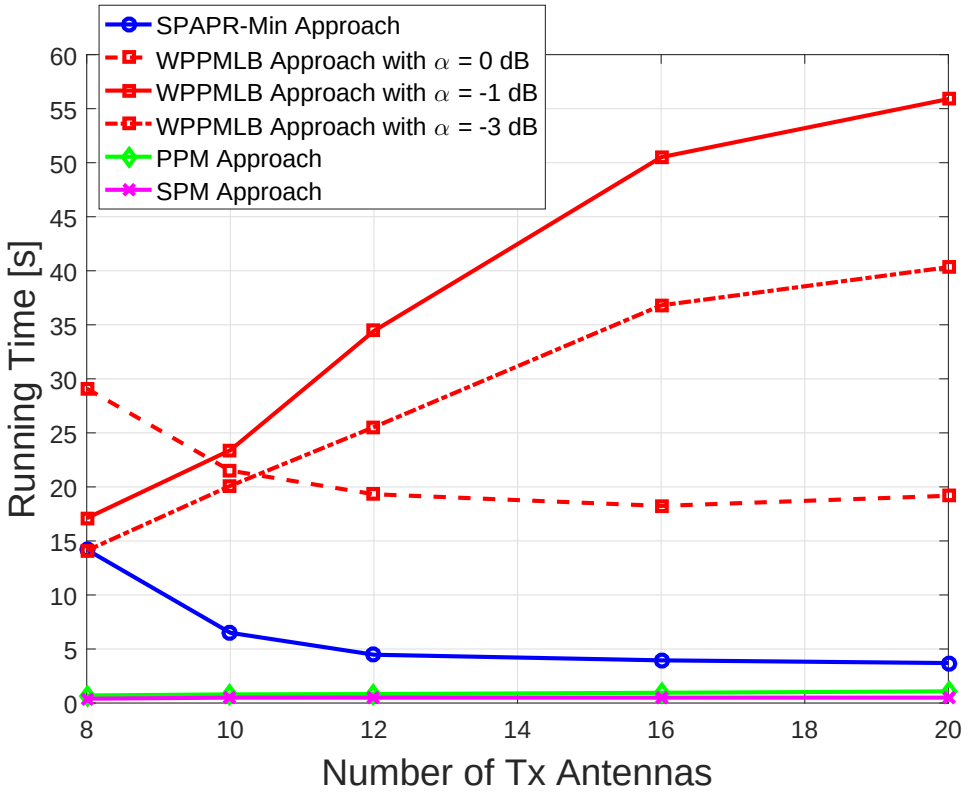

FIGURE 4.12: Average running time per iteration, in s, vs. number of transmit antennas.

show how the novel strategies outperform the existent symbol-level approaches with respect to the mentioned metrics. They also motivate using more transmit antennas than served users to improve the waveform characteristics of the transmitted signal. The WPPMLB scheme has been shown more flexible than the SPAPR-Min one, which however is able to achieve a slightly lower SER.

Part II

Spatio-temporal Symbol-level Precoding

Chapter 5

PAPR Minimization through Spatio-temporal Symbol-level Precoding

In practical multi-user multiple-input single-output (MISO) systems, the performance degradation induced by the non-linear amplification stage depends on the power variation of the signals both in the temporal and in the spatial dimensions. As already discussed, the latter one is referred to the variation of the instantaneous transmit power among the different antennas, which causes the problem of differential phase shift. The symbol-level precoding (SLP) schemes introduced in the previous chapters of this thesis tackle this problem by reducing the instantaneous power imbalances among the antennas, for each symbol slot. Nonetheless, these SLP schemes fail at improving the power dynamic of the waveforms in the temporal dimension, which is fundamental with respect to non-linearities, since they work on a symbol-by-symbol basis. In order to fill this gap, this chapter proposes a new SLP method, referred to as spatio-temporal SLP, which is able to optimize the power dynamic of the waveforms both in the spatial and in the temporal dimensions, thus further improving the robustness of the signals to non-linear effects. Specifically, the proposed strategy performs a minimization of the spatio-temporal peak-to-average power ratio (PAPR) of the transmitted waveforms, under Quality-of-Service (QoS) constraints, for multi-level modulation schemes. The related optimization problem can be formulated similarly to the spatial PAPR minimization of chapter 4, therefore it is addressed resorting once more to parametric programming and successive convex approximation (SCA). The optimization takes into account the oversampled waveforms, by modeling the pulse shaping operation at each antenna.

5.1 System Model

Let us consider a single-cell multiple-antenna downlink scenario, where a base-station delivers K independent data streams to K single-antenna user terminals through N transmit antennas, with $N \geq K$. Each data stream is divided in blocks of S symbols, and the channel is assumed to be quasi-static flat fading. Considering a data block, one can define the data information matrix $\boldsymbol{S} = [\boldsymbol{s}_1^T \dots \boldsymbol{s}_K^T]^T \in \mathbb{C}^{K \times S}$, which aggregates the symbol streams to be delivered to the different users. Similarly, the matrix $\boldsymbol{D} = [\boldsymbol{d}_1^T \dots \boldsymbol{d}_N^T]^T \in \mathbb{C}^{N \times S}$ aggregates the precoded symbol streams feeding the transmit filters. In fact, each symbol stream has to undergo pulse shaping before the actual transmission. The pulse shaping operation is performed using a unit energy symmetric pulse waveform[1] $\alpha(t)$. Denoting by T the symbol period and by ξ the oversampling factor, the transmitted waveform for the generic n-th antenna can be represented through its discrete samples spaced by $t_s = \frac{T}{\xi}$, as follows:

$$x_n[l] = \sum_{i=1}^{S} d_n[i]\alpha[(l-1)t_s - (i-1)T], \quad l = 1, \dots, \xi S, \tag{5.1}$$

where $d_n[i]$ is the i-th element of the symbol vector $\boldsymbol{d}_n$, which in turn is the n-th row of $\boldsymbol{D}$. Such relation can be rewritten in a compact matrix form as:

$$\boldsymbol{x}_n = \boldsymbol{d}_n \boldsymbol{A}_{\mathrm{TX}}, \tag{5.2}$$

where $\boldsymbol{x}_n \in \mathbb{C}^{1 \times \xi S}$ represents the output data stream (in the oversampled domain) from the n-th antenna and $\boldsymbol{A}_{\mathrm{TX}} \in \mathbb{R}^{S \times \xi S}$ is a block Toeplitz matrix modeling the pulse shaping operation, with its (i,l)-th element being:

$$[\boldsymbol{A}_{\mathrm{TX}}]_{(i,l)} = \alpha[(l-1)t_s - (i-1)T]. \tag{5.3}$$

By aggregating the output (oversampled) signals from all the antennas in a matrix $\boldsymbol{X} = [\boldsymbol{x}_1^T \dots \boldsymbol{x}_N^T]^T \in \mathbb{C}^{N \times \xi S}$, the pulse shaping operation can be represented in a compact matrix form as $\boldsymbol{X} = \boldsymbol{D}\boldsymbol{A}_{\mathrm{TX}}$.

According to the well-known multi-user MISO channel model, the received symbols at the users can be written in matrix form as:

$$\tilde{\boldsymbol{Y}} = \boldsymbol{H}\boldsymbol{X} + \tilde{\boldsymbol{Z}},$$

[1] The symmetry of the pulse is not a strict requirement for the system model. However, this assumption has been made in order to simplify the notation, and taking also into account that it is often met in practice (for example for SRRC pulses).

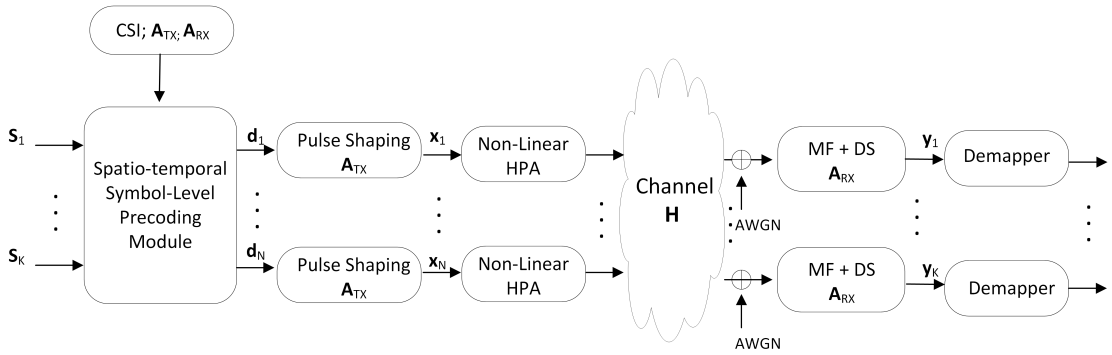

FIGURE 5.1: Block scheme of the considered system model relying on spatio-temporal SLP.

where the matrix $\tilde{\boldsymbol{Y}} = [\tilde{\boldsymbol{y}}_1^T \dots \tilde{\boldsymbol{y}}_K^T]^T \in \mathbb{C}^{K \times n_s S}$ represents the received samples at the K users, $\boldsymbol{H} = [\boldsymbol{h}_1^T \dots \boldsymbol{h}_K^T]^T \in \mathbb{C}^{K \times N}$ is the channel matrix modeling the interference among the different data streams, and $\tilde{\boldsymbol{Z}} = [\tilde{\boldsymbol{z}}_1^T \dots \tilde{\boldsymbol{z}}_K^T]^T \in \mathbb{C}^{K \times \xi S}$ models the additive white Gaussian noise (AWGN). In order to obtain the received signals at the users in the symbol domain, the matched filtering and downsampling operation needs to be modeled. This can be done again in a matrix form, using the block Toeplitz matrix $\boldsymbol{A}_{\mathrm{RX}} \in \mathbb{R}^{\xi S \times S}$, which can be defined in the same fashion of (5.3). Overall, grouping the received symbols at the K users in a matrix $\boldsymbol{Y} = [\boldsymbol{y}_1^T \dots \boldsymbol{y}_K^T]^T \in \mathbb{C}^{K \times S}$, the global communication model can be written as:

$$\boldsymbol{Y} = \tilde{\boldsymbol{Y}} \boldsymbol{A}_{\mathrm{RX}} = \boldsymbol{H}\boldsymbol{X}\boldsymbol{A}_{\mathrm{RX}} + \tilde{\boldsymbol{Z}}\boldsymbol{A}_{\mathrm{RX}} = \boldsymbol{H}\boldsymbol{D}\boldsymbol{A} + \boldsymbol{Z}, \tag{5.4}$$

where $\boldsymbol{A} = \boldsymbol{A}_{\mathrm{TX}}\boldsymbol{A}_{\mathrm{RX}} \in \mathbb{R}^{S \times S}$ represents the combination of the filters at the transmitter and at the receiver, while $\boldsymbol{Z} = \tilde{\boldsymbol{Z}}\boldsymbol{A}_{\mathrm{RX}} \in \mathbb{C}^{K \times S}$ is the noise in the symbol domain. Without loss of generality, the noise power is assumed to be 1.

As discussed in section 2.3 of chapter 2, it should be taken into account how the system model introduced in (5.4) is actually degraded by the non-linear effects introduced by the per-antenna high-power amplifiers (HPAs). In line with the previous chapters, the traveling-wave tube amplifier (TWTA) model introduced in Fig. 2.7 will be used as a practical reference[2]. The complete system model is represented in the block scheme of Fig. 5.1, where it is clear how the symbol matrix $\boldsymbol{D}$ is obtained as output of a spatio-temporal precoding module, which takes as input the channel state information (CSI), i.e. an estimate of $\boldsymbol{H}$, the filters matrices $\boldsymbol{A}_{\mathrm{TX}}$ and $\boldsymbol{A}_{\mathrm{RX}}$ and the data information matrix $\boldsymbol{S}$. Differently than in the previous chapters, the model in (5.4) represents the signals not only in the spatial dimension (i.e., how they vary between the antennas), but also in the temporal dimension, considering a whole block of S symbols per stream

[2]However, it should be stressed that the proposed scheme is general and applies to any non-linear model.

and the oversampled transmitted waveforms through $\boldsymbol{X}$. This feature allows to take an important step forward in SLP towards counteracting the non-linear effects. In fact, with the introduced model it is possible to design the matrix $\boldsymbol{D}$, namely the precoded symbol streams feeding the transmit filters, by optimizing the power dynamic of the transmitted samples $\boldsymbol{X}$ both in the spatial and in the temporal dimensions, thus making the signals more robust to non-linear effects.

In order to facilitate the formulation of the proposed optimization scheme, discussed in the next section, it is convenient to further manipulate the model of (5.4) by vectorizing the introduced signal matrices over the temporal dimension (rows first). Hence, the data information streams can be modeled through the vector $\boldsymbol{s} = \text{vec}(\boldsymbol{S}^T) = [\boldsymbol{s}_1 \dots \boldsymbol{s}_K]^T \in \mathbb{C}^{KS\times 1}$, the designed symbol streams through $\boldsymbol{d} = \text{vec}(\boldsymbol{D}^T) = [\boldsymbol{d}_1 \dots \boldsymbol{d}_K]^T \in \mathbb{C}^{NS\times 1}$, the transmitted signals through $\boldsymbol{x} = \text{vec}(\boldsymbol{X}^T) = [\boldsymbol{x}_1 \dots \boldsymbol{x}_N]^T \in \mathbb{C}^{N\xi S\times 1}$, the noise through $\boldsymbol{z} = \text{vec}(\boldsymbol{Z}^T) = [\boldsymbol{z}_1 \dots \boldsymbol{z}_K]^T \in \mathbb{C}^{KS\times 1}$, and the received symbols through $\boldsymbol{y} = \text{vec}(\boldsymbol{Y}^T) = [\boldsymbol{y}_1 \dots \boldsymbol{y}_K]^T \in \mathbb{C}^{KS\times 1}$. It is straightforward to check that the relation between $\boldsymbol{d}$ and $\boldsymbol{x}$ can be written as:

$$\boldsymbol{x} = (\boldsymbol{I}_N \otimes \boldsymbol{A}_{\text{TX}}^T)\boldsymbol{d}. \tag{5.5}$$

Further, by introducing the matrix $\hat{\boldsymbol{X}} = \boldsymbol{X}\boldsymbol{A}_{\text{RX}} = \boldsymbol{D}\boldsymbol{A} \in \mathbb{C}^{N\times S}$ and its vectorized version $\hat{\boldsymbol{x}} = \text{vec}(\hat{\boldsymbol{X}}^T) \in \mathbb{C}^{NS\times 1}$, and by accounting for (5.4), it is easy to check that $\hat{\boldsymbol{x}} = (\boldsymbol{I}_N \otimes \boldsymbol{A}^T)\boldsymbol{d}$ and that $\boldsymbol{y} = (\boldsymbol{H} \otimes \boldsymbol{I}_S)\hat{\boldsymbol{x}} + \boldsymbol{z}$. Finally, using the mixed-product property of the Kronecker product yields $(\boldsymbol{H} \otimes \boldsymbol{I}_S)(\boldsymbol{I}_N \otimes \boldsymbol{A}^T) = (\boldsymbol{H} \otimes \boldsymbol{A}^T)$, therefore the global communication model can be written as follows:

$$\boldsymbol{y} = (\boldsymbol{H} \otimes \boldsymbol{A}^T)\boldsymbol{d} + \boldsymbol{z} = \boldsymbol{G}\boldsymbol{d} + \boldsymbol{z}. \tag{5.6}$$

This final formulation represents the introduced spatio-temporal system model in a very simple way, formally similar to the spatial model used in the previous SLP literature. The matrix $\boldsymbol{G} = \boldsymbol{H} \otimes \boldsymbol{A}^T \in \mathbb{C}^{KS\times NS}$ is an equivalent representation of the channel matrix in this novel spatio-temporal model, therefore it will be referred to as spatio-temporal channel matrix.

5.2 Spatio-temporal Peak-to-average Power Ratio Minimization

In this section, a SLP scheme relying on the introduced spatio-temporal model is proposed. The scheme performs the minimization of the PAPR of the transmitted waveforms both in the spatial and in the temporal dimensions, under QoS constraints. Moreover, in line with the previous works on SLP [23], it targets a constructive interference effect at each receiver and for each symbol slot. Herein, the formulation is provided assuming an amplitude phase shift keying (APSK) modulation scheme for the data information[3]. The spatio-temporal peak-to-average power ratio (ST-PAPR) can be simply defined, based on the vectorized communication model of (5.6), as:

$$\text{ST-PAPR} = \frac{\|\boldsymbol{x}\|_\infty^2}{\|\boldsymbol{x}\|^2/N}. \tag{5.7}$$

Taking also into account the relation between $\boldsymbol{x}$ and $\boldsymbol{d}$, the optimization problem, referred to as ST-PAPR-Min, can be formulated as a non-linear fractional program as follows:

$$\begin{aligned} \boldsymbol{d}(\boldsymbol{s},\boldsymbol{H},\boldsymbol{A}_{\text{TX}},\boldsymbol{A}_{\text{RX}},\boldsymbol{\gamma}) = \arg\min_{\boldsymbol{d}} \quad & \frac{\|(\boldsymbol{I}_N \otimes \boldsymbol{A}_{\text{TX}}^T)\boldsymbol{d}\|_\infty^2}{\|(\boldsymbol{I}_N \otimes \boldsymbol{A}_{\text{TX}}^T)\boldsymbol{d}\|^2} \\ \text{s.t.} \qquad \mathcal{C}1: \quad & |\boldsymbol{g}_{ji}\boldsymbol{d}|^2 \trianglerighteq \kappa_{ji}^2\gamma_j,\ j=1,\dots,K, i=1,\dots,S, \\ \mathcal{C}2: \quad & \angle \boldsymbol{g}_{ji}\boldsymbol{d} = \angle s_j[i],\ j=1,\dots,K, i=1,\dots,S, \end{aligned} \tag{5.8}$$

where $\boldsymbol{g}_{ji}$ denotes the spatio-temporal channel related to the j-th user for the i-th symbol slot, thus it is the $[(j-1)S+i]$-th row of $\boldsymbol{G}$, and $s_j[i]$ is the i-th element of $\boldsymbol{s}_j$. Further, γ_j is the target signal-to-interference-plus-noise ratio (SINR) that should be granted for the j-th user, $\boldsymbol{\gamma} = [\gamma_1 \dots \gamma_K]^T \in \mathbb{C}^{K\times 1}$ stacks the target SINR for all the users, and $\kappa_{ji} = |s_j[i]|/\sqrt{\mathbb{E}_{j,i}[|s_j[i]|^2]}$ is a magnitude scaling factor for the symbol $s_j[i]$, which allows to account the different amplitudes of the symbols in the multi-level constellation (see also [23]). The notation $\trianglerighteq$ represents a generalized inequality, to be read as $\geq$ or $=$ depending whether the constraint is referred to a boundary symbol or to an inner symbol of the constellation, respectively. The set of constraints $\mathcal{C}1$ represents a QoS constraint for each user, while the set of constraints $\mathcal{C}2$ represents the constructive interference condition, guaranteeing that each user receives the desired data symbol with the correct phase.

[3]However, it can be easily extended to QAM modulations, as in [23] (see also chapter 6).

The optimization problem (5.8) is formally similar to the spatial PAPR minimization problem addressed in section 4.3 of chapter 4. Thus, it can be solved following the same strategy. In particular, as a first step the problem can be rewritten by reformulating the constraints, as follows[4]:

$$\begin{aligned}
\boldsymbol{d}(\boldsymbol{s},\boldsymbol{H},\boldsymbol{A}_{\mathrm{TX}},\boldsymbol{A}_{\mathrm{RX}},\boldsymbol{\gamma}) = \arg\min_{\boldsymbol{d}} \quad & \frac{\|\boldsymbol{x}\|_{\infty}^{2}}{\|\boldsymbol{x}\|^{2}} \\
\text{s.t.} \quad \mathcal{C}1: \quad & \mathrm{Re}(s_j[i])\frac{\boldsymbol{g}_{ji}\boldsymbol{d}+\boldsymbol{d}^{\dagger}\boldsymbol{g}_{ji}^{\dagger}}{2} \trianglerighteq \sqrt{\gamma_j}\,\mathrm{Re}^2(s_j[i]), \\
& j=1,\ldots,K, i=1,\ldots,S, \\
\mathcal{C}2: \quad & \mathrm{Im}(s_j[i])\frac{\boldsymbol{g}_{ji}\boldsymbol{d}-\boldsymbol{d}^{\dagger}\boldsymbol{g}_{ji}^{\dagger}}{2\iota} \trianglerighteq \sqrt{\gamma_j}\,\mathrm{Im}^2(s_j[i]), \\
& j=1,\ldots,K, i=1,\ldots,S, \\
\mathcal{C}3: \quad & (\iota t_{ji}-1)\boldsymbol{g}_{ji}\boldsymbol{d}+(\iota t_{ji}+1)\boldsymbol{d}^{\dagger}\boldsymbol{g}_{ji}^{\dagger}=0, \\
& j=1,\ldots,K, i=1,\ldots,S,
\end{aligned} \tag{5.9}$$

where $t_{ji}=\tan(\angle s_j[i])$, and $\boldsymbol{x}$ has been used in place of $(\boldsymbol{I}_N \otimes \boldsymbol{A}_{\mathrm{TX}}^{T})\boldsymbol{d}$ to simplify the notation.

The formulation in (5.9) is still challenging because of the non-linear fractional objective function. The problem can be solved based on the method followed in chapter 4, by applying in a joint fashion parametric programming [157] and SCA [152]. Accordingly, the function $\|\boldsymbol{x}\|^2$ can be approximated around a generic point $\boldsymbol{z}\in\mathbb{C}^{N\xi S\times 1}$ by a concave (affine) function as:

$$\begin{aligned}
(\boldsymbol{x}-\boldsymbol{z})^{\dagger}(\boldsymbol{x}-\boldsymbol{z}) &= \boldsymbol{x}^{\dagger}\boldsymbol{x}-2\,\mathrm{Re}(\boldsymbol{z}^{\dagger}\boldsymbol{x})+\boldsymbol{z}^{\dagger}\boldsymbol{z}\geq 0 \\
& \boldsymbol{x}^{\dagger}\boldsymbol{x}\geq 2\,\mathrm{Re}(\boldsymbol{z}^{\dagger}\boldsymbol{x})-\boldsymbol{z}^{\dagger}\boldsymbol{z} \\
& \boldsymbol{x}^{\dagger}\boldsymbol{x}\approx 2\,\mathrm{Re}(\boldsymbol{z}^{\dagger}\boldsymbol{x})-\boldsymbol{z}^{\dagger}\boldsymbol{z}.
\end{aligned} \tag{5.10}$$

Using this lower bound approximation, the problem in (5.9) can be rewritten as:

[4]This can be derived based based on the result of Theorem 4.2

$$
\begin{aligned}
\boldsymbol{d}(\boldsymbol{s},\boldsymbol{H},\boldsymbol{A}_{\mathrm{TX}},\boldsymbol{A}_{\mathrm{RX}},\boldsymbol{\gamma}) = \arg\min_{\boldsymbol{d}} \quad & \frac{\|\boldsymbol{x}\|_\infty^2}{2\,\mathrm{Re}(\boldsymbol{z}^\dagger\boldsymbol{x}) - \boldsymbol{z}^\dagger\boldsymbol{z}} \\
\text{s.t.} \quad \mathcal{C}1: \quad & \mathrm{Re}(s_j[i])\frac{\boldsymbol{g}_{ji}\boldsymbol{d} + \boldsymbol{d}^\dagger\boldsymbol{g}_{ji}^\dagger}{2} \trianglerighteq \sqrt{\gamma_j}\,\mathrm{Re}^2(s_j[i]), \\
& j = 1,\ldots,K, i = 1,\ldots,S, \\
\mathcal{C}2: \quad & \mathrm{Im}(s_j[i])\frac{\boldsymbol{g}_{ji}\boldsymbol{d} - \boldsymbol{d}^\dagger\boldsymbol{g}_{ji}^\dagger}{2\iota} \trianglerighteq \sqrt{\gamma_j}\,\mathrm{Im}^2(s_j[i]), \\
& j = 1,\ldots,K, i = 1,\ldots,S, \\
\mathcal{C}3: \quad & (\iota t_{ji} - 1)\boldsymbol{g}_{ji}\boldsymbol{d} + (\iota t_{ji} + 1)\boldsymbol{d}^\dagger\boldsymbol{g}_{ji}^\dagger = 0, \\
& j = 1,\ldots,K, i = 1,\ldots,S.
\end{aligned}
\tag{5.11}
$$

Then, by applying parametric programming to the formulation in (5.11) using an auxiliary variable λ, it is possible to define the optimization function $F(\lambda,\boldsymbol{z}) = \min_{\boldsymbol{d}\in\mathcal{S}}\{\|\boldsymbol{x}\|_\infty^2 - \lambda(2\,\mathrm{Re}(\boldsymbol{z}^\dagger\boldsymbol{x}) - \boldsymbol{z}^\dagger\boldsymbol{z})\}$, where $\mathcal{S}$ represents the sets of constraints $\mathcal{C}_1$, $\mathcal{C}_2$, $\mathcal{C}_3$. This yields the following optimization problem:

$$
\begin{aligned}
\boldsymbol{d}(\boldsymbol{s},\boldsymbol{H},\boldsymbol{A}_{\mathrm{TX}},\boldsymbol{A}_{\mathrm{RX}},\boldsymbol{\gamma}) = \arg\min_{\boldsymbol{d}} \quad & \|\boldsymbol{x}\|_\infty^2 - \lambda(2\,\mathrm{Re}(\boldsymbol{z}^\dagger\boldsymbol{x}) - \boldsymbol{z}^\dagger\boldsymbol{z}) \\
\text{s.t.} \quad \mathcal{C}1: \quad & \mathrm{Re}(s_j[i])\frac{\boldsymbol{g}_{ji}\boldsymbol{d} + \boldsymbol{d}^\dagger\boldsymbol{g}_{ji}^\dagger}{2} \trianglerighteq \sqrt{\gamma_j}\,\mathrm{Re}^2(s_j[i]), \\
& j = 1,\ldots,K, i = 1,\ldots,S, \\
\mathcal{C}2: \quad & \mathrm{Im}(s_j[i])\frac{\boldsymbol{g}_{ji}\boldsymbol{d} - \boldsymbol{d}^\dagger\boldsymbol{g}_{ji}^\dagger}{2\iota} \trianglerighteq \sqrt{\gamma_j}\,\mathrm{Im}^2(s_j[i]), \\
& j = 1,\ldots,K, i = 1,\ldots,S, \\
\mathcal{C}3: \quad & (\iota t_{ji} - 1)\boldsymbol{g}_{ji}\boldsymbol{d} + (\iota t_{ji} + 1)\boldsymbol{d}^\dagger\boldsymbol{g}_{ji}^\dagger = 0, \\
& j = 1,\ldots,K, i = 1,\ldots,S.
\end{aligned}
\tag{5.12}
$$

Ultimately, the algorithm in Table 5.1 is proposed, where λ and $\boldsymbol{z}$ are iteratively updated until convergence. The parametric problem (5.12) is convex and can be solved using the standard convex optimization tools [149]. Both the SCA approach [152] and the parametric programming [157] have been proven convergent. Moreover, a numerical analysis has evidenced a fast convergence of the proposed joint algorithm (see also chapter 4).

5.3 Numerical Results

In this section, numerical results are presented to assess the performance of the proposed ST-PAPR-Min scheme over non-linear channels. The presented results are obtained considering a scenario with $N = 5$ antennas and $K = 3$ users, a 16-APSK modulation

$$\boldsymbol{H} = \begin{bmatrix} 0.217 - 0.002\imath & -1.355 - 0.642\imath & 0.587 - 0.018\imath & -0.363 - 0.312\imath & -0.356 + 0.635\imath \\ -0.667 - 0.692\imath & 0.342 - 0.355\imath & -0.717 + 1.114\imath & 0.817 + 0.166\imath & 0.584 + 0.385\imath \\ 0.006 - 1.211\imath & 0.798 - 0.139\imath & 0.330 - 0.315\imath & 0.327 + 0.711\imath & 0.192 - 1.571\imath \end{bmatrix} \tag{5.13}$$

TABLE 5.1: Proposed Iterative Algorithm

1. Initialization: Set ϵ, $k = 0$, $\lambda = 0$, which results in solving $\min_{\boldsymbol{d} \in \mathcal{S}} \{\|\boldsymbol{x}\|_\infty^2\}$.
2. Evaluate $\lambda_0 = \frac{\|\boldsymbol{x}\|_\infty^2}{\|\boldsymbol{x}\|^2}$, $\boldsymbol{z}_0 = \boldsymbol{x}$.
3. Solve the following optimization:

$$\begin{aligned} \boldsymbol{d} = \arg\min_{\boldsymbol{d}} \quad & \|\boldsymbol{x}\|_\infty^2 - \lambda_k (2\,\mathrm{Re}(\boldsymbol{z}_k^\dagger \boldsymbol{x}) - \boldsymbol{z}_k^\dagger \boldsymbol{z}_k) \\ \text{s.t.} \quad & \mathcal{C}1, \mathcal{C}2, \mathcal{C}3. \end{aligned} \tag{5.14}$$

4. Evaluate $|F(\lambda_k, \boldsymbol{z}_k)|$ and $\|\boldsymbol{x} - \boldsymbol{z}_k\|$; if $|F(\lambda_k, \boldsymbol{z}_k)| \geq \epsilon$ or $\|\boldsymbol{x} - \boldsymbol{z}_k\| \geq \epsilon$ go to step 5.
5. Set $\lambda_{k+1} = \frac{\|\boldsymbol{x}\|_\infty^2}{\|\boldsymbol{x}\|^2}$, $\boldsymbol{z}_{k+1} = \boldsymbol{x}$, $k = k + 1$, go to step 3.

scheme for the data information, and a block length of $S = 100$ symbols, averaging over different realization of the data $\boldsymbol{S}$. The pulse shaping operation is performed using squared root raised cosine (SRRC) pulses with a roll-off factor of 0.25, while the oversampling factor ξ is set to 4. The target SINR, assumed the same for all the users, is set to 12 dB, while a fixed realization has been considered for the spatial channel coefficients[5] as in (5.13). The considered benchmarks are the spatial peak-to-average power ratio (SPAPR) minimization (SPAPR-Min) scheme of chapter 4, which minimizes the PAPR only in the spatial dimension, and the peak power minimization (PPM) scheme of chapter 3, which aims at minimizing the power peaks again only in the spatial dimension.

First of all, Table 5.2 compares the ST-PAPR, in dB, achieved by the proposed scheme and the benchmarks, together with the average per-antenna transmit power in dBW. Remarkably, the proposed scheme manages to reduce the ST-PAPR of 6.55 and 5.45 dB

[5] However, the main conclusions of this work still apply if more general channel conditions are considered.

TABLE 5.2: PAPR and transmit power for the different schemes.

	ST-PAPR-Min	SPAPR-Min	PPM
ST-PAPR [dB]	1.05	7.6	6.5
Temp. PAPR [dB]	1.09	7.3	5.8
Per-ant. Power [dBW]	14.4	9.4	6

compared to the two considered benchmarks, respectively, at the expense of a higher transmit power. The table also shows the attained temporal PAPR averaged between the antennas, in order to highlight that impressive gains are obtained in the temporal dimension for each radio frequency (RF) chain. The improved power dynamic obtained with the proposed scheme in the temporal dimension is clearly visible in Fig. 5.2, where the complementary cumulative distribution function (CCDF) of the instantaneous power transmitted by one antenna ($|x_1[l]|^2$, considering the antenna indexed by 1, with l being the sample index) is drawn. Notably, the ST-PAPR-Min approach shows a much lower power variation in time.

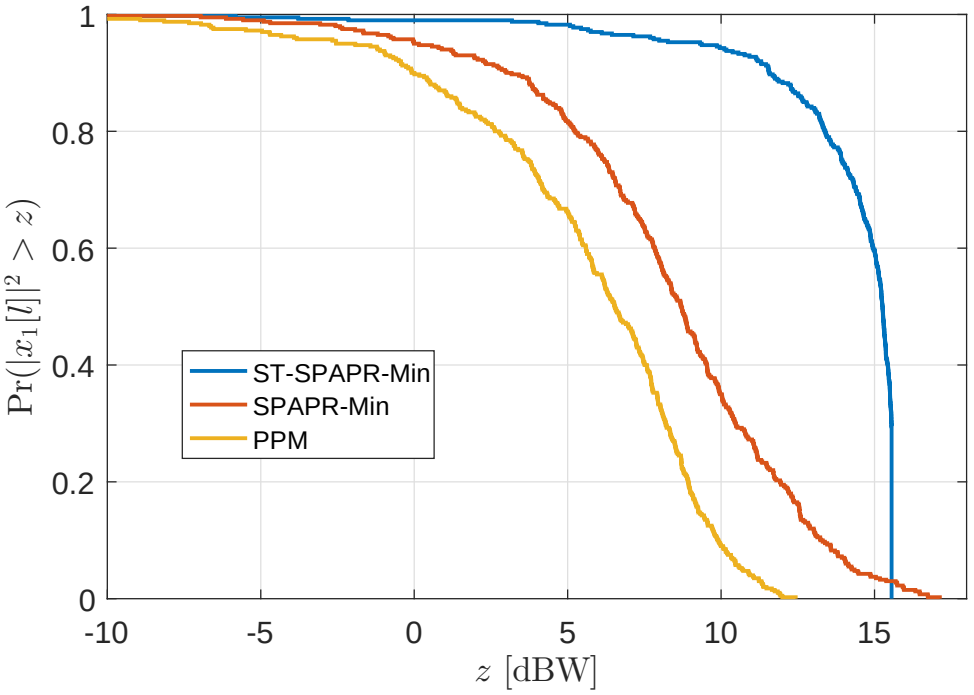

FIGURE 5.2: CCDF of the instantaneous transmit power for a single antenna.

Finally, to validate the performance of the proposed scheme with respect to non-linearities, Fig. 5.3 shows the symbol error rate (SER) attained by the proposed approach and by the benchmarks over a channel corrupted by the non-linear model of Fig. 2.7. The SER is shown as a function of the input back-off (IBO), in dB, applied to the signal feeding

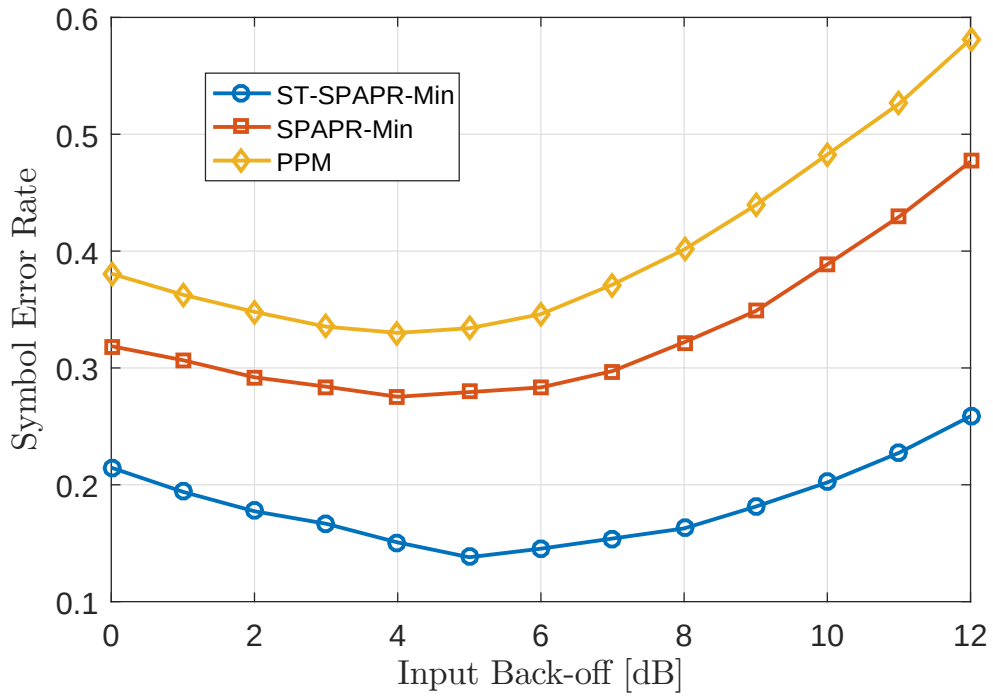

FIGURE 5.3: Achieved SER versus IBO, in dB, using the non-linear model of Fig. 2.7.

the non-linear HPAs. This result shows how the improved PAPR properties achieved by the proposed scheme result in a remarkable SER reduction when non-linearities are considered.

5.4 Conclusions

In this chapter, a new SLP method has been proposed, which allows to optimize the power dynamic of the waveforms both in the spatial and in the temporal dimensions, thus further improving the robustness of the signals to non-linear effects with respect to the space-only SLP schemes. In particular, the introduced spatio-temporal precoding model is utilized to minimize the spatio-temporal PAPR guaranteeing some specific Quality-of-Service targets, while at the same time exploiting the constructive interference effect typical of SLP. Numerical results have been presented, in terms of PAPR, power distribution, and symbol error rate over a non-linear channel, showing remarkable gains with respect to the SLP shemes previously discussed, at the expense of a higher transmit power.

Chapter 6

Faster-than-Nyquist Signaling through Spatio-temporal Symbol-level Precoding

In this chapter, the concept of spatio-temporal symbol-level precoding (SLP) previously introduced is applied in order to go beyond the classical precoding paradigm aimed at handling the multi-user interference (MUI). In particular, spatio-temporal SLP is used to enable faster-than-Nyquist (FTN) signaling over multi-user multiple-input single-output (MISO) systems, thus jointly leveraging the aggressive frequency reuse relying on precoding and the rate enhancement given by time packing, as discussed in section 2.4 of chapter 2. Considering a generic multi-user MISO system, the main idea is to apply spatio-temporal SLP in order to tackle at the transmitter side not only the interference in the spatial dimension (the MUI), but also the inter-symbol interference (ISI) in the temporal dimension. This extension of SLP is particularly relevant because it allows to solves the problem of complex FTN receivers, as the ISI is completely handled at the transmitter. Further, it is important to note that this approach allows to exploit in a constructive fashion the interference both in the temporal and in the spatial dimensions, thus gleaning benefits from both the domains. It should be also stressed that, unlike the previous chapters, this chapter is not addressed to non-linear systems. Overall, the main contributions of this chapter can be summarized as follows:

- The system model of spatio-temporal SLP, already introduced in chapter 5, is retraced, with specific regard to FTN signaling.
- This spatio-temporal SLP framework is used to apply FTN signaling over a multi-user MISO system, considering squared root raised cosine (SRRC) pulses and

coping with the ISI at the transmitter side: in particular, the focus is on a FTN SLP scheme performing sum power minimization under Quality-of-Service (QoS) constraints for a generic multi-level modulation, where the data streams are divided in blocks of symbols and the interference (MUI and ISI) is tackled within each block.

- Further, a more advanced sum power minimization scheme is proposed, which tackles not only the interference within each block of symbols but also the inter-block ISI arising between adjacent data blocks, borrowing concepts from dirty paper coding [33] and precoding under interference constraints. This scheme results in lower complexity as long frames can be broken down in shorter symbol blocks and processed separately.

6.1 System Model

In this section, the system model for spatio-temporal SLP, already introduced in chapter 5, is retraced for the reader's convenience. Further, the implications of applying FTN signaling are discussed based on this system model. Let us consider a single-cell multiple-antenna downlink scenario, where a base station simultaneously delivers K independent data streams to K single-antenna user terminals through N transmit antennas, with $N \geq K$. Each data stream is divided in blocks of S symbols, and the channel is assumed to be quasi-static flat fading. Considering a data block, the data information matrix can be defined as $\boldsymbol{S} = [\boldsymbol{s}_1^T \dots \boldsymbol{s}_K^T]^T \in \mathbb{C}^{K \times S}$. Such matrix aggregates the symbol streams to be conveyed to the different users, taken from a constellation having unit average power. Similarly, the matrix $\boldsymbol{D} = [\boldsymbol{d}_1^T \dots \boldsymbol{d}_N^T]^T \in \mathbb{C}^{N \times S}$ aggregates the precoded symbol streams which feed the transmit filters. In fact, each symbol stream has to undergo pulse shaping before the actual transmission. The pulse shaping operation is performed using a unit-power symmetric pulse waveform[1] $\alpha(t)$, having duration $2\eta T$, with T being the symbol period[2]. This implies that $\alpha(t) = 0$ for $|t| > \eta T$. Moving to a discrete time representation, and considering an oversampling factor ξ, the pulse waveform can be represented through its samples spaced by $\xi = \frac{T}{\xi}$, i.e., $\alpha[mt_s]$, with the index m such that $|m| \leq \eta\xi$ (accounting for the pulse duration).

With the introduced formalism, it is possible to write the expression of the discrete samples at the output of the pulse shaping filter of the generic n-th antenna, as follows:

[1] The symmetry of the pulse is not a strict requirement for the system model. However, this assumption has been made in order to simplify the notation, and taking also into account that it is often met in practice (for example for SRRC pulses).

[2] For infinite pulses, η is defined by the time (in symbol periods) at which the pulse amplitude decades below a sufficiently low level so that it can be considered negligible.

$$x_n[m] = \sum_{i=1}^{S} d_n[i]\alpha[(m-1)t_s - (i-1)T], \quad m = 1, \ldots, \xi S, \tag{6.1}$$

where $d_n[i]$ is the i-th element of the symbol vector $\boldsymbol{d}_n$, which in turn is the n-th row of $\boldsymbol{D}$. Such relation can be rewritten in a compact matrix form as:

$$\boldsymbol{x}_n = \boldsymbol{d}_n \boldsymbol{A}_{\mathrm{TX}}, \tag{6.2}$$

where $\boldsymbol{x}_n \in \mathbb{C}^{1\times \xi S}$ represents the output data stream (in the oversampled domain) from the n-th antenna and $\boldsymbol{A}_{\mathrm{TX}} \in \mathbb{R}^{S\times \xi S}$ is a block Toeplitz matrix modeling the pulse shaping operation, with its (i,m)-th element being:

$$[\boldsymbol{A}_{\mathrm{TX}}]_{(i,m)} = \alpha[(m-1)t_s - (i-1)T]. \tag{6.3}$$

Further, we can aggregate the output signals from all the antennas in a matrix $\boldsymbol{X} = [\boldsymbol{x}_1^T \ldots \boldsymbol{x}_N^T]^T \in \mathbb{C}^{N\times \xi S}$, which allows us to model the pulse shaping operation for all the N antennas simply as $\boldsymbol{X} = \boldsymbol{D}\boldsymbol{A}_{\mathrm{TX}}$.

According to the well-known multi-user MISO channel model, the received symbols at the users can be written in matrix form as:

$$\tilde{\boldsymbol{Y}} = \boldsymbol{H}\boldsymbol{X} + \tilde{\boldsymbol{Z}}$$

where the matrix $\tilde{\boldsymbol{Y}} = [\tilde{\boldsymbol{y}}_1^T \ldots \tilde{\boldsymbol{y}}_K^T]^T \in \mathbb{C}^{K\times \xi S}$ represents the received samples at the K users, $\boldsymbol{H} = [\boldsymbol{h}_1^T \ldots \boldsymbol{h}_K^T]^T \in \mathbb{C}^{K\times N}$ is the quasi-static flat fading channel[3] matrix modeling the MUI among the different data streams, and $\tilde{\boldsymbol{Z}} = [\tilde{\boldsymbol{z}}_1^T \ldots \tilde{\boldsymbol{z}}_K^T]^T \in \mathbb{C}^{K\times \xi S}$ models the additive white Gaussian noise (AWGN). In order to obtain the received signals at the users in the symbol domain, the matched filtering and downsampling operation needs to be modeled. This is done again in a matrix form, using the block Toeplitz matrix $\boldsymbol{A}_{\mathrm{RX}} \in \mathbb{R}^{\xi S\times S}$, which can be defined in the same fashion of (6.3). Overall, grouping the received symbols at the K users in a matrix $\boldsymbol{Y} = [\boldsymbol{y}_1^T \ldots \boldsymbol{y}_K^T]^T \in \mathbb{C}^{K\times S}$, the global communication model can be written as:

$$\boldsymbol{Y} = \tilde{\boldsymbol{Y}}\boldsymbol{A}_{\mathrm{RX}} = \boldsymbol{H}\boldsymbol{X}\boldsymbol{A}_{\mathrm{RX}} + \tilde{\boldsymbol{Z}}\boldsymbol{A}_{\mathrm{RX}} = \boldsymbol{H}\boldsymbol{D}\boldsymbol{A} + \boldsymbol{Z}, \tag{6.4}$$

where $\boldsymbol{A} = \boldsymbol{A}_{\mathrm{TX}}\boldsymbol{A}_{\mathrm{RX}} \in \mathbb{R}^{S\times S}$ is a matrix representing the convolution of the filters at the transmitter and at the receiver, while $\boldsymbol{Z} = \tilde{\boldsymbol{Z}}\boldsymbol{A}_{\mathrm{RX}} \in \mathbb{C}^{K\times S}$ is the noise in

[3] In principle, it is possible to extend the model accounting also for frequency selective fading channels, by representing the resulting channel induced ISI. Nevertheless, in order not to further complicate the system model, in this thesis the focus is on flat fading channels, while the extension to the general case will be considered in the future work.

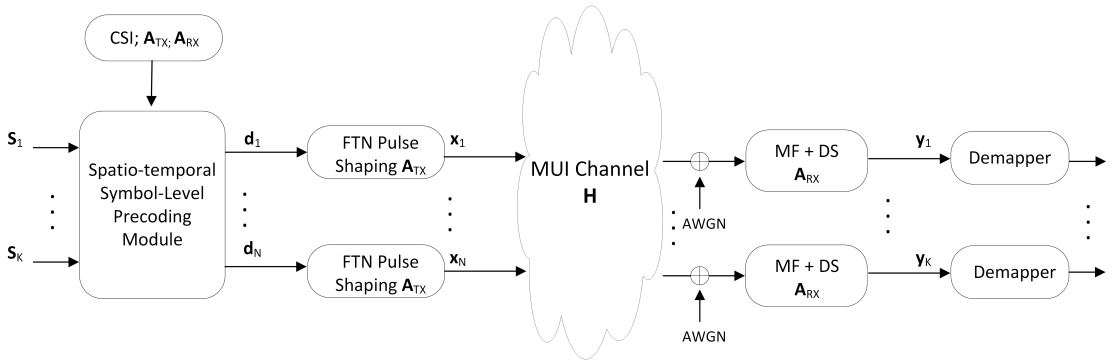

FIGURE 6.1: Block scheme of the considered system model relying on spatio-temporal SLP.

the symbol domain, having power σ_z^2. If we denote by $\beta(t)$ the impulse response of the overall filter composed by the convolution of the pulse shaping and the matched filtering, it can be seen that $\boldsymbol{A}$ is a symmetric Toeplitz matrix whose first row is $\boldsymbol{a} = [\beta[0]\beta[T]\dots\beta[2\eta T]0\dots0]$[4]. It should be stressed that the model in (6.4) takes into account the interference both in the spatial dimension (the MUI), through the spatial channel matrix $\boldsymbol{H}$, and in the temporal dimension (the ISI), through the temporal channel matrix $\boldsymbol{A}$. The complete system model is represented in the block scheme of Fig. 6.1, where it is clear how the symbol matrix $\boldsymbol{D}$ is obtained as output of a spatio-temporal precoding module, which takes as input the channel state information (CSI), i.e. an estimate of $\boldsymbol{H}$, the filters matrices $\boldsymbol{A}_{\text{TX}}$ and $\boldsymbol{A}_{\text{RX}}$ and the data information matrix $\boldsymbol{S}$.

The aim of the symbol-level precoding scheme is to optimize the matrix $\boldsymbol{D}$, namely the precoded symbol streams feeding the transmit filters, by constructively exploiting the interference in the spatial and in the temporal dimension. While this optimization procedure will be explained in detail in the following section, it is now convenient to further manipulate the model of (6.4) by vectorizing the introduced signal matrices over the temporal dimension (rows first). Accordingly, data information streams are modeled through the vector $\boldsymbol{s} = \text{vec}(\boldsymbol{S}^T) = [\boldsymbol{s}_1 \dots \boldsymbol{s}_K]^T \in \mathbb{C}^{KS\times 1}$, the designed symbol streams through $\boldsymbol{d} = \text{vec}(\boldsymbol{D}^T) = [\boldsymbol{d}_1 \dots \boldsymbol{d}_N]^T \in \mathbb{C}^{NS\times 1}$, the transmitted signals through $\boldsymbol{x} = \text{vec}(\boldsymbol{X}^T) = [\boldsymbol{x}_1 \dots \boldsymbol{x}_N]^T \in \mathbb{C}^{N\xi S\times 1}$, the noise through $\boldsymbol{z} = \text{vec}(\boldsymbol{Z}^T) = [\boldsymbol{z}_1 \dots \boldsymbol{z}_K]^T \in \mathbb{C}^{KS\times 1}$, and the received symbols through $\boldsymbol{y} = \text{vec}(\boldsymbol{Y}^T) = [\boldsymbol{y}_1 \dots \boldsymbol{y}_K]^T \in \mathbb{C}^{KS\times 1}$. It is straightforward to check that the relation between $\boldsymbol{d}$ and $\boldsymbol{x}$ can be written as:

$$\boldsymbol{x} = (\boldsymbol{I}_N \otimes \boldsymbol{A}_{\text{TX}}^T)\boldsymbol{d}. \tag{6.5}$$

Further, by introducing the matrix $\hat{\boldsymbol{X}} = \boldsymbol{X}\boldsymbol{A}_{\text{RX}} = \boldsymbol{D}\boldsymbol{A} \in \mathbb{C}^{N\times S}$ and its vectorized version $\hat{\boldsymbol{x}} = \text{vec}(\hat{\boldsymbol{X}}^T) \in \mathbb{C}^{NS\times 1}$, and by accounting for (6.4), it is easy to check that

[4]To ease the notation, the assumption that $S > 2\eta$ is considered.

$\hat{\boldsymbol{x}} = (\boldsymbol{I}_N \otimes \boldsymbol{A}^T)\boldsymbol{d}$ and that $\boldsymbol{y} = (\boldsymbol{H} \otimes \boldsymbol{I}_S)\hat{\boldsymbol{x}} + \boldsymbol{z}$. Finally, using the mixed-product property of the Kronecker product yields $(\boldsymbol{H} \otimes \boldsymbol{I}_S)(\boldsymbol{I}_N \otimes \boldsymbol{A}^T) = (\boldsymbol{H} \otimes \boldsymbol{A}^T)$, therefore the global communication model can be written as follows:

$$\boldsymbol{y} = (\boldsymbol{H} \otimes \boldsymbol{A}^T)\boldsymbol{d} + \boldsymbol{z} = \boldsymbol{G}\boldsymbol{d} + \boldsymbol{z}. \tag{6.6}$$

The matrix $\boldsymbol{G} = \boldsymbol{H} \otimes \boldsymbol{A}^T \in \mathbb{C}^{KS \times NS}$ incorporates both the spatial channel matrix $\boldsymbol{H}$ and the temporal one $\boldsymbol{A}$, thus it will be referred to as spatio-temporal channel matrix. Ultimately, the model of (6.6) allows to represent in a very simple way both the MUI and the ISI of the system. In the next section, the optimization problem modeling the proposed spatio-temporal SLP scheme will be detailed.

6.1.1 Faster-than-Nyquist

As already mentioned, FTN signaling manages to pack more information in the time domain by reducing the symbol period T below the minimum allowed by the Nyquist criterion, thus introducing controlled ISI. This is graphically shown in Fig. 6.2 for the case of a SRRC pulse. In the system model definition, no assumptions have been on the symbol-rate so far. It can be easily seen that if we do not apply FTN, then the Toeplitz matrix $\boldsymbol{A}$ simply reduces to a scaled identity, i.e., $\boldsymbol{A} = \beta[0]\boldsymbol{I}_S$. In this case there is no ISI and the model in (6.4) boils down to the classic multi-user MISO case.

Now, let us assume that we apply a signaling acceleration factor $\tau \in [0, 1]$, so that the effective symbol period is $T = \tau T_{\text{ny}}$, with T_{ny} indicating the minimum symbol period allowed by the Nyquist criterion. It can be easily seen that the lower is the acceleration factor τ (i.e., the more the transmissions are accelerated) the larger is the number of non-zero values in the matrix $\boldsymbol{A}$, thus the higher is the ISI level in the system. This can be easily explained by the fact that more pulses are packed in the time domain. Furthermore, as the total duration of the individual pulse remains constant, the value of η increases as τ decreases[5]. The schemes proposed in this chapter apply regardless of the chosen pulse. In the numerical results section, SRRC pulses will be considered, as they are the most used in practical applications. It should be noted that no complex equalization or decoding is needed at the receivers, as they are oblivious to the FTN operation. The receivers have to be informed only about the baud-rate of the communication for sampling purposes.

[5]In the remainder of the chapter the FTN operation will be represented solely through the acceleration factor τ, as η is directly dependent on it for a given pulse.

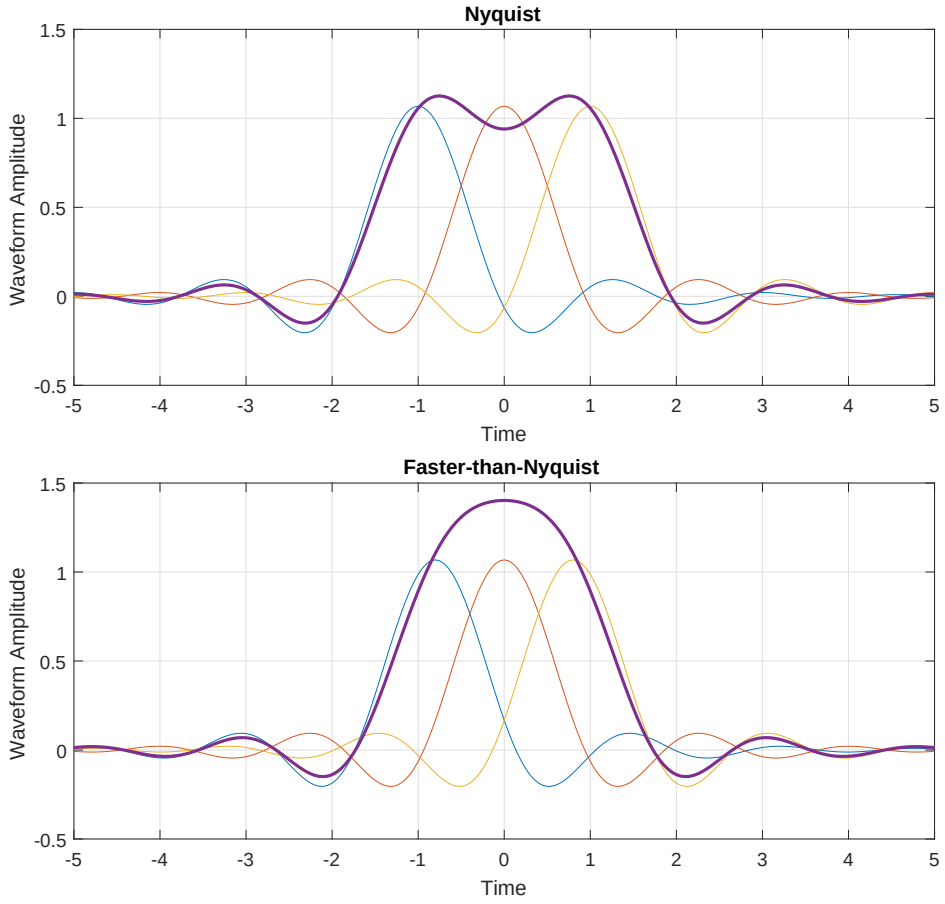

FIGURE 6.2: Nyquist vs. Faster-than-Nyquist for a SRRC pulse, in the time domain.

6.2 Faster-than-Nyquist SLP for Sum Power Minimization with QoS Constraints

In this section a novel SLP scheme accounting for FTN signaling is presented, which exploits in a constructive fashion [22] the interference both in the spatial and in the temporal domain. The novelty with respect to the previous SLP solutions lies in the ability of the new scheme to model and handle the ISI, together with the MUI, and in the consequent capacity of exploting the potential of FTN signaling in the context of multi-user MISO systems. More specifically, a sum power minimization scheme under QoS constraints is proposed. As common in the precoding literature, the QoS constraints are expressed in terms of target SINR, which represents a predefined per-user SINR threshold to be guaranteed at the receivers' side. The target SINR, which is an input parameter to the precoding scheme, has to be selected in order to ensure a sufficiently good performance (e.g. in terms of symbol error rate or bit error rate) for the considered application, and strongly depends on the adopted modulation as well as on the use of forward error correction (FEC) schemes. Therefore, in a practical system the target SINR should not be selected a priori, but it shall be rather chosen through a training

phase based on pilots, which allows to evaluate the performance associated to different target SINR values for the specific system at hand. Since the aim is to minimize the total transmit power P_{tot}, it is convenient to explicit its expression before formalizing the proposed scheme, as follows:

$$P_{\text{tot}} = \frac{1}{\xi S} \sum_{m=1}^{nsS} \sum_{n=1}^{N} |[\boldsymbol{X}]_{(n,m)}|^2 = \frac{1}{\xi S} \|\boldsymbol{X}\|_F^2 = \frac{1}{\xi S} \|\boldsymbol{x}\|^2. \tag{6.7}$$

Accordingly, taking also into account that $\boldsymbol{X} = \boldsymbol{D}\boldsymbol{A}_{\text{TX}}$, a general formulation of the optimization problem for the proposed scheme, using the matrix notation introduced in section 6.1, is the following:

$$\begin{aligned} \boldsymbol{D}(\boldsymbol{S}, \boldsymbol{H}, \boldsymbol{A}_{\text{TX}}, \boldsymbol{A}_{\text{RX}}, \boldsymbol{\gamma}) = \arg\min_{\boldsymbol{D}} \quad & \|\boldsymbol{D}\boldsymbol{A}_{\text{TX}}\|_F^2 \\ \text{s.t.} \quad & \boldsymbol{H}\boldsymbol{D}\boldsymbol{A} \triangleright \sigma_z \boldsymbol{Q} \circ \boldsymbol{S}, \end{aligned} \tag{6.8}$$

where the quantities in brackets are given as input to the optimization problem. Among them, the vector $\boldsymbol{\gamma} = [\gamma_1 \dots \gamma_K]^T \in \mathbb{R}^{K \times 1}$ represents the target SINR for all the users and appears in the optimization problem through the matrix $\boldsymbol{Q} = \sqrt{\boldsymbol{\gamma}} \otimes \boldsymbol{1}_{1 \times S}$. The operator $\triangleright$ used in the constraint, which applies element-wise, imposes that the received symbols at each user (represented respectively by the elements of $\boldsymbol{HDA}$) lie in their correct detection regions. Further, the correct detection regions, which clearly depend on the data information matrix $\boldsymbol{S}$, are scaled accounting for the target SINR $\boldsymbol{\gamma}$, which has to be guaranteed at each user[6]. The introduced constraint allows the exploitation of the constructive interference effect, in the same fashion as [23]. In order to express it in a more explicit form it is necessary to refer to a specific modulation scheme, as will be done later in this section. The problem (6.8) can be rewritten resorting to the vectorized formalism and the spatio-temporal channel matrix introduced in (6.5)-(6.6), as follows:

$$\begin{aligned} \boldsymbol{d}(\boldsymbol{s}, \boldsymbol{H}, \boldsymbol{A}_{\text{TX}}, \boldsymbol{A}_{\text{RX}}, \boldsymbol{\gamma}) = \arg\min_{\boldsymbol{d}} \quad & \|\boldsymbol{x}\|^2 \\ \text{s.t.} \quad & \boldsymbol{G}_k \boldsymbol{d} \triangleright \sigma_z \sqrt{\gamma_k} \boldsymbol{s}_k^T, \; k = 1, \dots, K, \end{aligned} \tag{6.9}$$

where $\boldsymbol{G}_k = [\boldsymbol{g}_{k1}^T \dots \boldsymbol{g}_{kS}^T]^T \in \mathbb{C}^{S \times NS}$ is a submatrix of $\boldsymbol{G}$ denoting the spatio-temporal channel matrix for the k-th user, and $\boldsymbol{s}_k \in \mathbb{C}^{1 \times S}$ represents the data information related to the k-th user. The optimization problem can be further manipulated by using (6.5), and by specifying the constraints for each symbol slot, as follows:

[6]However, it should be stressed that the target SINR does not need to be known a priori at the receivers. In fact, the receivers estimate the attained SINR based on pilots (see also [160]) and normalize the received constellation accordingly.

$$\begin{aligned} \boldsymbol{d}(\boldsymbol{s},\boldsymbol{H},\boldsymbol{A}_{\mathrm{TX}},\boldsymbol{A}_{\mathrm{RX}},\boldsymbol{\gamma}) = \arg\min_{\boldsymbol{d}} \quad & \|(\boldsymbol{I}_N \otimes \boldsymbol{A}_{\mathrm{TX}}^T)\boldsymbol{d}\|^2 \\ \text{s.t.} \quad & \boldsymbol{g}_{ki}\boldsymbol{d} \triangleright \sigma_z\sqrt{\gamma_k}\boldsymbol{s}_k[i],\ k=1,\ldots,K,\ i=1,\ldots,S. \end{aligned} \tag{6.10}$$

It should be stressed that the quantity $\boldsymbol{g}_{ki}\boldsymbol{d}$ represents the received symbol at the k-th user terminal in the i-th symbol slot, and that the imposed constraint forces it to lie in the correct detection region of the corresponding data information symbol $\boldsymbol{s}_k[i]$. It is also worth highlighting that the SINR corresponding to the k-th user is given by $\mathbb{E}_i\left[\frac{|\boldsymbol{g}_{ki}\boldsymbol{d}|^2}{\sigma_z^2}\right]$, therefore the scaling factor $\sigma_z\sqrt{\gamma_k}$ introduced in the constraint allows to guarantee the target SINR γ_k. It is important now to take a further step in the formalization of the power minimization problem at hand, by expressing the introduced constraints in an explicit form. To this aim, let us focus on a quadrature amplitude modulation (QAM) modulation scheme for the data information. In this case the optimization problem can be written by decomposing the constraints along the in-phase and quadrature components of the symbols, as follows:

$$\begin{aligned} \boldsymbol{d}(\boldsymbol{s},\boldsymbol{H},\boldsymbol{A}_{\mathrm{TX}},\boldsymbol{A}_{\mathrm{RX}},\boldsymbol{\gamma}) = \arg\min_{\boldsymbol{d}} \quad & \|(\boldsymbol{I}_N \otimes \boldsymbol{A}_{\mathrm{TX}}^T)\boldsymbol{d}\|^2 \\ \text{s.t.} \quad \mathcal{C}1: \quad & \mathrm{Re}(\boldsymbol{g}_{ki}\boldsymbol{d}) \gtreqless \sigma_z\sqrt{\gamma_k}\,\mathrm{Re}(\boldsymbol{s}_k[i]),\ k=1,\ldots,K,\ i=1,\ldots,S, \\ \mathcal{C}2: \quad & \mathrm{Im}(\boldsymbol{g}_{ki}\boldsymbol{d}) \gtreqless \sigma_z\sqrt{\gamma_k}\,\mathrm{Im}(\boldsymbol{s}_k[i]),\ k=1,\ldots,K,\ i=1,\ldots,S, \end{aligned} \tag{6.11}$$

where the notation $\gtreqless$ denotes a generalized inequality, which shall be read as $>$,$<$ or $=$ depending on the position of the data $\boldsymbol{s}_k[i]$ within the QAM constellation and, accordingly, on its detection region. A detailed formulation of the constraints $\mathcal{C}1$, $\mathcal{C}2$ is explained hereafter:

- For the inner constellation symbols, which are labeled by A in the 16-QAM example of Fig. 6.3, the constraints $\mathcal{C}1$, $\mathcal{C}2$ should guarantee that the received signal achieves the exact constellation point. Hence, the constraints are equality constraints, as follows:

$$\begin{aligned} \mathcal{C}1: \quad & \mathrm{Re}(\boldsymbol{g}_{ki}\boldsymbol{d}) = \sigma_z\sqrt{\gamma_k}\,\mathrm{Re}(\boldsymbol{s}_k[i]), \\ \mathcal{C}2: \quad & \mathrm{Im}(\boldsymbol{g}_{ki}\boldsymbol{d}) = \sigma_z\sqrt{\gamma_k}\,\mathrm{Im}(\boldsymbol{s}_k[i]). \end{aligned} \tag{6.12}$$

- For the outer constellation symbols, which are labeled by B in the 16-QAM example of Fig. 6.3, the constraints $\mathcal{C}1$, $\mathcal{C}2$ guaranteeing the correct detections and exploiting the constructive interference are:

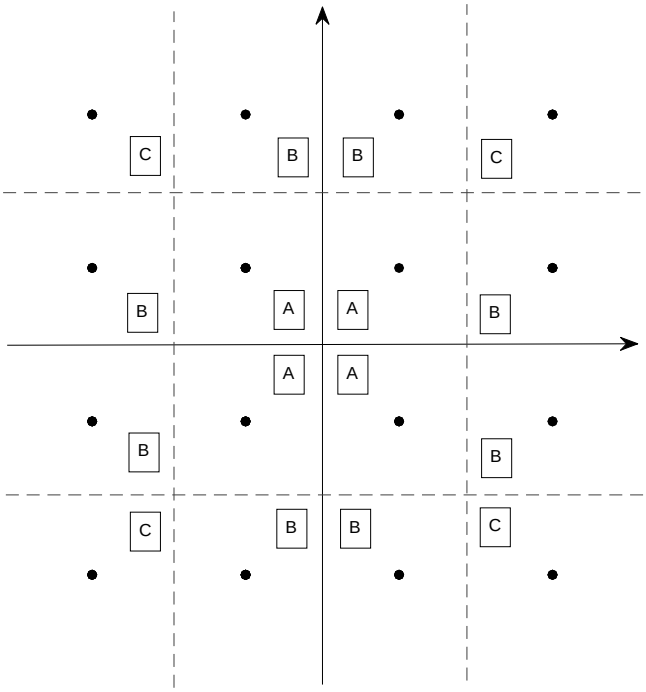

FIGURE 6.3: Classification of the constellation points into inner (A), outer (B) and outermost (C), for a 16-QAM modulation scheme.

$$\begin{aligned} \mathcal{C}1: \quad & \mathrm{Re}(\boldsymbol{g}_{ki}\boldsymbol{d}) \geq \sigma_z\sqrt{\gamma_k}\,\mathrm{Re}(\boldsymbol{s}_k[i]), \text{ if } \mathrm{Re}\,\boldsymbol{s}_k[i] > 0, \\ & \mathrm{Re}(\boldsymbol{g}_{ki}\boldsymbol{d}) \leq \sigma_z\sqrt{\gamma_k}\,\mathrm{Re}(\boldsymbol{s}_k[i]), \text{ if } \mathrm{Re}\,\boldsymbol{s}_k[i] < 0, \\ \mathcal{C}2: \quad & \mathrm{Im}(\boldsymbol{g}_{ki}\boldsymbol{d}) = \sigma_z\sqrt{\gamma_k}\,\mathrm{Im}(\boldsymbol{s}_k[i]), \end{aligned} \tag{6.13}$$

when $\boldsymbol{s}_k[i]$ lies on the left/right side of the constellation, and:

$$\begin{aligned} \mathcal{C}1: \quad & \mathrm{Re}(\boldsymbol{g}_{ki}\boldsymbol{d}) = \sigma_z\sqrt{\gamma_k}\,\mathrm{Re}(\boldsymbol{s}_k[i]), \\ \mathcal{C}2: \quad & \mathrm{Im}(\boldsymbol{g}_{ki}\boldsymbol{d}) \geq \sigma_z\sqrt{\gamma_k}\,\mathrm{Im}(\boldsymbol{s}_k[i]), \text{ if } \mathrm{Im}\,\boldsymbol{s}_k[i] > 0, \\ & \mathrm{Im}(\boldsymbol{g}_{ki}\boldsymbol{d}) \leq \sigma_z\sqrt{\gamma_k}\,\mathrm{Im}(\boldsymbol{s}_k[i]), \text{ if } \mathrm{Im}\,\boldsymbol{s}_k[i] < 0, \end{aligned} \tag{6.14}$$

when $\boldsymbol{s}_k[i]$ lies on the upper/lower side of the constellation.

- Finally, for the outermost symbols lying on the edges of the QAM constellation, which are labeled by C in the 16-QAM example of Fig. 6.3, the constraints $\mathcal{C}1$, $\mathcal{C}2$ can exploit the constructive interference effect by imposing inequalities along both the in-phase and the quadrature components of the signals, as follows:

$$
\begin{aligned}
\mathcal{C}1: \quad & \mathrm{Re}(\boldsymbol{g}_{ki}\boldsymbol{d}) \geq \sigma_z\sqrt{\gamma_k}\,\mathrm{Re}(\boldsymbol{s}_k[i]), \text{ if } \mathrm{Re}\,\boldsymbol{s}_k[i] > 0, \\
& \mathrm{Re}(\boldsymbol{g}_{ki}\boldsymbol{d}) \leq \sigma_z\sqrt{\gamma_k}\,\mathrm{Re}(\boldsymbol{s}_k[i]), \text{ if } \mathrm{Re}\,\boldsymbol{s}_k[i] < 0, \\
\mathcal{C}2: \quad & \mathrm{Im}(\boldsymbol{g}_{ki}\boldsymbol{d}) \geq \sigma_z\sqrt{\gamma_k}\,\mathrm{Im}(\boldsymbol{s}_k[i]), \text{ if } \mathrm{Im}\,\boldsymbol{s}_k[i] > 0, \\
& \mathrm{Im}(\boldsymbol{g}_{ki}\boldsymbol{d}) \leq \sigma_z\sqrt{\gamma_k}\,\mathrm{Im}(\boldsymbol{s}_k[i]), \text{ if } \mathrm{Im}\,\boldsymbol{s}_k[i] < 0.
\end{aligned}
\tag{6.15}
$$

The final optimization problem in (6.11) presents a convex quadratic objective function and affine constraints, therefore it is convex and can be solved resorting to the standard convex optimization tools [149]. As a final remark, it should be mentioned that, although herein we solely focused on QAM constellations, the optimization problem (6.10) can be straightforwardly expressed for different constellations, by tailoring the constraints to the different detection regions. In particular, if the data information symbols belong to a phase shift keying (PSK) or to an amplitude phase shift keying (APSK) constellation, it is convenient to express the constraints in (6.10) focusing on the amplitude and the phase of the symbols, rather than their in-phase and quadrature components, as done in chapters 4-5. Although in this case the optimization problem appears more constrained with respect to (6.11), due to the different detection regions, it is still possible to exploit the constructive interference effect of SLP.

6.3 Sequential Faster-than-Nyquist SLP: processing subsequent blocks

So far a single data block of S symbols per stream has been considered, and an approach to constructively handle the interference within the block has been devised. However, it is clear that the optimization problem (6.11) cannot handle any arbitrary block length S, as the dimension of the involved optimization variables, as well as the number of constraints, linearly grow with S[7]. This implies that in a practical system the scheme needs to process subsequently different information blocks of a manageable length S. If the framing structure of the system allows to neglect the mutual interference between adjacent blocks (for instance, because subsequent information blocks are separated by a sufficient number of non-precoded signaling symbols, such as headers and pilots), then the problem formulation in (6.11) still applies. Nevertheless, in general we also need to account for the ISI arising between subsequent blocks, i.e., the inter-block ISI. In this section the proposed approach is extended so as to cope with the problem of inter-block interference, thus moving closer to the practical application of the discussed FTN SLP scheme.

[7] A numerical evaluation of the complexity of (6.11), as a function of S, is given in section 6.4.

As a first step towards extending the previous scheme, the ISI between two adjacent blocks needs to be modeled. In particular, denoting the current block under processing by an index l, one needs to model the residual ISI coming from the previous $(l-1)$-th block, as well as the ISI that the current l-th block is causing to the $(l-1)$-th one[8]. This inter-block interference can be taken into account by extending the communication model in (6.6) as follows:

$$\begin{bmatrix} \boldsymbol{y}_{l-1} \\ \boldsymbol{y}_l \end{bmatrix} = \begin{bmatrix} \boldsymbol{G} & \boldsymbol{G}_U \\ \boldsymbol{G}_P & \boldsymbol{G} \end{bmatrix} \begin{bmatrix} \boldsymbol{d}_{l-1} \\ \boldsymbol{d}_l \end{bmatrix} + \begin{bmatrix} \boldsymbol{z}_{l-1} \\ \boldsymbol{z}_l \end{bmatrix}, \tag{6.16}$$

where $\boldsymbol{G}_P = \boldsymbol{H} \otimes \boldsymbol{A}_P^T \in \mathbb{C}^{KS \times NS}$ and $\boldsymbol{G}_U = \boldsymbol{H} \otimes \boldsymbol{A}_U^T \in \mathbb{C}^{KS \times NS}$ respectively, and the matrices $\boldsymbol{A}_P \in \mathbb{R}^{S \times S}$ and $\boldsymbol{A}_U \in \mathbb{R}^{S \times S}$ model the ISI coming from the previous block and the ISI caused to the previous block, respectively. It is straightforward to observe that $\boldsymbol{A}_P$ is a Toeplitz matrix whose first column is given by $\boldsymbol{a}_{Pc} = [0 \dots 0 \; \beta[-2\eta T] \; \dots \beta[-T]]^T$ and whose first row is a zero-entries row vector. Similarly, $\boldsymbol{A}_U$ is a Toeplitz matrix whose last column is given by $\boldsymbol{a}_{Uc} = [\beta[T] \dots \beta[2\eta T] \; 0 \dots 0]^T$ and whose last row is a zero-entries row vector.

Now, assuming that blocks are serially processed, the ISI caused by the $(l-1)$-th block to the l-th one will be represented by the vector $\boldsymbol{v} = \boldsymbol{G}_P \boldsymbol{d}_{l-1} \in \mathbb{C}^{KS \times 1}$, which is known and can be used in the optimization scheme designing $\boldsymbol{d}_l$. It should be noted that this concept is similar to the dirty paper coding principle [33], where a known state is taken into account while designing the transmit signal. Analogously to the other introduced vectorized quantities, $\boldsymbol{v}$ can also be decomposed by indexing the components related to the different users, i.e., $\boldsymbol{v} = [\boldsymbol{v}_1 \dots \boldsymbol{v}_K]^T$. Besides accounting for the ISI coming from the previous block, one should also try to minimize the ISI that the l-th block is causing to the previous one, which is represented by the vector $\boldsymbol{G}_U \boldsymbol{d}_l$. This is achieved by setting interference constraints towards the previous block, following a strategy which resembles cognitive precoding schemes [107, 161, 162]. With these considerations, the following sequential FTN SLP optimization problem can be formalized, which performs a sum power minimization with QoS constraints:

$$\begin{aligned} \boldsymbol{d}_l(\boldsymbol{s}, \boldsymbol{H}, \boldsymbol{A}_{\mathrm{TX}}, \boldsymbol{A}_{\mathrm{RX}}, \boldsymbol{\gamma}, \boldsymbol{v}, \epsilon) = \arg\min_{\boldsymbol{d}_l} \quad & \|\boldsymbol{x}_l\|^2 \\ \text{s.t.} \quad \mathcal{C}1: \quad & \boldsymbol{G}_k \boldsymbol{d}_l + \boldsymbol{v}_k^T \triangleright \sigma_z \sqrt{\gamma_k} \boldsymbol{s}_k^T, \; k = 1, \dots, K, \\ \mathcal{C}2: \quad & |\boldsymbol{G}_U \boldsymbol{d}_l|^{\circ 2} \leq \epsilon \mathbf{1}_{KS \times 1}, \end{aligned} \tag{6.17}$$

[8] In principle, it could be possible to consider also the $(l-2)$-th block or even previous blocks in the model. However, in most practical scenarios the residual ISI coming from such blocks would be negligible, and considering it would not significantly improve the performance. Thus, in order to keep the complexity of the scheme to a manageable level, only two adjacent blocks are considered.

where the Hadamard notation $\circ$ in $\mathcal{C}2$ is used to indicate that the squaring operation applies element-wise (moreover, the inequality has also to be considered element-wise). The novelty with respect to the problem in (6.9) is in the fact that the constraints $\mathcal{C}1$ is now also accounting the ISI coming from the previous block, so as to guarantee constructive interference at each user. Further, the constraint $\mathcal{C}2$ imposes a maximum level of ISI that the l-th block is causing to the previous one, through a predefined threshold ϵ. Although the best in terms of ISI reduction would be to impose a zero-forcing condition in $\mathcal{C}2$, i.e., fixing $\epsilon = 0$, a numerical analysis has shown how such choice would make the problem unfeasible for most scenarios due to the lack of degrees of freedom. In the numerical results section different values for ϵ will be considered and discussed.

The constraint $\mathcal{C}2$ can be decomposed by considering for each user the relative submatrix of the matrix $\boldsymbol{G}_U$, similarly to what was done in (6.9) for $\boldsymbol{G}$. Accordingly, $\boldsymbol{G}_{Uk} = [\boldsymbol{g}_{Uk1}^T \dots \boldsymbol{g}_{UkS}^T]^T \in \mathbb{C}^{S \times NS}$ is a submatrix of $\boldsymbol{G}_U$ related to the k-th user, hence the problem (6.17) can be rewritten as:

$$\begin{aligned} \boldsymbol{d}_l(\boldsymbol{s}, \boldsymbol{H}, \boldsymbol{A}_{\text{TX}}, \boldsymbol{A}_{\text{RX}}, \boldsymbol{\gamma}, \boldsymbol{v}, \epsilon) = \arg\min_{\boldsymbol{d}_l} \quad & \|\boldsymbol{x}_l\|^2 \\ \text{s.t.} \quad \mathcal{C}1: \quad & \boldsymbol{G}_k \boldsymbol{d}_l + \boldsymbol{v}_k^T \triangleright \sigma_z \sqrt{\gamma_k} \boldsymbol{s}_k^T, \ k = 1, \dots, K, \\ \mathcal{C}2: \quad & |\boldsymbol{G}_{Uk} \boldsymbol{d}_l|^{\circ 2} \leq \epsilon \mathbf{1}_{S \times 1}, \ k = 1, \dots, K, \end{aligned} \tag{6.18}$$

and, expressing the constraints for each symbol slot, in the same fashion of (6.10), as:

$$\begin{aligned} \boldsymbol{d}_l(\boldsymbol{s}, \boldsymbol{H}, \boldsymbol{A}_{\text{TX}}, \boldsymbol{A}_{\text{RX}}, \boldsymbol{\gamma}, \boldsymbol{v}, \epsilon) = \arg\min_{\boldsymbol{d}_l} \quad & \|(\boldsymbol{I}_N \otimes \boldsymbol{A}_{\text{TX}}^T) \boldsymbol{d}_l\|^2 \\ \text{s.t.} \quad \mathcal{C}1: \quad & \boldsymbol{g}_{ki} \boldsymbol{d}_l + \boldsymbol{v}_k[i] \triangleright \sigma_z \sqrt{\gamma_k} \boldsymbol{s}_k[i], \ k = 1, \dots, K, \ i = 1, \dots, S, \\ \mathcal{C}2: \quad & |\boldsymbol{g}_{Uki} \boldsymbol{d}_l|^2 \leq \epsilon, \ k = 1, \dots, K, \ i = 1, \dots, S. \end{aligned} \tag{6.19}$$

Interestingly, it can be noticed how in this sequential scheme the SINR corresponding to the k-th user is given by $\mathbb{E}_i \left[\frac{|\boldsymbol{g}_{ki} \boldsymbol{d}_l + \boldsymbol{v}_k[i]|^2}{\sigma_z^2} \right]$, since the ISI coming from the previous block, modeled by $\boldsymbol{v}_k$, also contributes to the constructive interference effect.

Furthermore, by focusing on a QAM modulation scheme, the problem can be finally written decomposing the constraints $\mathcal{C}1$ along the in-phase and quadrature components of the symbols, as follows:

$$\begin{aligned}\boldsymbol{d}_l(\boldsymbol{s},\boldsymbol{H},\boldsymbol{A}_{\mathrm{TX}},\boldsymbol{A}_{\mathrm{RX}},\boldsymbol{\gamma},\boldsymbol{v},\epsilon) = \arg\min_{\boldsymbol{d}_l} \quad & \|(\boldsymbol{I}_N \otimes \boldsymbol{A}_{\mathrm{TX}}^T)\boldsymbol{d}_l\|^2 \\ \text{s.t.} \quad \mathcal{C}1: \quad & \mathrm{Re}(\boldsymbol{g}_{ki}\boldsymbol{d}_l + \boldsymbol{v}_k[i]) \gtrless \sigma_z\sqrt{\gamma_k}\,\mathrm{Re}(\boldsymbol{s}_k[i]),\ k=1,\dots,K,\ i=1,\dots,S, \\ \mathcal{C}2: \quad & \mathrm{Im}(\boldsymbol{g}_{ki}\boldsymbol{d}_l + \boldsymbol{v}_k[i]) \gtrless \sigma_z\sqrt{\gamma_k}\,\mathrm{Im}(\boldsymbol{s}_k[i]),\ k=1,\dots,K,\ i=1,\dots,S, \\ \mathcal{C}3: \quad & |\boldsymbol{g}_{Uki}\boldsymbol{d}_l|^2 \le \epsilon,\ k=1,\dots,K,\ i=1,\dots,S.\end{aligned} \tag{6.20}$$

In the last proposed formulation, the same considerations given in the previous section apply for the constraints $\mathcal{C}1$, $\mathcal{C}2$, while the constraints introduced in $\mathcal{C}3$ are convex quadratic ones. Therefore, the final optimization problem in (6.20) is convex and can be solved resorting to the standard convex optimization tools [149].

6.4 Numerical Results

This section presents numerical results to show the effectiveness of the proposed scheme with respect to the classical SLP approach [22, 23], which can handle only the interference in the spatial dimension. As shown in [23, 25], SLP already outperforms the conventional block-level precoding schemes and this is why it was selected as benchmark. The performance of the proposed approaches will be assessed in terms of symbol error rate (SER), total transmit power, effective rate and energy efficiency, considering different acceleration factors τ applied to the FTN system[9]. Further, bit error rate (BER) results will be presented to assess the performance of the techniques when a FEC scheme is used.

All the results presented in the remainder of this section are obtained assuming a 16-QAM modulation scheme for the data information, while the number of antennas N and the number of users K are both fixed to 4 (unless specified otherwise). As to the pulse shaping operation, it is modeled using a SRRC pulse waveform, which is the most used in practical systems, with a roll-off factor of 0.25. The considered oversampling factor ξ is 20. The target SINR is assumed the same for all the users for the sake of simplicity, and it is fixed to 12 dB for all the results[10], while the noise variance σ_z^2 is

[9] This thesis does not provide a performance bound (for instance, in terms of information rate as in [140]). This is not straightforward in the context of SLP, because of the irregular received constellations due to the constructive interference effect (see also [23]), and is an issue for the future work.

[10] As already mentioned, in practical systems the target SINR should be selected based on a training phase. Herein a 12 dB target is considered as a reference value for the assumed 16-QAM modulation scheme. It can be numerically checked that this value can lead to good BER performance when an appropriate FEC scheme is employed (see also Section 6.4.3). However, it should be kept in mind that, when needed for a specific application, the SER/BER performance can always be improved by considering a higher target SINR.

assumed unitary. Unless specified otherwise, the results are obtained by averaging over several realizations of the spatial channel matrix which is generated, for the generic user k, as $\boldsymbol{h}_k \sim \mathcal{CN}(0, \sigma_h^2 \boldsymbol{I}_N)$, with $\sigma_h^2 = 1$. Finally, the block length S has been set to 50 symbols. In the following, first the focus is on the scheme presented in section 6.2, which does not consider any inter-block interference. Then, the sequential FTN SLP scheme of section 6.3 is evaluated.

6.4.1 Performance Analysis without Inter-block Interference

Herein a scenario with no ISI between multiple symbol blocks is considered. This is the case when a single data block is handled by the SLP scheme, or when the framing structure ensures that the adjacent blocks do not mutually interfere. Accordingly, the focus is on the scheme presented in section 6.2. The presented results are obtained by averaging over several realizations of the data information matrix $\boldsymbol{S}$.

Fig. 6.4 shows a SER result comparing the proposed FTN SLP approach with the SLP scheme of [23], as a function of the acceleration factor τ. Since the SLP scheme of [23] operates only in the spatial dimension, for each symbol slot, this technique is referred to as space-only SLP. As expected, the SER achieved by the two approaches is the same when no acceleration is applied, since in this case there is no ISI so the schemes are equivalent. When τ is reduced[11], it is apparent how the space-only approach severely suffers the introduced ISI, which is not handled by such scheme, showing a higher and higher SER with decreasing values of τ. On the other hand, the result shows the ability of the proposed technique in managing the ISI for all the considered acceleration factors. Interestingly, the constructive interference effect over the temporal dimension even allows to improve the achieved SER performance[12] when the system is more accelerated.

Another interesting performance metric is the effective sum rate of the system. This quantity can be defined as:

$$\bar{R} = \frac{1}{\tau} \sum_{k=1}^{K} R_k (1 - \mathrm{SER}_k), \tag{6.21}$$

where R_k is the error-free rate for the user k. Such error-free rate (the maximum rate that can be achieved by the used modulation) can be written in turn as $W \log_2(M)$, with W being the user bandwidth and M the modulation order. Considering a user

[11] For the sake of clarity, it should be stressed again that the acceleration factor τ defines the symbol period fraction of the accelerated system compared to the Nyquist system. Thus lower τ means higher acceleration, as discussed in section 6.1.1.

[12] The attained SER values can be further reduced by increasing the target SINR. However, the application of FEC allows to strongly boost the performance in terms of BER without any SINR increase, as shown later in this section (see also footnote 10).

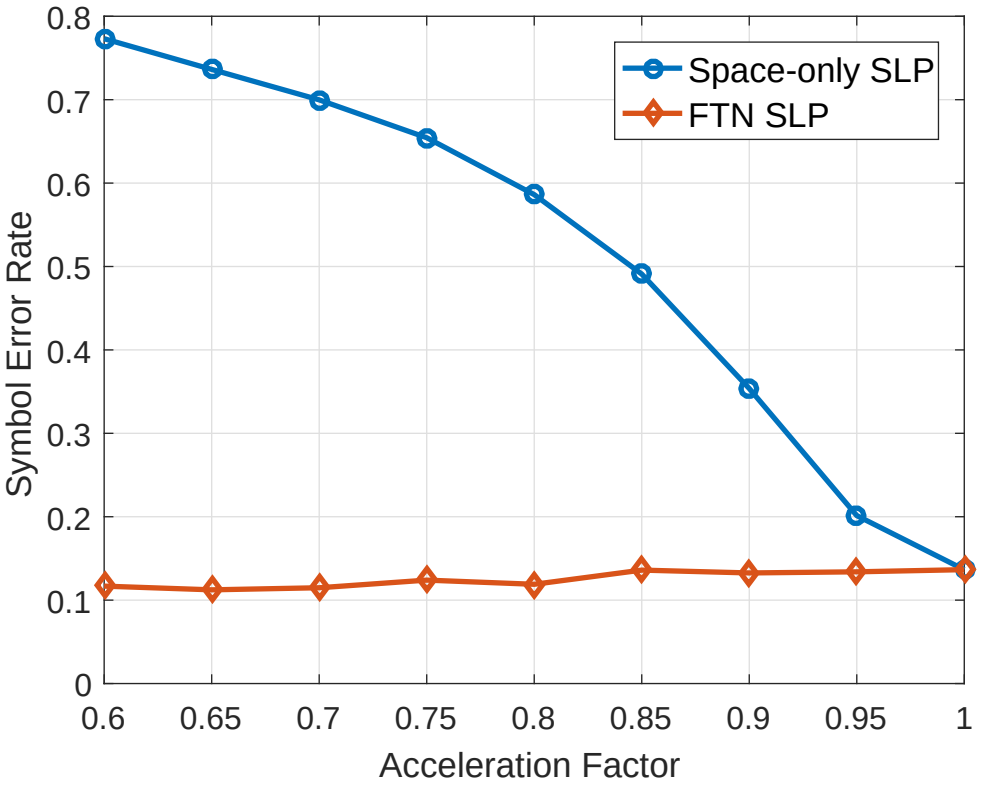

FIGURE 6.4: Attained symbol error rate versus acceleration factor.

bandwidth of 10 MHz (this value will be also used in the remainder of this section), Fig. 6.5 compares the effective rate (in Mbps) of the proposed technique with the space-only benchmark, for different acceleration factors. This result shows again the effectiveness of the FTN SLP scheme in exploiting the FTN signaling and handling the ISI.

It is now essential to assess the transmit power required by the proposed scheme, and how it varies with the acceleration factor. The total transmit power, defined in (6.7), is shown, in dBW, in Fig. 6.6 as a function of τ. While the transmit power does not depend on τ for the space-only SLP (as this approach does not take into account the acceleration), it is visible how with the FTN SLP it significantly depends on τ. In particular, when τ is too low the required power becomes prohibitive. Nevertheless, if a τ not lower than 0.8 (which determines a 25% gain in the rate with respect to the non accelerated case) is used, the power increase is moderate.

Finally, a fundamental performance metric which allows to jointly account for the effective rate and the consumed power is the energy efficiency, defined as $\mathcal{E} = \bar{R}/P_{\text{tot}}$, with $\bar{R}$ and P_{tot} defined in (6.21) and (6.7) respectively[13]. The related result, in Mbits/J,

[13]For simplicity, in the computation of the consumed power only the transmit power is considered, while additional terms due to, for instance, the digital-to-analog conversion or the power amplifiers

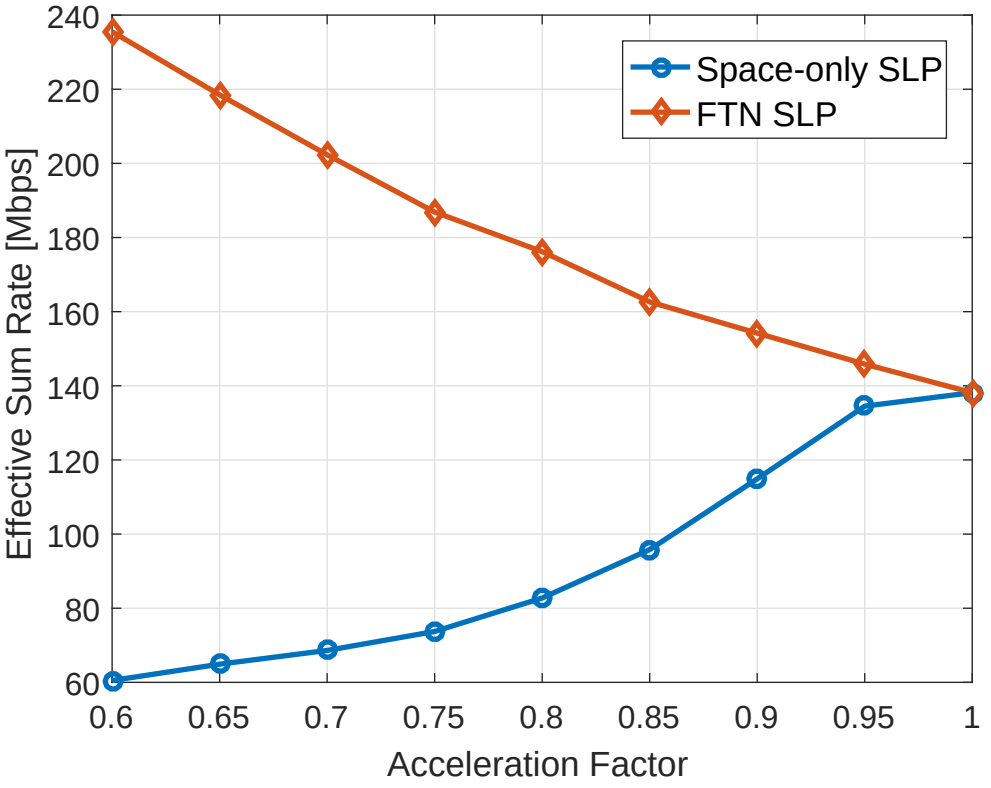

FIGURE 6.5: Attained effective sum rate, in Mbps, versus acceleration factor.

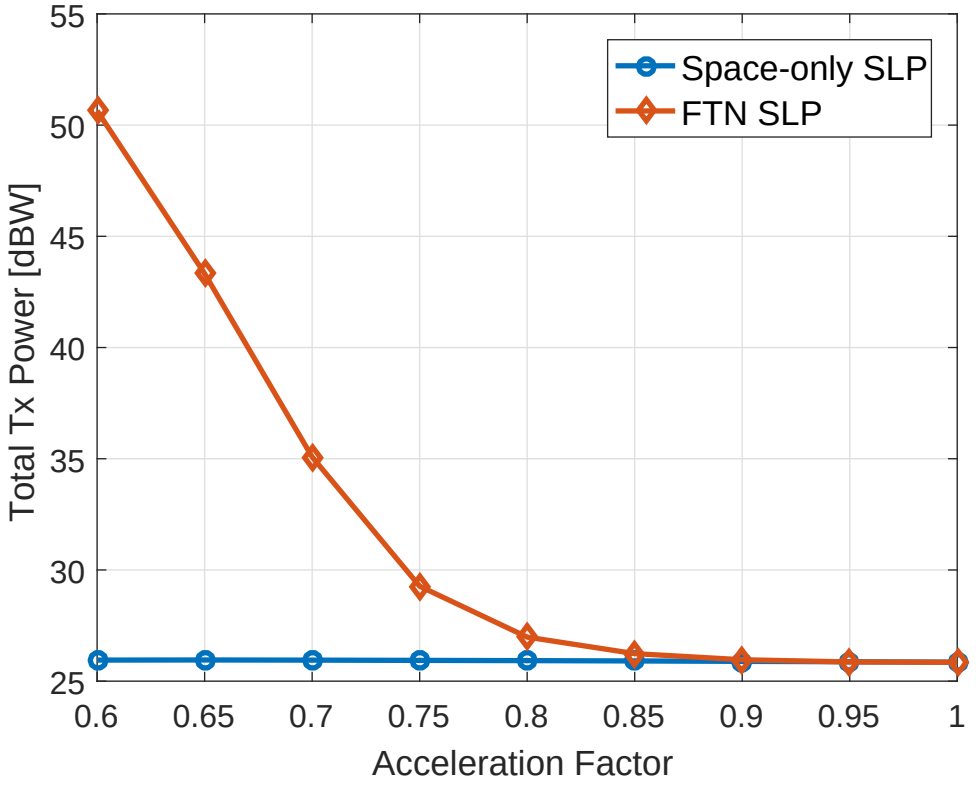

FIGURE 6.6: Total transmit power, in dBW, versus acceleration factor.

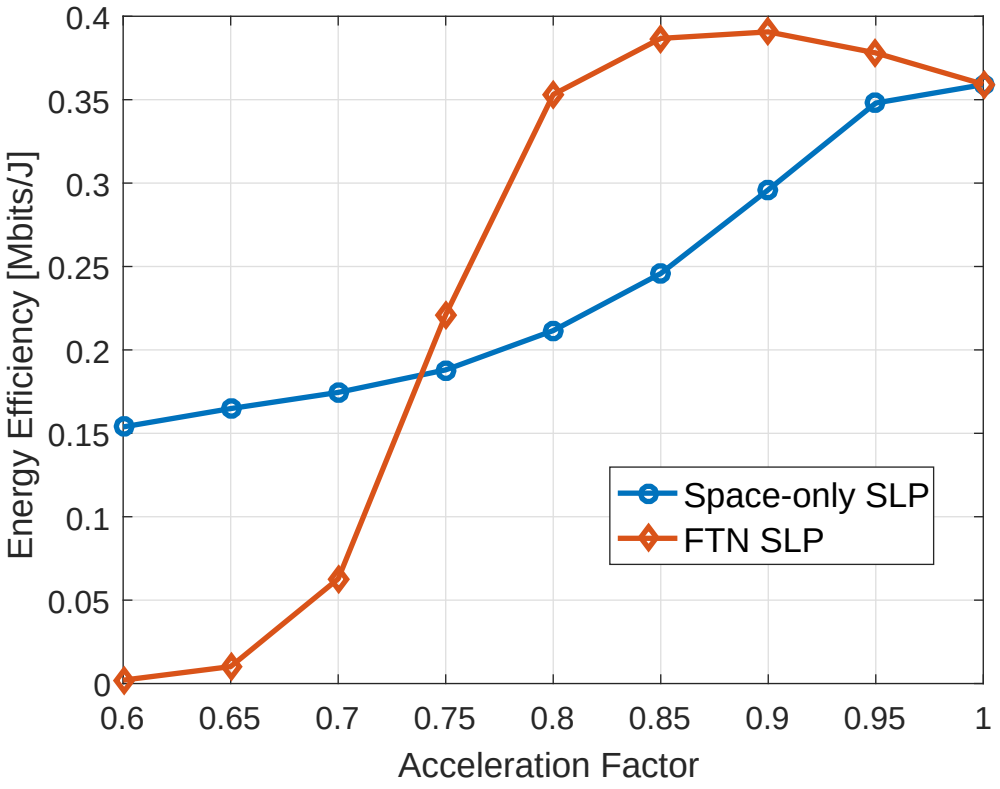

FIGURE 6.7: Attained energy efficiency, in Mbits/J, versus acceleration factor.

is shown in Fig. 6.7. From the result, it turns out that the proposed approach outperforms the space-only scheme in terms of energy efficiency only in a certain range of the acceleration factor, starting from 0.75. Further, it should be highlighted that when $\tau < 0.85$ the energy efficiency of the FTN scheme becomes lower with respect to the non accelerated case, with $\tau = 1$. This means that accelerating the transmission beyond this threshold, although determining a higher rate, is not convenient for the energy efficiency of the system. We can conclude that the optimal τ in this scenario is 0.85, which allows an 18% gain in the rate with respect to the non FTN case.

6.4.2 Performance Analysis accounting for the Inter-block Interference

In this section, a scenario where multiple data blocks are sequentially transmitted is considered, without assuming any separation between the blocks. In this case, there is inter-block ISI between adjacent blocks, and the performance of the scheme proposed in section 6.3 can be assessed. The presented results are obtained by simulating $L = 10$ sequential blocks. As anticipated, the choice of the parameter ϵ in (6.20) affects the feasibility of the optimization problem. Moreover, since the problem (6.20) is more

losses, are neglected. Nevertheless, the main conclusions of this work still apply if a more complicated power model is used.

constrained than the one in (6.11), the permissible range for the acceleration factor τ turns out to be tighter. In fact, the performed numerical analysis has shown that there is a lower bound for τ, which depends on ϵ, under which the problem becomes unfeasible. Hereafter we consider acceleration factors τ in the range $[0.8, 1]$, and the performance of the scheme in (6.20) is assessed for different values of ϵ. In particular, the evaluation is performed for $\epsilon = 3\sigma_z^2$, $\epsilon = 6\sigma_z^2$, and $\epsilon = +\infty$, with the last case corresponding to solving the problem in (6.20) without the constraint $\mathcal{C}3$.

The obtained numerical results are presented in Figs. 6.8-6.11, based on the previously introduced performance metrics. The sequential FTN SLP approach is compared with the non sequential one of section 6.2, which has to tolerate the inter-block interference arising in the system. Moreover, the space-only SLP is also used as a benchmark. In Figs. 6.8-6.9 the obtained SER and the effective sum rate are shown, respectively, as a function of the acceleration factor τ. It is notable how, when the acceleration becomes significant, the non sequential FTN SLP scheme suffers the ISI, showing worse SER and rate performance. On the other hand, the introduced sequential FTN SLP scheme is able to handle the inter-block interference, and it does not show any SER degradation when τ is reduced with $\epsilon = 3\sigma_z^2$ and $\epsilon = 6\sigma_z^2$, without a significant difference among these two cases. When the constraint $\mathcal{C}3$ in (6.20) is relaxed, i.e. for $\epsilon = +\infty$, it can be seen how even the sequential scheme shows a SER degradation for low values of τ, because of the residual inter-block ISI. Nevertheless, it is apparent how the sequential scheme outperforms the benchmarks in terms of SER and effective rate even when ϵ is set to $+\infty$.

As previously discussed, it is fundamental to evaluate the performance also in terms of transmit power and, ultimately, in terms of energy efficiency. The related results are shown in Figs. 6.10-6.11. Concerning the total transmit power, it appears from Fig. 6.10 how the power requirement of the sequential scheme is higher than the non sequential one for $\epsilon = 3\sigma_z^2$ and $\epsilon = 6\sigma_z^2$, especially for low values of τ within the considered range. On the other hand, it emerges how when $\epsilon = +\infty$ the transmit power is comparable to the non sequential scheme, since in this case the problem in (6.20) has more degrees of freedom. Taking this into account, it is interesting to notice from Fig. 6.11 how the best approach in terms of energy efficiency is the sequential FTN scheme with $\epsilon = +\infty$, which outperforms the non sequential scheme for all the considered acceleration factors. Conversely, the constrained cases with $\epsilon = 3\sigma_z^2$ and $\epsilon = 6\sigma_z^2$ show a worse energy efficiency due to their higher transmit power. For this reason, in the remainder of this section the main focus will be on the case with $\epsilon = +\infty$, which is assumed when not specified otherwise. Concerning the acceleration factor, it can be observed how for $\tau \geq 0.85$ the energy efficiency attained by the proposed sequential FTN scheme is not lower than the non accelerated case ($\tau = 1$). Accordingly, also in this multi-block

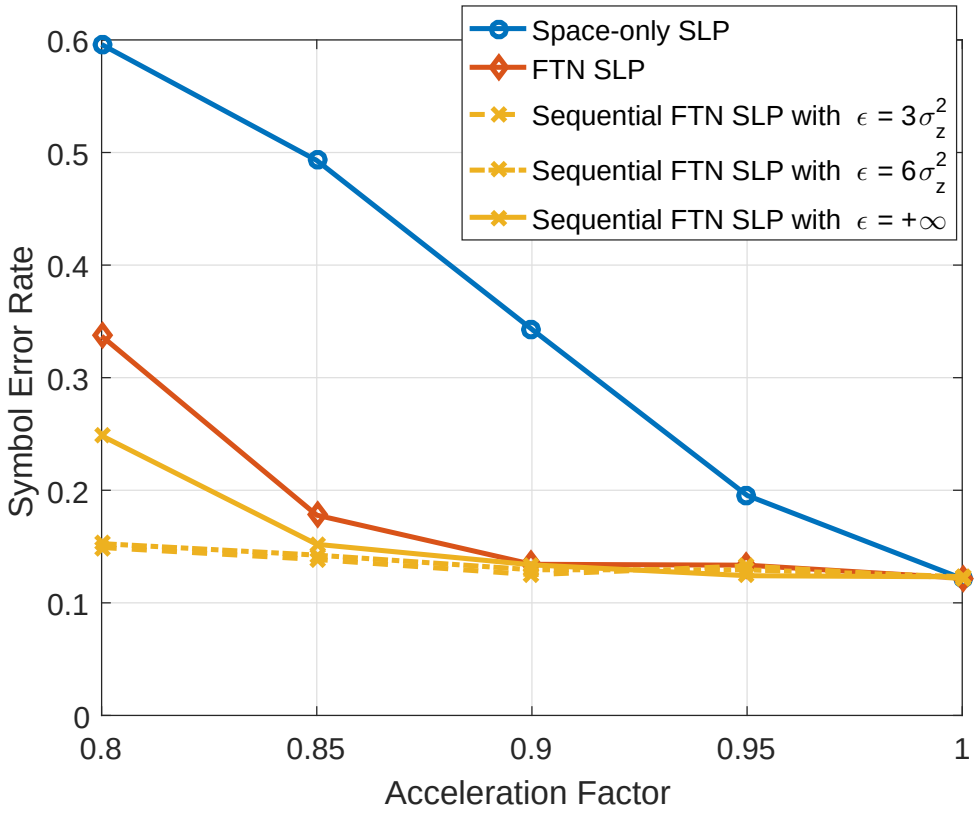

FIGURE 6.8: Attained symbol error rate versus acceleration factor, in a multi-block scenario.

scenario the optimal τ is 0.85, which allows an 18% gain in the rate with respect to the non FTN case.

An additional result is displayed in Fig. 6.12, which shows how the achieved performance changes when more antennas are utilized at the transmitter. More specifically, the energy efficiency and the effective rate are represented as a function of the number of antennas N, when $\tau = 0.85$. Remarkably, while the effective rate does not show substantial changes, the attained energy efficiency considerably grows with N due to the reduced transmit power required to achieve the target SINR. This effect is related to the improved constructive interference effect taking place when more antennas are used, and has been discussed also in [23].

6.4.3 Effect of imperfect CSI and BER analysis with FEC

So far, a perfect knowledge of the CSI has been assumed for the presented techniques, as a robust version of them to CSI errors falls out of the scope of this thesis. Nevertheless, it is worth analyzing how the different schemes are sensitive to channel uncertainties, which are usually present in practical applications. Consequently we can model the

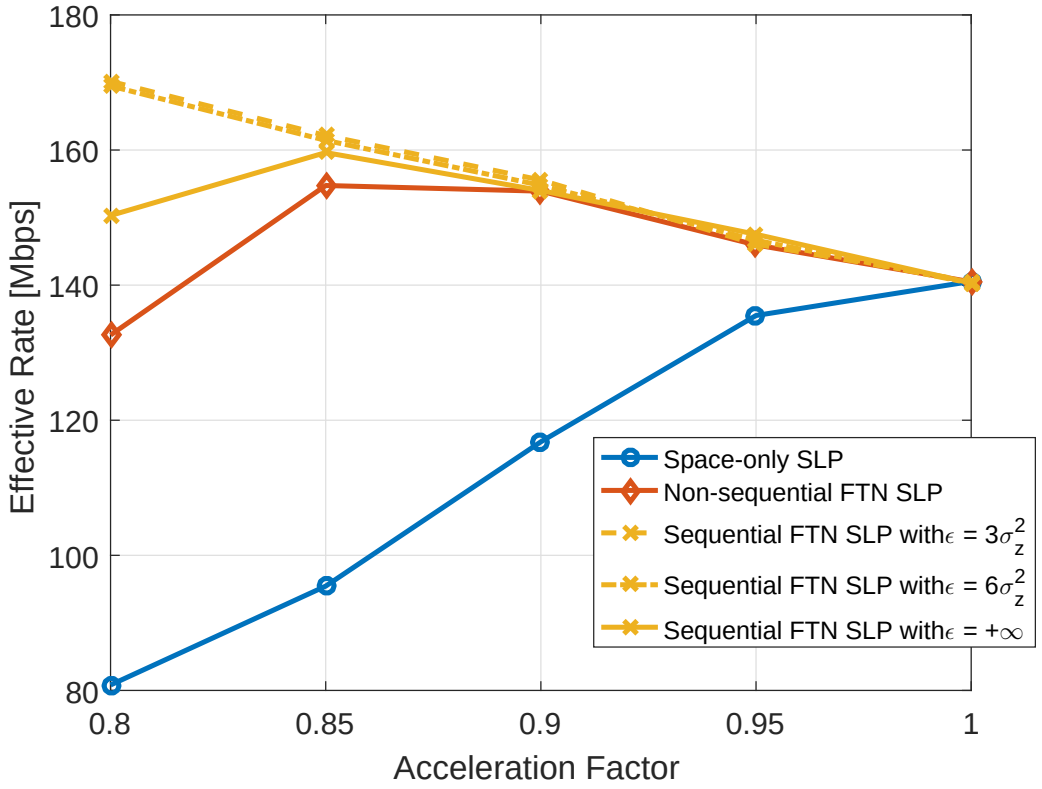

FIGURE 6.9: Attained effective sum rate, in Mbps, versus acceleration factor, in a multi-block scenario.

CSI estimate for the k-th user as $\hat{\boldsymbol{h}}_k = \boldsymbol{h}_k + \boldsymbol{e}_k$ (see also [13]), with $\boldsymbol{e}_k$ being an error vector modeled as $\boldsymbol{e}_k \sim \mathcal{CN}(0, \sigma_e^2 \boldsymbol{I}_N)$. In Fig. 6.13 the obtained SER for the introduced schemes is presented, for different values of τ and σ_e^2, focusing on the multi-block scenario (moreover, for simplicity from now on a fixed channel matrix $\boldsymbol{H}$ is considered, as in (6.22)). First of all, it can be noticed how the SER degradation induced by the CSI error is limited for $\sigma_e^2 = 10^{-4}$ and $\sigma_e^2 = 10^{-3}$, while when $\sigma_e^2 = 10^{-2}$ the performance is extremely degraded for all the schemes. Notably, the non sequential FTN SLP scheme and the sequential one show a comparable sensitivity to CSI errors, and their SER degradation does not substantially vary with τ. As to the space-only scheme, it shows the same sensitivity of the proposed ones only for high acceleration factors ($\tau > 0.9$), while when τ is decreased the SER degradation is reduced (however, it should be noted that in this case the SER is already very high with perfect CSI, thus the CSI errors are less determinant).

Besides the imperfect CSI, the performance of precoding can be degraded by timing errors. In fact, a common assumption in the precoding literature is to have a perfect synchronization between the transmitted waveforms. However, in many practical systems (for instance in satellite communications) there is a timing misalignment across

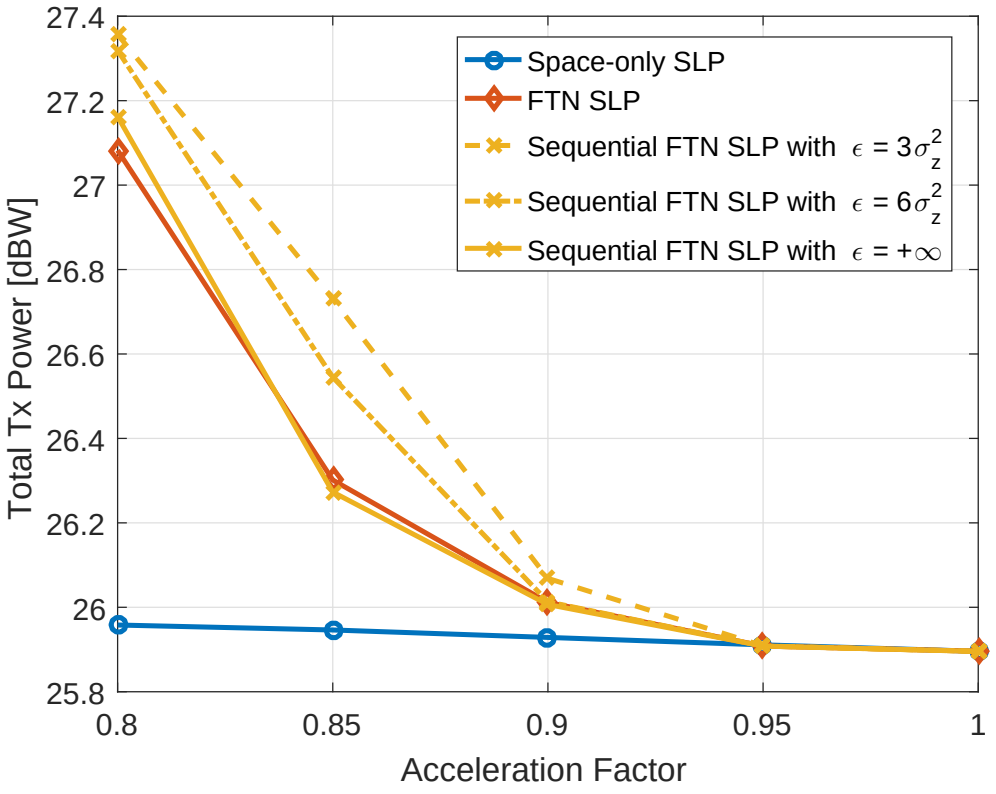

FIGURE 6.10: Total transmit power, in dBW, versus acceleration factor, in a multi-block scenario.

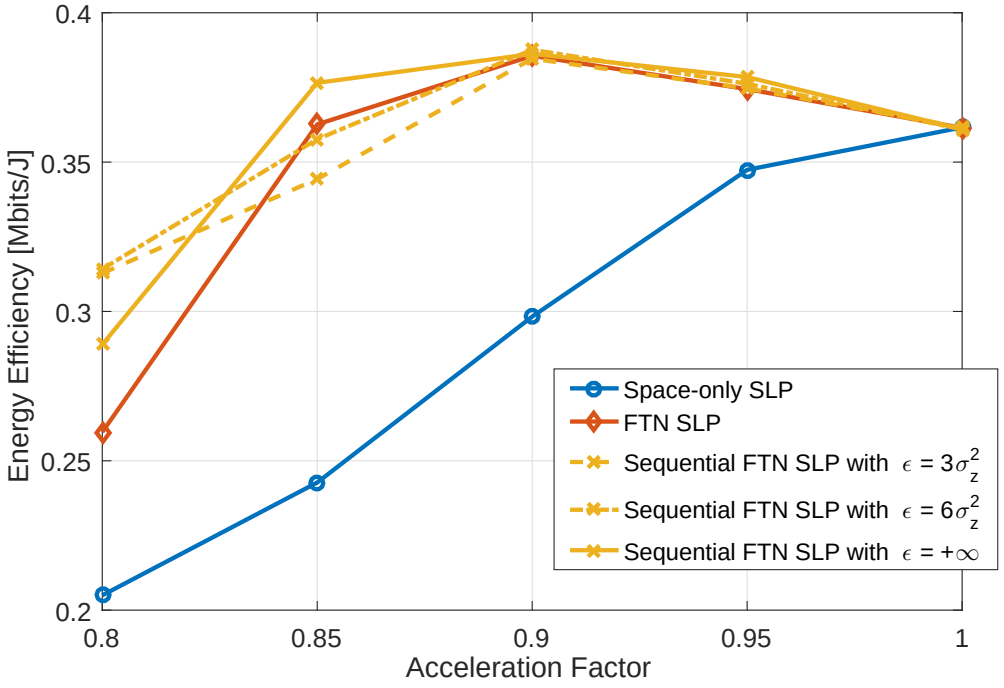

FIGURE 6.11: Attained energy efficiency, in Mbits/J, versus acceleration factor, in a multi-block scenario.

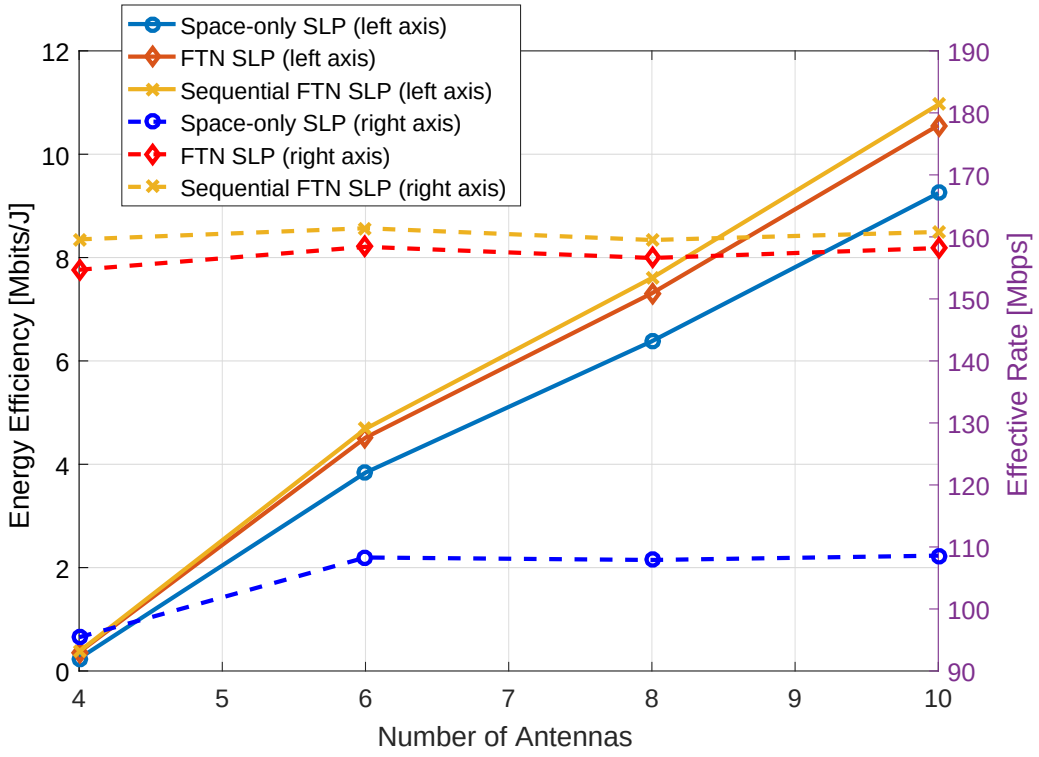

FIGURE 6.12: Attained energy efficiency and effective rate versus number of antennas, for $\tau = 0.85$.

$$\boldsymbol{H} = \begin{bmatrix} -0.6753 + 0.7875\imath & -0.9406 + 0.3229\imath & -0.1814 + 0.2493\imath & 0.1856 - 0.7855\imath \\ -0.0214 + 0.3383\imath & -1.1166 + 1.0522\imath & 0.0435 - 1.1963\imath & -0.8914 - 0.2106\imath \\ 0.1734 - 1.0120\imath & -1.1399 + 1.5326\imath & -0.5112 + 1.3084\imath & -0.8879 + 0.3026\imath \\ 0.0145 - 0.0956\imath & -0.5300 + 0.0520\imath & -0.5749 - 0.0975\imath & -0.2097 + 0.3532\imath \end{bmatrix}, \tag{6.22}$$

the different antennas which, if not compensated, can deteriorate the precoding gains. Timing errors are an issue in the general context of precoding, and have been addressed for instance in [163]. A study of timing errors in the specific context of SLP falls out of the scope of this thesis (which assumes synchronized transmissions), and is left for the future work.

Finally, Fig. 6.14 presents a result in terms of BER obtained using a FEC scheme with the proposed techniques. In particular, the low-density parity check (LDPC) code of the DVB-S2 standard [130], which is available in Matlab, is considered as an example of FEC. The frame length is 64800 bits, while the code rate is 5/6 (for more details on this specific LDPC scheme the reader is referred to [130]). The presented result has been obtained by simulating 10 frames[14]. The coded BER is shown for the different approaches as a function of τ, and the case with $\epsilon = 6\sigma_z^2$ is also considered (besides $\epsilon = +\infty$) for the sequential FTN SLP scheme. Remarkably, it can be seen how the application of LDPC

[14]The simulation requires to solve numerically the optimization problems using CVX, and this makes prohibitive to simulate a higher number of frames

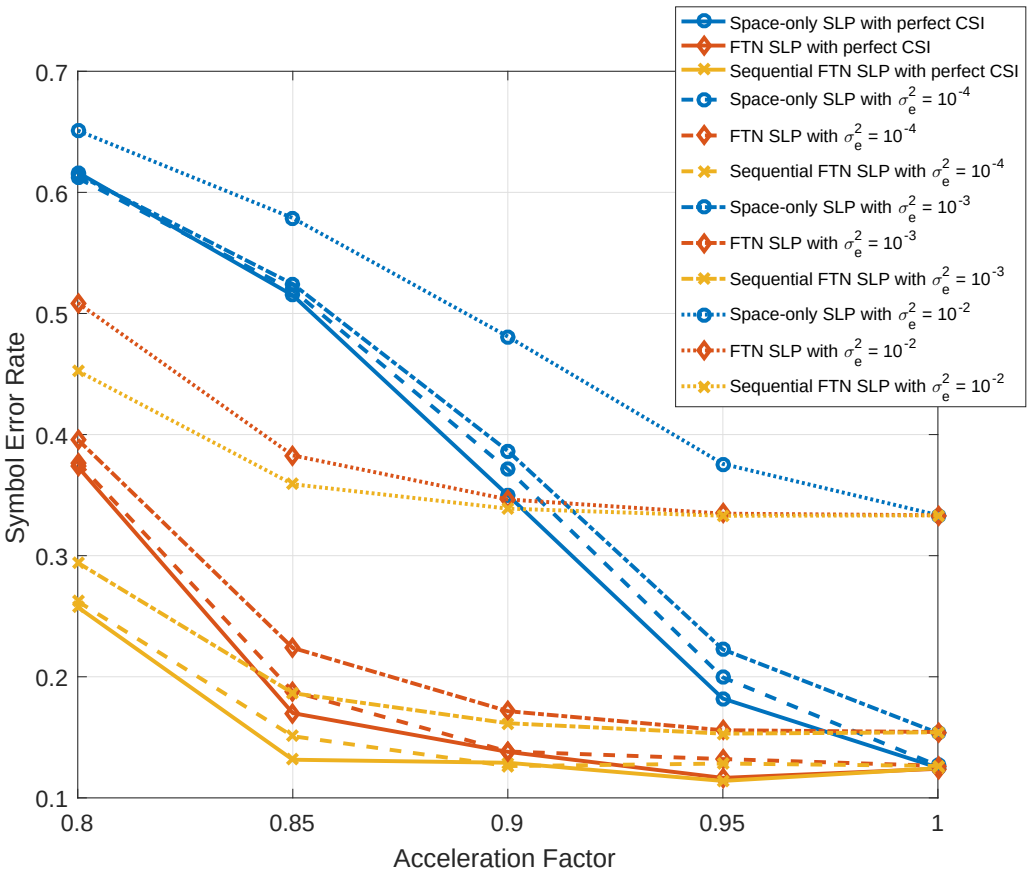

FIGURE 6.13: Attained symbol error rate versus acceleration factor, considering CSI errors.

provides considerable improvement in the BER performance achieved by the proposed schemes, with an error-free communication (i.e., a zero BER for the simulated scenario) for $\tau \geq 0.9$ for the sequential SLP with $\epsilon = 6\sigma_z^2$.

6.4.4 Numerical Evaluation of the Complexity

To conclude this section, a complexity evaluation of the proposed approaches is provided, as a function of the number of symbols to be processed (for each user stream). Since the proposed optimization problems are tackled resorting to numerical convex optimization tools [149], analytical expressions for the complexity are hard to derive. Thus herein the complexity is numerically evaluated in terms of average running time of the algorithms over the same machine. Before presenting such evaluation, it should be stressed that in general complexity is one of the key challenges of SLP with respect to conventional channel-level precoding schemes: in fact, while in the latter ones the precoder optimization is performed once per channel coherence time, SLP (e.g. [23]) presents a much

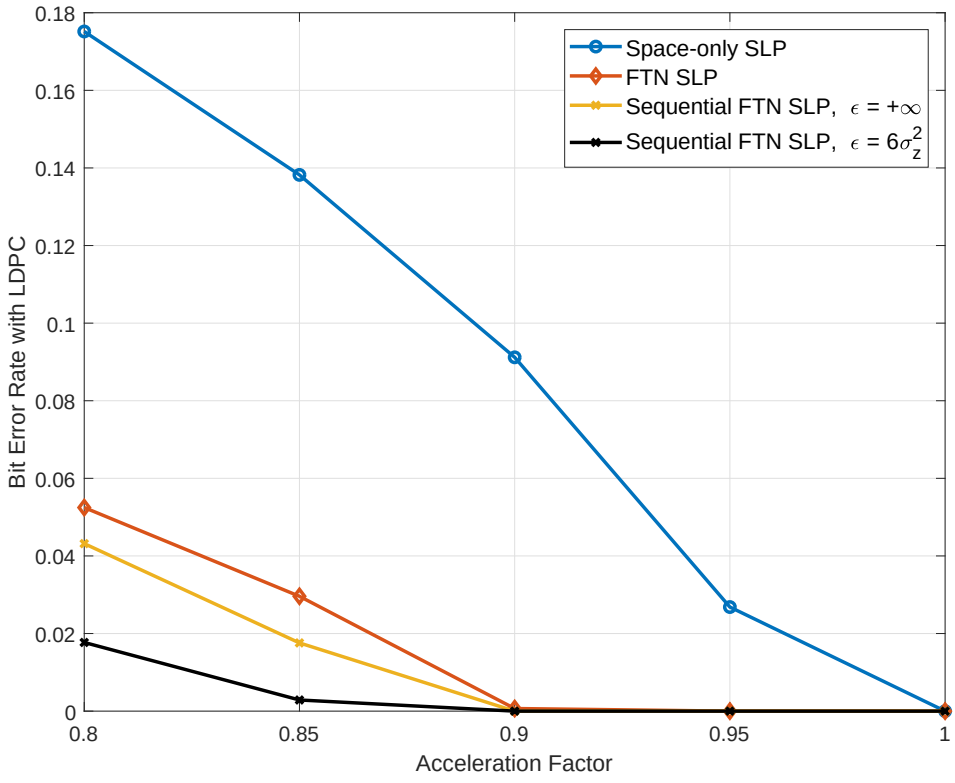

FIGURE 6.14: Attained bit error rate versus acceleration factor, considering a LDPC scheme.

higher switching rate, equal to the baud rate. Nonetheless, the spatio-temporal precoding introduced herein has an advantage in this regard, since the optimization procedure applies once per block and not once per symbol slot. This can be observed in Fig. 6.15, which presents how the average running time varies with the number of symbols to be processed per stream, for $\tau = 0.85$. The considered schemes are the spatio-temporal SLP, which performs the optimization symbol by symbol, the non sequential FTN SLP, which processes the whole symbol stream all at once, and the sequential FTN SLP scheme, which processes the data divided in blocks of $S = 50$ symbols. As expected, it can be observed how both the space-only approach and the sequential FTN one present a linear dependence between the running time and the number of symbols (blocks), but the latter one shows a remarkably reduced running time due to the block processing. On the other hand, it can be also noticed how, in the case of the non sequential FTN SLP, the complexity grows in a superlinear way with the number of processed symbols, and this justifies the need of resorting to a serial processing of multiple sequential blocks. Overall, the sequential FTN SLP scheme appears to be the most suitable in terms of complexity. In general, complexity still remains an open challenge of the SLP framework, especially when the system dimensions (e.g. number of users/antennas) is high.

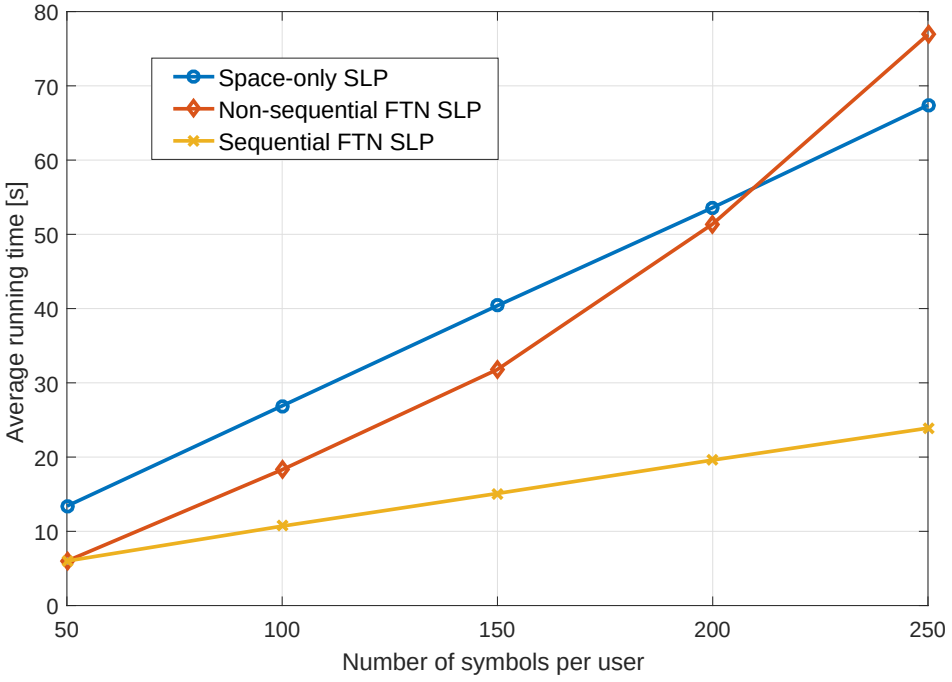

FIGURE 6.15: Average running time of the algorithms, in seconds, versus stream length.

An efficient implementation of SLP schemes aimed at reducing their inherent complexity, and eventually at allowing a real-time processing, is part of the ongoing and future work [164].

6.5 Conclusions

In this chapter, a novel symbol-level precoding strategy has been proposed, which handles, at the transmitter side, not only the interference in the spatial dimension (the MUI), but also the interference in the temporal dimension (the ISI). This new precoding method, named spatio-temporal symbol-level precoding, is used to apply faster-than-Nyquist signaling over multiuser MISO systems. The introduced strategy splits the data streams in blocks of symbols, and processes the blocks so as to exploit in a constructive fashion the interference both in the temporal dimension and in the spatial one, thus gleaning benefits from both the domains. Firstly, a sum power minimization scheme which tackles the interference within each data block has been proposed. Afterwards, an extension of the optimization scheme has been presented, which tackles a scenario with multiple mutually interfering data blocks, and is able to manage the inter-block ISI arising between adjacent blocks. The performance of the proposed schemes has been assessed through numerical simulations over a multiuser MISO system using SRRC pulse shaping and a 16-QAM modulation scheme, in terms of achieved SER, effective sum rate,

energy efficiency, and total transmit power. The results have shown how the proposed spatio-temporal precoding outperforms the existent symbol-level precoding solutions in terms of effective rate and energy efficiency, for acceleration factors in the order of 0.8-0.9. Further, the gain in the system rate (thus, in energy efficiency) of the FTN schemes has been discussed with respect to the classical Nyquist transmission.

Chapter 7

Conclusions and Future Work

In this chapter, the main conclusions of this thesis are summarized, and the issues for future work are identified and discussed. The main focus of this thesis has been the investigation of novel symbol-level precoding (SLP) schemes suitable to non-linear systems, where the per-antenna high-power amplifiers (HPAs) introduce an amplitude and phase distortion on the transmitted signals. In this context, the objective was to exploit the potential of SLP not only for constructive interference, but also to improve the power dynamics of the transmitted waveforms, in order to enhance the robustness to non-linear effects.

In the first part of the thesis novel SLP schemes have been proposed in order to improve the power dynamics of the transmitted signals in the spatial dimension, by reducing the instantaneous power imbalances across the different antennas. First, a SLP per-antenna power minimization scheme has been presented, followed by a related max-min fair formulation with per-antenna power constraints. These schemes allow to take into account the per-antenna power limitations of practical multi-user multiple-input single-output (MISO) systems. In fact, a common practice in multi-antenna systems is the use of separate per-antenna amplifiers, thus considering the power constraints individually for each transmitting antenna is particularly important. Moreover, these SLP schemes reduce the power peaks among the different antennas, for each symbol slot. Then, more advanced SLP schemes have been formulated and solved, with the objective of further improving the spatial dynamics of the signals and therefore counteracting the problem of differential phase shift. Specifically, a first proposed scheme performs a per-antenna power minimization, under QoS constraints and under a lower bound constraint on the per-antenna transmit power. The related optimization problem has been solved through an iterative procedure relying on successive convex approximation (SCA). A second scheme performs a minimization of the spatial peak-to-average power

ratio (SPAPR), evaluated amongst the transmitting antennas, under Quality-of-Service (QoS) constraints. The related optimization problem has been tackled by resorting jointly to parametric programming and SCA. Numerical results have been presented, showing how the proposed schemes outperform the state of the art in SLP in terms of SPAPR and spatial dynamic range, at the expense of a higher average transmitted power. Further, the enhanced robustness of the proposed schemes to non-linear effects has been assessed based on symbol error rate (SER) results over a channel corrupted by a non-linear HPA model.

In the second part of the thesis a novel SLP method has been developed, referred to as spatio-temporal SLP, where the temporal variation of the transmit power is also considered in the SLP optimization. The main aim of this extension was to improve the power dynamics of the transmitted waveforms also in the temporal dimension, which are particular important in the context of non-linear channels, in order to counteract the distortion and the saturation effect. Specifically, spatio-temporal SLP has been used to minimize the peak-to-average power ratio (PAPR) of the transmitted waveforms both in space and time, while at the same time exploiting the constructive interference effect. The related optimization problem has been formulated in a similar fashion to the SPAPR minimization carried out in the first part of the thesis, therefore parametric programming and SCA have been used to tackle the problem. Numerical results have been shown that accounting also for the temporal dimension significantly improves the performance over non-linear channels, in terms of SER and in terms of power distribution, at the expense of a higher average transmitted power. Then, one step further has been taken in the context of spatio-temporal SLP. In particular, a spatio-temporal SLP scheme is proposed which enables faster-than-Nyquist (FTN) signaling over multi-user systems, by constructively handling at the transmitter side not only the multi-user interference (MUI) but also the inter-symbol interference (ISI). This strategy, which is not referred to non-linear systems, allows to benefit from the increased throughput provided by FTN signaling without imposing additional complexity at the user terminals. Numerical results have been presented in a comparative fashion to show the effectiveness of the this novel FTN approach, which outperform the state of the art symbol-level precoding schemes in terms of SER, effective rate, and energy efficiency.

7.1 Future Work

The work carried out in this thesis can be extended in several directions. The main issues left for future work are discussed below:

- The accuracy of the estimated channel state information (CSI) plays an important role in designing accurate precoding that can exploit the interference created from the simultaneous spatial transmissions. Designing robust precoding strategies to CSI errors is an important topic to tackle, especially in the context of SLP for non-linear channels.

- Complexity is an open challenge in the context of SLP, especially when the system dimension (e.g. number of users/antennas) is high. An efficient implementation of the proposed SLP schemes aimed at reducing their inherent complexity, and eventually at allowing a real-time processing, is an issue for future work.

- The proposed schemes refer to a unicast scenario, where each data stream is addressed to a single user. In general, SLP has been applied so far only in the unicast framework. The investigation of the proposed schemes for multicast scenarios is an interesting problem for future work. In particular, a multicast evolution of the proposed schemes would allow their application in communication systems where the framing structure imposes that groups of user receive the same data.

- The exploitation of multiple antennas at the receivers has never been discussed for SLP (however, it has been considered in the context of single link directional modulation [165, 166]). An investigation of SLP, and of the proposed schemes in particular, in a multiple-input multiple-output (MIMO) context where more degrees of freedom are available, is an issue for future work.

- Another issue to be addressed is the study of the proposed schemes accounting for adaptive coding and modulation (ACM) schemes. This is particularly important in the context of SLP for FTN signaling, where it is important to assess if the discussed energy efficiency gains hold in a system supporting ACM.

- The study of the introduced schemes under frequency selective fading channels is an important extension left for future work. It is well known that frequency selective fading introduces ISI. In this regard, an interesting research avenue would be to tackle such ISI analogously to the FTN case, resorting to spatio-temporal SLP.

- As remarked, the FTN SLP scheme introduced in chapter 6 is not addressed to non-linear channels. Nonetheless, it can be extended to the non-linear case by modifying the related optimization formulation in the same fashion as in chapters 4-5. Further, the spatio-temporal processing could be used to handle non-linear channels with memory, by addressing the resulting ISI.

- Finally, a further extension of the proposed FTN SLP scheme could be considered for multi-carrier systems. In this case, it has been shown that a similar concept

to FTN can be applied in the frequency domain, by handling the resulting ISI. Although it is a challenging problem, an extension of the proposed FTN SLP scheme to the frequency domain would allow to jointly handle at the transmitter the interference in the spatial domain (MUI), temporal domain (ISI), and frequency domain (ICI).

Appendix A

Proof of Theorem 4.1.

This proof is based on a number of steps through which the optimization problem (4.3) is transformed into the formulation in (4.4).

First of all, following the method of [125, 126, 142], the constraint $\mathcal{C}3$ in (4.3) can be rewritten, by applying the tangent operator[1], as:

$$\frac{\mathrm{Im}(\boldsymbol{h}_j\boldsymbol{x})}{\mathrm{Re}(\boldsymbol{h}_j\boldsymbol{x})} = t_j,\ j = 1, \ldots, K, \tag{A.1}$$

where $t_j = \tan(\angle d_j)$. However, since the tangent is not a one-to-one function, the following conditions should be added, in order to ensure that the received symbol and the intended one lie in the same quadrant:

$$\begin{aligned} \mathrm{Re}(d_j)\,\mathrm{Re}(\boldsymbol{h}_j\boldsymbol{x}) \geq 0,\ j = 1, \ldots, K, \\ \mathrm{Im}(d_j)\,\mathrm{Im}(\boldsymbol{h}_j\boldsymbol{x}) \geq 0,\ j = 1, \ldots, K. \end{aligned} \tag{A.2}$$

Secondly, the QoS constraint $\mathcal{C}2$ in the problem (4.3) can be rewritten, again in the same fashion of [125, 126, 142], referring to the amplitude levels of the in-phase and quadrature components of the corresponding symbols, as follows:

$$\begin{aligned} |\,\mathrm{Re}(\boldsymbol{h}_j\boldsymbol{x})| \trianglerighteq \sigma_z\sqrt{\gamma_j}|\,\mathrm{Re}(d_j)|,\ j = 1, \ldots, K, \\ |\,\mathrm{Im}(\boldsymbol{h}_j\boldsymbol{x})| \trianglerighteq \sigma_z\sqrt{\gamma_j}|\,\mathrm{Im}(d_j)|,\ j = 1, \ldots, K, \end{aligned} \tag{A.3}$$

[1] This does not apply for data symbols laying on the imaginary axis, since the tangent is not defined in such case. Although this case can be easily handled, it is not considered herein, since we can always assume a phase offset preventing this situation.

where the absolute value is necessary for accounting negative components. By multiplying both the members of the above equations by $\mathrm{Re}(d_j)$ and $\mathrm{Im}(d_j)$ respectively, and by taking into account the conditions in (A.2), the above constraints become:

$$\begin{aligned} &\mathrm{Re}(d_j)\,\mathrm{Re}(\boldsymbol{h}_j\boldsymbol{x}) \trianglerighteq \sigma_z\sqrt{\gamma_j}\,\mathrm{Re}^2(d_j),\ j=1,\dots,K,\\ &\mathrm{Im}(d_j)\,\mathrm{Im}(\boldsymbol{h}_j\boldsymbol{x}) \trianglerighteq \sigma_z\sqrt{\gamma_j}\,\mathrm{Im}^2(d_j),\ j=1,\dots,K. \end{aligned} \tag{A.4}$$

Thus, the problem becomes:

$$\begin{aligned} \boldsymbol{x}(\boldsymbol{d},\boldsymbol{H},\boldsymbol{\gamma},\boldsymbol{p}) = \arg\min_{r,\boldsymbol{x}}\quad & r\\ \text{s.t.}\quad \mathcal{C}1:\quad & \alpha r^2 \le \frac{|x_i|^2}{p_i} \le r^2,\ i=1,\dots,N,\\ \mathcal{C}2:\quad & \mathrm{Re}(d_j)\,\mathrm{Re}(\boldsymbol{h}_j\boldsymbol{x}) \trianglerighteq \sigma_z\sqrt{\gamma_j}\,\mathrm{Re}^2(d_j),\\ & j=1,\dots,K,\\ \mathcal{C}3:\quad & \mathrm{Im}(d_j)\,\mathrm{Im}(\boldsymbol{h}_j\boldsymbol{x}) \trianglerighteq \sigma_z\sqrt{\gamma_j}\,\mathrm{Im}^2(d_j),\\ & j=1,\dots,K,\\ \mathcal{C}4:\quad & \frac{\mathrm{Im}(\boldsymbol{h}_j\boldsymbol{x})}{\mathrm{Re}(\boldsymbol{h}_j\boldsymbol{x})} = t_j,\ j=1,\dots,K. \end{aligned} \tag{A.5}$$

Ultimately, the problem can be rewritten in a more compact form as:

$$\begin{aligned} \boldsymbol{x}(\boldsymbol{d},\boldsymbol{H},\boldsymbol{\gamma},\boldsymbol{p}) = \arg\min_{r,\boldsymbol{x}}\quad & r\\ \text{s.t.}\quad \mathcal{C}1:\quad & \frac{|x_i|^2}{p_i} \le r^2,\ i=1,\dots,N,\\ \mathcal{C}2:\quad & \frac{|x_i|^2}{p_i} \ge \alpha r^2,\ i=1,\dots,N,\\ \mathcal{C}3:\quad & \mathrm{Re}(\boldsymbol{D})\,\mathrm{Re}(\boldsymbol{H}\boldsymbol{x}) \trianglerighteq \boldsymbol{\beta_R}\\ \mathcal{C}4:\quad & \mathrm{Im}(\boldsymbol{D})\,\mathrm{Im}(\boldsymbol{H}\boldsymbol{x}) \trianglerighteq \boldsymbol{\beta_I}\\ \mathcal{C}5:\quad & \boldsymbol{T}\,\mathrm{Re}(\boldsymbol{H}\boldsymbol{x}) - \mathrm{Im}(\boldsymbol{H}\boldsymbol{x}) = \boldsymbol{0}, \end{aligned} \tag{A.6}$$

where $\boldsymbol{D}=\mathrm{diag}(\boldsymbol{d})$, $\boldsymbol{T}=\mathrm{diag}(t_1,\dots,t_K)$, $\boldsymbol{\beta_r}=\sigma_z\sqrt{\boldsymbol{\gamma}}\circ\mathrm{Re}(\boldsymbol{d})^{\circ 2}$, $\boldsymbol{\beta_i}=\sigma_z\sqrt{\boldsymbol{\gamma}}\circ\mathrm{Im}(\boldsymbol{d})^{\circ 2}$.

A further step for simplifying the problem (A.6) is to rewrite it in the real domain, in the stacked variable $\tilde{\boldsymbol{x}}=[\mathrm{Re}(\boldsymbol{x})^T,\mathrm{Im}(\boldsymbol{x})^T]^T\in\mathbb{R}^{2N\times 1}$. To this end, the constraints should be modified accordingly.

Regarding the weighted per-antenna transmit power, it is not difficult to see that:

$$\frac{|x_i|^2}{p_i} = \|\boldsymbol{B}_i\tilde{\boldsymbol{x}}\|^2, \tag{A.7}$$

where $\boldsymbol{B}_i \in \mathbb{R}^{2\times 2N}$ is a matrix used for selecting $\mathrm{Re}(x_i)$ and $\mathrm{Im}(x_i)$ in the stacked vector $\tilde{\boldsymbol{x}}$ and, $\forall i = 1, \ldots, N$, is defined as:

$$\frac{1}{\sqrt{p_i}} \begin{bmatrix} \boldsymbol{e}_i & \boldsymbol{0}_N \\ \boldsymbol{0}_N & \boldsymbol{e}_i \end{bmatrix}, \tag{A.8}$$

with $\boldsymbol{e}_i$ being a the i-th row of an identity matrix with size N, and $\boldsymbol{0}_N$ being the all zero entries vector in $\mathbb{R}^{1\times N}$.

Concerning the QoS constraints, it is convenient to split the vector $\boldsymbol{Hx}$ into its real and imaginary parts:

$$\begin{aligned} \boldsymbol{Hx} = &\,\mathrm{Re}(\boldsymbol{H})\,\mathrm{Re}(\boldsymbol{x}) - \mathrm{Im}(\boldsymbol{H})\,\mathrm{Im}(\boldsymbol{x}) + \\ &+ \iota[\mathrm{Re}(\boldsymbol{H})\,\mathrm{Im}(\boldsymbol{x}) + \mathrm{Im}(\boldsymbol{H})\,\mathrm{Re}(\boldsymbol{x})], \end{aligned} \tag{A.9}$$

which leads straightforwardly to:

$$\mathrm{Re}(\boldsymbol{Hx}) = \boldsymbol{H_1}\tilde{\boldsymbol{x}}, \quad \mathrm{Im}(\boldsymbol{Hx}) = \boldsymbol{H_2}\tilde{\boldsymbol{x}}, \tag{A.10}$$

where $\boldsymbol{H_1} = [\mathrm{Re}(\boldsymbol{H}), -\mathrm{Im}(\boldsymbol{H})]$, $\boldsymbol{H_2} = [\mathrm{Im}(\boldsymbol{H}), \mathrm{Re}(\boldsymbol{H})]$.

With the above positions, the problem (A.6) can be expressed as:

$$\begin{aligned} \boldsymbol{x}(\boldsymbol{d}, \boldsymbol{H}, \boldsymbol{\gamma}, \boldsymbol{p}) = \arg\min_{r,\boldsymbol{x}} \quad & r \\ \text{s.t.} \quad \mathcal{C}1: \quad & \|\boldsymbol{B}_i\tilde{\boldsymbol{x}}\| \le r,\ i = 1, \ldots, N, \\ \mathcal{C}2: \quad & \|\boldsymbol{B}_i\tilde{\boldsymbol{x}}\|^2 \ge \alpha r^2,\ i = 1, \ldots, N, \\ \mathcal{C}3: \quad & \mathrm{Re}(\boldsymbol{D})\boldsymbol{H_1}\tilde{\boldsymbol{x}} \succeq \boldsymbol{\beta_r}, \\ \mathcal{C}4: \quad & \mathrm{Im}(\boldsymbol{D})\boldsymbol{H_2}\tilde{\boldsymbol{x}} \succeq \boldsymbol{\beta_i}, \\ \mathcal{C}5: \quad & (\boldsymbol{T}\boldsymbol{H_1} - \boldsymbol{H_2})\tilde{\boldsymbol{x}} = \boldsymbol{0}. \end{aligned} \tag{A.11}$$

Finally, by defining the matrices $\boldsymbol{A}_i = -\boldsymbol{B}_i^{\dagger}\boldsymbol{B}_i$ the problem becomes the one in (4.4), hence the Theorem 4.1 is proved.

□

Appendix B

Proof of Theorem 4.2.

Retracing the procedure followed in the proof in Appendix A, and specifically considering the equations (A.1)-(A.4), the problem (4.10) can be rewritten as follows:

$$\begin{aligned}
\boldsymbol{x}(\boldsymbol{d},\boldsymbol{H},\boldsymbol{\gamma}) = \arg\min_{\boldsymbol{x}} \quad & \frac{\|\boldsymbol{x}\|_\infty^2}{\|\boldsymbol{x}\|^2} \\
\text{s.t.} \quad \mathcal{C}1: \quad & \operatorname{Re}(d_j)\operatorname{Re}(\boldsymbol{h}_j\boldsymbol{x}) \trianglerighteq \sigma_z\sqrt{\gamma_j}\operatorname{Re}^2(d_j), \\
& j = 1,\dots,K, \\
\mathcal{C}2: \quad & \operatorname{Im}(d_j)\operatorname{Im}(\boldsymbol{h}_j\boldsymbol{x}) \trianglerighteq \sigma_z\sqrt{\gamma_j}\operatorname{Im}^2(d_j), \\
& j = 1,\dots,K. \\
\mathcal{C}3: \quad & t_j\operatorname{Re}(\boldsymbol{h}_j\boldsymbol{x}) - \operatorname{Im}(\boldsymbol{h}_j\boldsymbol{x}) = 0,\ j = 1,\dots,K.
\end{aligned} \tag{B.1}$$

By applying the following equalities:

$$\begin{aligned}
\operatorname{Re}(\boldsymbol{h}_j\boldsymbol{x}) &= \frac{\boldsymbol{h}_j\boldsymbol{x} + \boldsymbol{x}^\dagger\boldsymbol{h}_j^\dagger}{2}, \\
\operatorname{Im}(\boldsymbol{h}_j\boldsymbol{x}) &= \frac{\boldsymbol{h}_j\boldsymbol{x} - \boldsymbol{x}^\dagger\boldsymbol{h}_j^\dagger}{2\iota},
\end{aligned} \tag{B.2}$$

the problem (4.10) can be straightforwardly expressed as in (4.11). Thus, the Theorem 4.2 is proved.

□

Bibliography

[1] R. Roy and B. Ottersten, "Spatial division multiple access wireless communication systems," May 1996, US Patent 5,515,378. [Online]. Available: https://www.google.com/patents/US5515378

[2] D. Gesbert, S. Hanly, H. Huang, S. S. Shitz, O. Simeone, and W. Yu, "Multi-cell MIMO cooperative networks: A new look at interference," *IEEE Journal on Selected Areas in Communications*, vol. 28, no. 9, pp. 1380–1408, Dec 2010.

[3] S. Bassoy, H. Farooq, M. A. Imran, and A. Imran, "Coordinated multi-point clustering schemes: A survey," *IEEE Communications Surveys & Tutorials*, vol. 19, no. 2, pp. 743 – 764, Secondquarter 2017.

[4] S. Schwarz and M. Rupp, "Exploring coordinated multipoint beamforming strategies for 5G cellular," *IEEE Access*, vol. 2, pp. 930–946, 2014.

[5] G. Y. Li, J. Niu, D. Lee, J. Fan, and Y. Fu, "Multi-cell coordinated scheduling and MIMO in LTE," *IEEE Communications Surveys & Tutorials*, vol. 16, no. 2, pp. 761–775, 2014.

[6] P. Marsch and G. P. Fettweis, *Coordinated Multi-Point in Mobile Communications: From Theory to Practice*. Cambridge University Press, 2011.

[7] P.-D. Arapoglou, K. Liolis, M. Bertinelli, A. Panagopoulos, P. Cottis, and R. D. Gaudenzi, "MIMO over satellite: A review," *IEEE Communications Surveys & Tutorials*, vol. 13, no. 1, pp. 27–51, 2011.

[8] M. A. Vazquez, A. Perez-Neira, D. Christopoulos, S. Chatzinotas, B. Ottersten, P.-D. Arapoglou, A. Ginesi, and G. Tarocco, "Precoding in multibeam satellite communications: Present and future challenges," *IEEE Wireless Communications*, vol. 23, no. 6, pp. 88–95, Dec 2016.

[9] P.-D. Arapoglou, A. Ginesi, S. Cioni, S. Erl, F. Clazzer, S. Andrenacci, and A. Vanelli-Coralli, "DVB-S2X-enabled precoding for high throughput satellite systems," *International Journal of Satellite Communications and Networking*, vol. 34, no. 3, pp. 439–455, Jun 2015.

[10] Q. Wang, Z. Wang, and L. Dai, "Multiuser MIMO-OFDM for visible light communications," *IEEE Photonics Journal*, vol. 7, no. 6, pp. 1–11, Dec 2015.

[11] H. Shen, Y. Deng, W. Xu, and C. Zhao, "Rate-maximized zero-forcing beamforming for VLC multiuser MISO downlinks," *IEEE Photonics Journal*, vol. 8, no. 1, pp. 1–13, Feb 2016.

[12] K. Cai, M. Jiang, and X. Ma, "Photodetector selection aided multiuser MIMO optical OFDM imaging visible light communication system," *IEEE Access*, vol. 4, pp. 9870–9879, 2016.

[13] M. Bengtsson and B. Ottersten, "Optimal and suboptimal transmit beamforming," in *Handbook of Antennas in Wireless Communications*. CRC Press, 2001.

[14] ——, "Optimal downlink beamforming using semidefinite optimization," in *Proc. of Annual Allert. Conf. on Commun. Control and Computing*, vol. 37. Citeseer, 1999, pp. 987–996.

[15] M. Schubert and H. Boche, "Solution of the multiuser downlink beamforming problem with individual SINR constraints," *IEEE Transactions on Vehicular Technology*, vol. 53, no. 1, pp. 18–28, Jan 2004.

[16] W. Yu and T. Lan, "Transmitter optimization for the multi-antenna downlink with per-antenna power constraints," *IEEE Transactions on Signal Processing*, vol. 55, no. 6, pp. 2646–2660, June 2007.

[17] G. Dartmann, X. Gong, W. Afzal, and G. Ascheid, "On the duality of the max min beamforming problem with per-antenna and per-antenna-array power constraints," *IEEE Transactions on Vehicular Technology*, vol. 62, no. 2, pp. 606–619, Feb 2013.

[18] E. Karipidis, N. D. Sidiropoulos, and Z.-Q. Luo, "Far-field multicast beamforming for uniform linear antenna arrays," *IEEE Transactions on Signal Processing*, vol. 55, no. 10, pp. 4916–4927, Oct 2007.

[19] E. Karipidis, N. Sidiropoulos, and Z.-Q. Luo, "Quality of service and max-min fair transmit beamforming to multiple cochannel multicast groups," *IEEE Trans. Signal Process.*, vol. 56, no. 3, pp. 1268–1279, 2008.

[20] C. Masouros and E. Alsusa, "Dynamic linear precoding for the exploitation of known interference in MIMO broadcast systems," *IEEE Transactions on Wireless Communications*, vol. 8, no. 3, pp. 1396–1404, March 2009.

[21] C. Masouros, "Correlation rotation linear precoding for MIMO broadcast communications," *IEEE Transactions on Signal Processing*, vol. 59, no. 1, pp. 252–262, Jan. 2011.

[22] M. Alodeh, S. Chatzinotas, and B. Ottersten, "Constructive multiuser interference in symbol level precoding for the MISO downlink channel," *IEEE Transactions on Signal Processing*, vol. 63, no. 9, pp. 2239–2252, May 2015.

[23] ——, "Symbol-level multiuser MISO precoding for multi-level adaptive modulation," *IEEE Transactions on Wireless Communications*, vol. 16, no. 8, pp. 5511–5524, Aug 2017.

[24] ——, "Energy-efficient symbol-level precoding in multiuser MISO based on relaxed detection region," *IEEE Transactions on Wireless Communications*, vol. 15, no. 5, pp. 3755–3767, May 2016.

[25] C. Masouros and G. Zheng, "Exploiting known interference as green signal power for downlink beamforming optimization," *IEEE Transactions on Signal Processing*, vol. 63, no. 14, pp. 3628–3640, July 2015.

[26] G. Auer, V. Giannini, C. Desset, I. Gódor, P. Skillermark, M. Olsson, M. A. Imran, D. Sabella, M. J. Gonzalez, O. Blume, and A. Fehske, "How much energy is needed to run a wireless network?" *IEEE Wireless Communications*, vol. 18, no. 5, pp. 40–49, October 2011.

[27] S. Cripps, *RF Power Amplifiers for Wireless Communications*, 2nd ed. Artech House Microwave Library, 2006.

[28] R. Piazza, M. R. B. Shankar, and B. Ottersten, "Data predistortion for multicarrier satellite channels based on direct learning," *IEEE Transactions on Signal Processing*, vol. 62, no. 22, pp. 5868–5880, Nov 2014.

[29] S. K. Mohammed and E. G. Larsson, "Per-antenna constant envelope precoding for large multi-user MIMO systems," *IEEE Transactions on Communications*, vol. 61, no. 3, pp. 1059–1071, March 2013.

[30] C. Studer and E. G. Larsson, "PAR-aware large-scale multi-user MIMO-OFDM downlink," *IEEE Journal on Selected Areas in Communications*, vol. 31, no. 2, pp. 303–313, February 2013.

[31] C. Mollén and E. G. Larsson, "Multiuser MIMO precoding with per-antenna continuous-time constant-envelope constraints," in *2015 IEEE 16th International Workshop on Signal Processing Advances in Wireless Communications (SPAWC)*, June 2015, pp. 261–265.

[32] P. V. Amadori and C. Masouros, "Constant envelope precoding by interference exploitation in phase shift keying-modulated multiuser transmission," *IEEE Transactions on Wireless Communications*, vol. 16, no. 1, pp. 538–550, Jan 2017.

[33] M. Costa, "Writing on dirty paper," *IEEE Trans. Inf. Theory*, vol. 29, no. 3, pp. 439–441, 1983.

[34] H. Weingarten, Y. Steinberg, and S. Shamai, "On the capacity region of the multi-antenna broadcast channel with common messages," in *Information Theory, 2006 IEEE International Symposium on*, July 2006, pp. 2195–2199.

[35] B. Hassibi and H. Vikalo, "On the expected complexity of integer least-squares problems," in *2002 IEEE International Conference on Acoustics, Speech, and Signal Processing*, vol. 2, May 2002, pp. II–1497–II–1500.

[36] M. Tomlinson, "New automatic equalizer employing modulo arithmetic," *Electron. Lett.*, vol. 7, pp. 138–139, Mar 1971.

[37] A. Garcia-Rodriguez and C. Masouros, "Power-efficient Tomlinson-Harashima precoding for the downlink of multi-user MISO systems," *IEEE Transactions on Communications*, vol. 62, no. 6, pp. 1884–1896, June 2014.

[38] Y.-F. Liu, Y.-H. Dai, and Z.-Q. Luo, "Coordinated beamforming for MISO interference channel: Complexity analysis and efficient algorithms," *IEEE Transactions on Signal Processing*, vol. 59, no. 3, pp. 1142–1157, 2011.

[39] E. Björnson, M. Bengtsson, and B. Ottersten, "Optimal multiuser transmit beamforming: A difficult problem with a simple solution structure [lecture notes]," *IEEE Signal Processing Magazine*, vol. 31, no. 4, pp. 142–148, July 2014.

[40] A. B. Gershman, N. D. Sidiropoulos, S. Shahbazpanahi, M. Bengtsson, and B. Ottersten, "Convex optimization-based beamforming," *IEEE Signal Processing Magazine*, vol. 27, no. 3, pp. 62–75, May 2010.

[41] M. Kobayashi, N. Jindal, and G. Caire, "Training and feedback optimization for multiuser MIMO downlink," *IEEE Transactions on Communications*, vol. 59, no. 8, pp. 2228–2240, August 2011.

[42] G. Caire and S. Shamai, "On the achievable throughput of a multiantenna Gaussian broadcast channel," *IEEE Transactions on Information Theory*, vol. 49, no. 7, pp. 1691–1706, Jul 2003.

[43] E. Karipidis, N. Sidiropoulos, and Z.-Q. Luo, "Transmit beamforming to multiple co-channel multicast groups," in *Proc. of 1st Int. Workshop on Comput. Adv. in Multi-Sensor Adapt. Process. (CAMSAP)*, 2005, pp. 109–112.

[44] D. Christopoulos, S. Chatzinotas, and B. Ottersten, "Full frequency reuse multi-beam satellite systems: Frame based precoding and user scheduling," *IEEE Trans. Wireless Commun.*, 2014, *preprint:* arXiv:1406.7699 [cs.IT].

[45] ——, "Multicast multigroup beamforming under per-antenna power constraints," in *2014 IEEE International Conference on Communications (ICC)*, Jun 2014.

[46] ——, "Weighted fair multicast multigroup beamforming under per-antenna power constraints," *IEEE Transactions on Signal Processing*, vol. 62, no. 19, pp. 5132–5142, Oct 2014.

[47] ——, "Multicast multigroup beamforming for per-antenna power constrained large-scale arrays," in *2015 IEEE 16th International Workshop on Signal Processing Advances in Wireless Communications (SPAWC)*, Jun 2015.

[48] V. Joroughi, M. Ángel Vàzquez, and A. I. Pérez-Neira, "Generalized multicast multibeam precoding for satellite communications," *IEEE Transactions on Wireless Communications*, vol. 16, no. 2, pp. 952 – 966, February 2017.

[49] Y. Gao and M. Schubert, "Group-oriented beamforming for multi-stream multicasting based on quality-of-service requirements," in *Computational Advances in Multi-Sensor Adaptive Processing, 2005 1st IEEE International Workshop on.* IEEE, 2005, pp. 193–196.

[50] Y. Silva and A. Klein, "Linear transmit beamforming techniques for the multigroup multicast scenario," *IEEE Transactions on Vehicular Technology*, vol. 58, no. 8, pp. 4353–4367, Oct 2009.

[51] K. L. Law, I. Wajid, and M. Pesavento, "Robust downlink beamforming in multi-group multicasting using trace bounds on the covariance mismatches," in *2012 IEEE International Conference on Acoustics, Speech and Signal Processing (ICASSP)*, Mar 2012.

[52] S. X. Wu, Q. Li, M.-C. So, and W.-K. Ma, "A stochastic beamformed amplify-and-forward scheme in a multigroup multicast MIMO relay network with per-antenna power constraints," *IEEE Transactions on Wireless Communications*, pp. 1–1, 2016.

[53] M. Sadeghi, L. Sanguinetti, R. Couillet, and C. Yuen, "Reducing the computational complexity of multicasting in large-scale antenna systems," *IEEE Transactions on Wireless Communications*, vol. 16, no. 5, pp. 2963–2975, May 2017.

[54] N. Sidiropoulos, T. Davidson, and Z.-Q. Luo, "Transmit beamforming for physical-layer multicasting," *IEEE Transactions on Signal Processing*, vol. 54, no. 6, pp. 2239–2251, Jun 2006.

[55] N. Jindal and Z. quan Luo, "Capacity limits of multiple antenna multicast," in *2006 IEEE International Symposium on Information Theory*, Jul 2006.

[56] M.-C. Yue, S. X. Wu, and A. M.-C. So, "A robust design for MISO physical-layer multicasting over line-of-sight channels," *IEEE Signal Processing Letters*, vol. 23, no. 7, pp. 939 – 943, July 2016.

[57] A. Abdelkader, A. B. Gershman, and N. D. Sidiropoulos, "Multiple-antenna multicasting using channel orthogonalization and local refinement," *IEEE Transactions on Signal Processing*, vol. 58, no. 7, pp. 3922 – 3927, 2010.

[58] B. Gopalakrishnan and N. D. Sidiropoulos, "High performance adaptive algorithms for single-group multicast beamforming," *IEEE Transactions on Signal Processing*, vol. 63, no. 16, pp. 4373 – 4384, August 2015.

[59] V. Ntranos, N. D. Sidiropoulos, and L. Tassiulas, "On multicast beamforming for minimum outage," *IEEE Transactions on Wireless Communications*, vol. 8, no. 6, pp. 1536–1276, June 2009.

[60] I. H. Kim, D. J. Love, and S. Y. Park, "Optimal and successive approaches to signal design for multiple antenna physical layer multicasting," *IEEE Transactions on Communications*, vol. 59, no. 8, pp. 2316 – 2327, 2011.

[61] X. Xu, B. Du, and C. Wang, "On the bottleneck users for multiple-antenna physical-layer multicasting," *IEEE Transactions on Vehicular Technology*, vol. 63, no. 6, pp. 2977 – 2982, 2014.

[62] T. Yoo and A. Goldsmith, "Optimality of zero-forcing beamforming with multiuser diversity," in *IEEE International Conference on Communications (ICC 2005)*, vol. 1, May 2005, pp. 542–546.

[63] ——, "Capacity and power allocation for fading MIMO channels with channel estimation error," *IEEE Trans. Inf. Theory*, vol. 52, no. 5, pp. 2203–2214, May 2006.

[64] E. Björnson, M. Bengtsson, and B. Ottersten, "Optimal multiuser transmit beamforming: A difficult problem with a simple solution structure [lecture notes]," *IEEE Signal Processing Magazine*, vol. 31, no. 4, pp. 142–148, Jul 2014.

[65] M. Joham, W. Utschick, and J. Nossek, "Linear transmit processing in MIMO communications systems," *IEEE Transactions on Signal Processing*, vol. 53, no. 8, pp. 2700–2712, Aug 2005.

[66] C. Peel, B. Hochwald, and A. Swindlehurst, "A vector-perturbation technique for near-capacity multiantenna multiuser communication - part i: channel inversion and regularization," *IEEE Trans. Commun.*, vol. 53, no. 1, pp. 195–202, 2005.

[67] W. Yang and G. Xu, "New method for designing smart antenna downlink weighting vectors based on the filter bank concept," in *Advanced Signal Processing: Algorithms, Architectures, and Implementations VII*, F. T. Luk, Ed. SPIE-Intl Soc Optical Eng, Oct 1997.

[68] V. K. Nguyen and J. S. Evans, "Multiuser transmit beamforming via regularized channel inversion: A large system analysis," in *IEEE GLOBECOM 2008 - 2008 IEEE Global Telecommunications Conference*, 2008.

[69] R. Muharar, R. Zakhour, and J. Evans, "Optimal power allocation and user loading for multiuser MISO channels with regularized channel inversion," *IEEE Transactions on Communications*, vol. 61, no. 12, pp. 5030–5041, Dec 2013.

[70] T. Lo, "Maximum ratio transmission," *IEEE Transactions on Communications*, vol. 47, no. 10, pp. 1458–1461, 1999.

[71] Y. Wu, M. Wang, C. Xiao, Z. Ding, and X. Gao, "Linear precoding for MIMO broadcast channels with finite-alphabet constraints," *IEEE Transactions on Wireless Communications*, pp. 1–15, 2012.

[72] A. Lozano, A. Tulino, and S. Verdu, "Optimum power allocation for parallel gaussian channels with arbitrary input distributions," *IEEE Transactions on Information Theory*, vol. 52, no. 7, pp. 3033–3051, Jul 2006.

[73] F. Perez-Cruz, M. R. D. Rodrigues, and S. Verdu, "MIMO gaussian channels with arbitrary inputs: Optimal precoding and power allocation," *IEEE Transactions on Information Theory*, vol. 56, no. 3, pp. 1070–1084, Mar 2010.

[74] M. Bengtsson and B. Ottersten, "Optimal and suboptimal transmit beamforming," in *Handbook of Antennas in Wireless Communications*. CRC Press, 2001, pp. 18–1–18–33.

[75] M. Schubert and H. Boche, "Solution of the multiuser downlink beamforming problem with individual SINR constraints," *IEEE Transactions on Vehicular Technology*, vol. 53, no. 1, pp. 18–28, Jan 2004.

[76] H. Shen, W. Xu, A. L. Swindlehurst, and C. Zhao, "Transmitter optimization for per-antenna power constrained multi-antenna downlinks: An SLNR maximization methodology," *IEEE Transactions on Signal Processing*, vol. 64, no. 10, pp. 2712–2725, May 2016.

[77] G. Zheng, S. Chatzinotas, and B. Ottersten, "Generic optimization of linear precoding in multibeam satellite systems," *IEEE Transactions on Wireless Communications*, vol. 11, no. 6, pp. 2308–2320, June 2012.

[78] H. Dahrouj and W. Yu, "Coordinated beamforming for the multicell multi-antenna wireless system," *IEEE Transactions on Wireless Communications*, vol. 9, no. 5, pp. 1748–1759, May 2010.

[79] V.-D. Nguyen, L.-N. Tran, T. Duong, O.-S. Shin, and R. Farrell, "An efficient precoder design for multiuser MIMO cognitive radio networks with interference constraints," *IEEE Transactions on Vehicular Technology*, pp. 1–1, 2016.

[80] H. Zhang, C. Li, Y. Huang, and L. Yang, "Secure beamforming for SWIPT in multiuser MISO broadcast channel with confidential messages," *IEEE Communications Letters*, vol. 19, no. 8, pp. 1347–1350, Aug 2015.

[81] X. Chen and Y. Zhang, "Mode selection in MU-MIMO downlink networks: A physical-layer security perspective," *IEEE Systems Journal*, pp. 1–9, 2015.

[82] J. Xu, L. Liu, and R. Zhang, "Multiuser MISO beamforming for simultaneous wireless information and power transfer," *IEEE Transactions on Signal Processing*, vol. 62, no. 18, pp. 4798–4810, sep 2014.

[83] S. Ji, S. X. Wu, A. M.-C. So, and W.-K. Ma, "Multi-group multicast beamforming in cognitive radio networks via rank-two transmit beamformed alamouti space-time coding," *IEEE International Conference on Acoustic, Speech, and Signal Processing*, 2013.

[84] Özlem Tuğfe Demir and T. E. Tuncer, "Max-min fair resource allocation for swipt in multi-group multicast ofdm systems," *to appear in IEEE Communications Letter*, 2017.

[85] M. Sadeghi, L. Sanguinetti, and C. Yuen, "Hybrid precoding for multi-group physical layer multicasting," *arXiv preprint arXiv:1703.10329*, 2017.

[86] B. Liu, L. Shi, and X.-G. Xia, "Robust rank-two multicast beamforming under a unified CSI uncertainty model," *IEEE Signal Processing Letters*, vol. 23, no. 10, pp. 1419–1423, Oct 2016.

[87] K. L. Law, X. Wen, M. T. Vu, and M. Pesavento, "General rank multiuser downlink beamforming with shaping constraints using real-valued ostbc," *IEEE Transactions on Signal Processing*, vol. 63, no. 21, pp. 5758–5771, 2015.

[88] A. Schad, K. L. Law, and M. Pesavento, "Rank-two beamforming and power allocation in multicasting relay networks." *IEEE Trans. Signal Processing*, vol. 63, no. 13, pp. 3435–3447, 2015.

[89] Y. Huang, Q. Li, W.-K. Ma, and S. Zhang, "Robust multicast beamforming for spectrum sharing-based cognitive radios," *IEEE Transactions on Signal Processing*, vol. 60, no. 1, pp. 527–533, Jan 2012.

[90] M. R. A. Khandaker and K.-K. Wong, "SWIPT in MISO multicasting systems," *IEEE Wireless Communications Letters*, vol. 3, no. 3, pp. 277–280, Jun 2014.

[91] Z. Xiang, M. Tao, and X. Wang, "Coordinated multicast beamforming in multicell networks," *IEEE Transactions on Wireless Communications*, vol. 12, no. 1, pp. 12–21, jan 2013.

[92] B. Clerckx, H. Joudeh, C. Hao, M. Dai, and B. Rassouli, "Rate splitting for MIMO wireless networks: a promising PHY-layer strategy for LTE evolution," *IEEE Communications Magazine*, vol. 54, no. 5, pp. 98–105, May 2016.

[93] H. Joudeh and B. Clerckx, "Robust transmission in downlink multiuser MISO systems: A rate-splitting approach," *IEEE Transactions on Signal Processing*, vol. 64, no. 23, pp. 6227–6242, Dec 2016.

[94] ——, "Sum-rate maximization for linearly precoded downlink multiuser miso systems with partial csit: A rate-splitting approach," *IEEE Transactions on Communications*, vol. 64, no. 11, pp. 4847 – 4861, November 2016.

[95] D. Christopoulos, S. Chatzinotas, and B. Ottersten, "Cellular-broadcast service convergence through caching for CoMP cloud RANs," in *2015 IEEE Symposium on Communications and Vehicular Technology in the Benelux (SCVT)*, Nov 2015.

[96] E. G. Larsson and H. V. Poor, "Joint beamforming and broadcasting in massive MIMO," *IEEE Transactions on Wireless Communications*, vol. 15, no. 4, pp. 3058–3070, Apr 2016.

[97] M. Tao, E. Chen, H. Zhou, and W. Yu, "Content-centric sparse multicast beamforming for cache-enabled cloud RAN," *IEEE Transactions on Wireless Communications*, vol. 15, no. 9, pp. 6118–6131, Sep 2016.

[98] B.-X. Wu, K. C.-J. Lin, K.-C. Hsu, and H.-Y. Wei, "HybridCast: Joint multicast-unicast design for multiuser MIMO networks," in *2015 IEEE Conference on Computer Communications (INFOCOM)*, Apr 2015.

[99] J. Zhao, O. Simeone, D. G. üz, and D. Gómez-Barquero, "Non-orthogonal unicast and broadcast transmission via joint beamforming and ldm in cellular networks," *IEEE Global Communications Conference (GLOBECOM)*, 2016.

[100] C. Masouros and T. Ratnarajah, "Interference as a source of green signal power in cognitive relay assisted co-existing MIMO wireless transmissions," *IEEE Transactions on Communications*, vol. 60, no. 2, pp. 525–536, Feb 2012.

[101] C. Masouros, M. Sellathurai, and T. Ratnarajah, "Interference optimization for transmit power reduction in tomlinson-harashima precoded MIMO downlinks," *IEEE Transactions on Signal Processing*, vol. 60, no. 5, pp. 2470–2481, May 2012.

[102] F. A. Khan, C. Masouros, and T. Ratnarajah, "Interference-driven linear precoding in multiuser MISO downlink cognitive radio network," *IEEE Transactions on Vehicular Technology*, vol. 61, no. 6, pp. 2531–2543, Jul 2012.

[103] M. Alodeh, S. Chatzinotas, and B. Ottersten, "A multicast approach for constructive interference precoding in MISO downlink channel," in *2014 IEEE International Symposium on Information Theory*, Jun 2014.

[104] ——, "Symbol based precoding in the downlink of cognitive MISO channel," in *Lecture Notes of the Institute for Computer Sciences, Social Informatics and Telecommunications Engineering*. Springer Nature, 2015, pp. 370–380.

[105] ——, "Energy efficient symbol-level precoding in multiuser MISO channels," in *2015 IEEE 16th International Workshop on Signal Processing Advances in Wireless Communications (SPAWC)*, Jun 2015.

[106] ——, "Constructive interference through symbol level precoding for multi-level modulation," in *2015 IEEE Global Communications Conference (GLOBECOM)*, Dec 2015.

[107] M. Alodeh, D. Spano, S. Chatzinotas, and B. Ottersten, "Peak power minimization in symbol-level precoding for cognitive miso downlink channels," in *2016 IEEE International Conference on Digital Signal Processing (DSP)*, Oct 2016, pp. 240–244.

[108] D. Kwon, W.-Y. Yeo, and D. K. Kim, "A new precoding scheme for constructive superposition of interfering signals in multiuser MIMO systems," *IEEE Communications Letters*, vol. 18, no. 11, pp. 2047–2050, Nov 2014.

[109] C. Masouros and G. Zheng, "Exploiting known interference as green signal power for downlink beamforming optimization," *IEEE Transactions on Signal Processing*, vol. 63, no. 14, pp. 3628–3640, Jul 2015.

[110] D. Kwon, H. S. Kang, and D. K. Kim, "Robust interference exploitation-based precoding scheme with quantized CSIT," *IEEE Communications Letters*, vol. 20, no. 4, pp. 780–783, Apr 2016.

[111] K. Ntougias, D. Ntaikos, and C. B. Papadias, "Robust low-complexity arbitrary user- and symbol-level multi-cell precoding with single-fed load-controlled parasitic antenna arrays," in *International Conference on Telecommunications (ICT)*, May 2016.

[112] P. V. Amadori and C. Masouros, "Constant envelope precoding by interference exploitation in phase shift keying-modulated multiuser transmission," *IEEE Transactions on Wireless Communications*, vol. 16, no. 1, pp. 538–550, Jan 2017.

[113] A. Haqiqatnejad, F. Kayhan, and B. Ottersten, "Constructive interference for generic constellations," *IEEE Signal Processing Letters*, vol. 25, no. 4, pp. 586–590, April 2018.

[114] S. M. Razavi and T. Ratnarajah, "Adaptively regularized phase alignment precoding for multiuser multiantenna downlink," *IEEE Transactions on Vehicular Technology*, vol. 64, no. 10, pp. 4863–4869, Oct 2015.

[115] A. Li and C. Masouros, "Hybrid massive MIMO unlicensed transmission with 1-bit quantization," in *2017 IEEE Globecom Workshops (GC Wkshps)*, Dec 2017, pp. 1–6.

[116] K. L. Law, C. Masouros, and M. Pesavento, "Transmit precoding for interference exploitation in the underlay cognitive radio z-channel," *IEEE Transactions on Signal Processing*, vol. 65, no. 14, pp. 3617–3631, July 2017.

[117] M. R. A. Khandaker, C. Masouros, and K. K. Wong, "Constructive interference based secure precoding: A new dimension in physical layer security," *IEEE Transactions on Information Forensics and Security*, vol. 13, no. 9, pp. 2256–2268, Sept 2018.

[118] T. Hong, M.-Z. Song, and Y. Liu, "Dual-beam directional modulation technique for physical-layer secure communication," *IEEE Antennas and Wireless Propagation Letters*, vol. 10, pp. 1417–1420, 2011.

[119] N. Valliappan, A. Lozano, and R. W. Heath, "Antenna subset modulation for secure millimeter-wave wireless communication," *IEEE Transactions on Communications*, vol. 61, no. 8, pp. 3231–3245, Aug 2013.

[120] Y. Ding and V. Fusco, "BER-driven synthesis for directional modulation secured wireless communication," *International Journal of Microwave and Wireless Technologies*, vol. 6, no. 02, pp. 139–149, Nov 2013.

[121] ——, "Directional modulation transmitter radiation pattern considerations," *IET Microwaves, Antennas & Propagation*, vol. 7, no. 15, pp. 1201–1206, Dec 2013.

[122] Y. Ding and V. F. Fusco, "Constraining directional modulation transmitter radiation patterns," *IET Microwaves, Antennas & Propagation*, vol. 8, no. 15, pp. 1408–1415, Dec 2014.

[123] H. Shi and A. Tennant, "Enhancing the security of communication via directly modulated antenna arrays," *IET Microwaves, Antennas & Propagation*, vol. 7, no. 8, pp. 606–611, Jun 2013.

[124] J. Hu, F. Shu, and J. Li, "Robust synthesis method for secure directional modulation with imperfect direction angle," *IEEE Communications Letters*, vol. 20, no. 6, pp. 1084–1087, Jun 2016.

[125] A. Kalantari, M. Soltanalian, S. Maleki, S. Chatzinotas, and B. Ottersten, "Secure M-PSK communication via directional modulation," in *2016 IEEE International Conference on Acoustics, Speech and Signal Processing (ICASSP)*, March 2016, pp. 3481–3485.

[126] ——, "Directional modulation via symbol-level precoding: A way to enhance security," *IEEE Journal of Selected Topics in Signal Processing*, vol. 10, no. 8, pp. 1478–1493, Dec 2016.

[127] E. Casini, R. D. Gaudenzi, and A. Ginesi, "DVB-S2 modem algorithms design and performance over typical satellite channels," *International Journal of Sat. Comm. and Netw.*, vol. 22, no. 3, pp. 281–318, 2004. [Online]. Available: http://dx.doi.org/10.1002/sat.791

[128] D. Spano, D. Christopoulos, S. Andrenacci, S. Chatzinotas, J. Krause, and B. Ottersten, "Total degradation analysis of precoded signals onto non-linear satellite channels," in *21st Ka and Broadband Communications Conference*, Oct 2015.

[129] D. Spano, S. Chatzinotas, J. Krause, and B. Ottersten, "Symbol-level precoding with per-antenna power constraints for the multi-beam satellite downlink," in *2016 8th Advanced Satellite Multimedia Systems Conference and the 14th Signal Processing for Space Communications Workshop (ASMS/SPSC)*, Sept 2016, pp. 1–8.

[130] ETSI EN 302 307-1, "Digital video broadcasting (DVB); second generation framing structure, channel coding and modulation systems for broadcasting, interactive services, news gathering and other broadband satellite applications; part 1: DVB-S2."

[131] ETSI EN 302 307-2, "Digital video broadcasting (DVB); second generation framing structure, channel coding and modulation systems for broadcasting, interactive services, news gathering and other broadband satellite applications; part 2: DVB-S2 extensions (DVB-S2X)."

[132] A. A. M. Saleh, "Frequency-independent and frequency-dependent nonlinear models of TWT amplifiers," *IEEE Transactions on Communications*, vol. 29, no. 11, pp. 1715–1720, November 1981.

[133] M. O'Droma, S. Meza, and Y. Lei, "New modified Saleh models for memoryless nonlinear power amplifier behavioural modelling," *IEEE Communications Letters*, vol. 13, no. 12, pp. 1007–1007, December 2009.

[134] C. Mollén, E. G. Larsson, and T. Eriksson, "Waveforms for the massive MIMO downlink: Amplifier efficiency, distortion, and performance," *IEEE Transactions on Communications*, vol. 64, no. 12, pp. 5050–5063, Dec 2016.

[135] J. E. Mazo, "Faster-than-Nyquist signaling," *The Bell System Technical Journal*, vol. 54, no. 8, pp. 1451–1462, Oct 1975.

[136] A. D. Liveris and C. N. Georghiades, "Exploiting faster-than-Nyquist signaling," *IEEE Transactions on Communications*, vol. 51, no. 9, pp. 1502–1511, Sept 2003.

[137] Y. J. D. Kim, J. Bajcsy, and D. Vargas, "Faster-than-Nyquist broadcasting in gaussian channels: Achievable rate regions and coding," *IEEE Transactions on Communications*, vol. 64, no. 3, pp. 1016–1030, March 2016.

[138] F. Rusek and J. B. Anderson, "The two dimensional Mazo limit," in *Proceedings. International Symposium on Information Theory, 2005. ISIT 2005.*, Sept 2005, pp. 970–974.

[139] A. Barbieri, D. Fertonani, and G. Colavolpe, "Time-frequency packing for linear modulations: spectral efficiency and practical detection schemes," *IEEE Transactions on Communications*, vol. 57, no. 10, pp. 2951–2959, October 2009.

[140] A. Modenini, F. Rusek, and G. Colavolpe, "Faster-than-Nyquist signaling for next generation communication architectures," in *2014 22nd European Signal Processing Conference (EUSIPCO)*, Sept 2014, pp. 1856–1860.

[141] J. B. Anderson, F. Rusek, and V. Öwall, "Faster-than-Nyquist signaling," *Proceedings of the IEEE*, vol. 101, no. 8, pp. 1817–1830, Aug 2013.

[142] D. Spano, M. Alodeh, S. Chatzinotas, and B. Ottersten, "Per-antenna power minimization in symbol-level precoding," in *2016 IEEE Global Communications Conference (GLOBECOM)*, Dec 2016, pp. 1–6.

[143] D. Spano, S. Chatzinotas, S. Andrenacci, J. Krause, and B. Ottersten, "Per-antenna power minimization in symbol-level precoding for the multi-beam satellite downlink," *International Journal of Satellite Communications and Networking*, May 2018.

[144] D. Spano, M. Alodeh, S. Chatzinotas, J. Krause, and B. Ottersten, "Spatial PAPR reduction in symbol-level precoding for the multi-beam satellite downlink," in *2017 IEEE 18th International Workshop on Signal Processing Advances in Wireless Communications (SPAWC)*, July 2017. [Online]. Available: http://hdl.handle.net/10993/31224

[145] D. Spano, M. Alodeh, S. Chatzinotas, and B. Ottersten, "Symbol-level precoding for the nonlinear multiuser MISO downlink channel," *IEEE Transactions on Signal Processing*, vol. 66, no. 5, pp. 1331–1345, March 2018.

[146] ——, "PAPR minimization through spatio-temporal symbol-level precoding for the non-linear multi-user MISO channel," in *2018 IEEE International Conference on Acoustics, Speech and Signal Processing (ICASSP)*, April 2018.

[147] M. Alodeh, D. Spano, S. Chatzinotas, and B. Ottersten, "Faster-than-Nyquist spatiotemporal symbol-level precoding in the downlink of multiuser MISO channels," in *2017 IEEE International Conference on Acoustics, Speech and Signal Processing (ICASSP)*, March 2017.

[148] D. Spano, M. Alodeh, S. Chatzinotas, and B. Ottersten, "Faster-than-Nyquist signaling through spatio-temporal symbol-level precoding for the multiuser MISO downlink channel," *IEEE Transactions on Wireless Communications*, July 2018.

[149] S. Boyd and L. Vandenberghe, *Convex optimization*. Cambridge Univ. Press, 2004.

[150] E. Larsson, O. Edfors, F. Tufvesson, and T. Marzetta, "Massive mimo for next generation wireless systems," *IEEE Communications Magazine*, vol. 52, no. 2, pp. 186–195, February 2014.

[151] M. Diaz, N. Courville, C. Mosquera, G. Liva, and G. Corazza, "Non-linear interference mitigation for broadband multimedia satellite systems," in *Proc. Int. Work. Sat. Space Commun. (IWSSC)*, Sept. 2007, pp. 61–65.

[152] A. Beck, A. Ben-Tal, and L. Tetruashvili, "A sequential parametric convex approximation method with applications to nonconvex truss topology design problems," *Journal of Global Optimization*, vol. 47, no. 01, pp. 29–51, 2010.

[153] O. Mehanna, K. Huang, B. Gopalakrishnan, A. Konar, and N. D. Sidiropoulos, "Feasible point pursuit and successive approximation of non-convex QCQPs," *IEEE Signal Processing Letters*, vol. 22, no. 7, pp. 804–808, July 2015.

[154] M. Hong, Q. Li, and Y. F. Liu, "Decomposition by successive convex approximation: A unifying approach for linear transceiver design in heterogeneous networks," *IEEE Transactions on Wireless Communications*, vol. 15, no. 2, pp. 1377–1392, Feb 2016.

[155] I. Iofedov and D. Wulich, "MIMO-OFDM with nonlinear power amplifiers," *IEEE Transactions on Communications*, vol. 63, no. 12, pp. 4894–4904, Dec 2015.

[156] Y. Rahmatallah and S. Mohan, "Peak-to-average power ratio reduction in OFDM systems: A survey and taxonomy," *IEEE Communications Surveys Tutorials*, vol. 15, no. 4, pp. 1567–1592, 2013.

[157] W. Dinkelbach, "On nonlinear fractional programming," *Management Science*, vol. 13, no. 7, pp. 492–498, March 1967.

[158] R. Jagannathan, "On some properties of programming problems in parametric form pertaining to fractional programming," *Management Science*, vol. 12, no. 7, pp. 609–615, 1966.

[159] A. Hjørungnes, *Complex-Valued Matrix Derivatives With Applications in Signal Processing and Communications*. Cambridge University Press, 2011.

[160] S. Andrenacci, D. Spano, D. Christopoulos, S. Chatzinotas, J. Krause, and B. Ottersten, "Optimized link adaptation for DVB-S2X precoded waveforms based on SNIR estimation," in *2016 50th Asilomar Conference on Signals, Systems and Computers*, Nov 2016, pp. 502–506.

[161] S. Haykin, "Cognitive radio: brain-empowered wireless communications," *IEEE Journal on Selected Areas in Communications*, vol. 23, no. 2, pp. 201–220, Feb 2005.

[162] A. Goldsmith, S. A. Jafar, I. Maric, and S. Srinivasa, "Breaking spectrum gridlock with cognitive radios: An information theoretic perspective," *Proceedings of the IEEE*, vol. 97, no. 5, pp. 894–914, May 2009.

[163] S. Andrenacci, S. Chatzinotas, A. Vanelli-Coralli, S. Cioni, A. Ginesi, and B. Ottersten, "Exploiting orthogonality in DVB-S2X through timing pre-compensation," in *2016 8th Advanced Satellite Multimedia Systems Conference and the 14th Signal Processing for Space Communications Workshop (ASMS/SPSC)*, Sept 2016, pp. 1–8.

[164] J. Krivochiza, A. Kalantari, S. Chatzinotas, and B. Ottersten, "Low complexity symbol-level design for linear precoding systems," in *Symposium on Information Theory and Signal Processing in the Benelux*, May 2017.

[165] A. Kalantari, C. Tsinos, M. Soltanalian, S. Chatzinotas, W. K. Ma, and B. Ottersten, "MIMO directional modulation M-QAM precoding for transceivers performance enhancement," in *2017 IEEE 18th International Workshop on Signal Processing Advances in Wireless Communications (SPAWC)*, July 2017, pp. 1–5.

[166] ——, "Spatial peak power minimization for relaxed phase M-PSK MIMO directional modulation transmitter," in *2017 25th European Signal Processing Conference (EUSIPCO)*, Aug 2017, pp. 2011–2015.